Regulation and Function of Cerebral Cavernous Malformation Proteins

Asya Lazarova Borikova

A dissertation of thesis submitted to the faculty of the University of North Carolina at Chapel Hill in partial fulfillment of the requirements for the degree of Doctor of Philosophy in the Department of Pharmacology.

Chapel Hill
2012

Approved by:

Gary Johnson, Ph.D.

Lee Graves, Ph.D.

Keith Burridge, Ph.D.

Leslie Parise, Ph.D.

David Siderovski, Ph.D.

ABSTRACT

ASYA LAZAROVA BORIKOVA: Regulation and Function of the Cerebral Cavernous Malformation Proteins
(Under the direction of Gary L. Johnson, Ph.D.)

Cerebral Cavernous Malformations (CCM) is a genetic disease that causes dilated, leaky blood vessels in the brain and manifests with neurological deficits, seizures and hemorrhagic stroke. CCM is linked with loss-of-function mutations in *ccm1*, *ccm2*, and *ccm3*. CCM1, 2 and 3 are adaptor-like proteins that form a ternary complex, which has suggested that they regulate a common molecular pathway for the maintenance of endothelial cell function. We provide subcellular localization evidence in support of a common molecular role for CCM1 and 2, and define the only two known signaling pathways that are coordinately regulated by CCM1, 2 and 3.

Using molecular and functional approaches, we report that ^{433}MISDISSDIEAL^{444} is a nuclear export sequence in CCM2, the localization of CCM1 patterns that of wildtype and nuclear export deficient CCM2 and that the cytosolic localization of CCM2 is required for normal endothelial function. Regulated co-localization of CCM1 and CCM2 within the same subcellular compartment is consistent with a common function for CCM1 and 2. Consistent with these

observations a finding from Crose *et al.* showed that CCM2 binds the E3 ubiquitin ligase Smurf1 and localizes Smurf1 to sites of RhoA at the plasma membrane for the degradation of RhoA. We utilized molecular, FRET-based biosensor, biophysical and functional approaches to define that CCM1, 2 and 3 co-regulate the abundance and activity of RhoA and RhoA-dependent cytoskeletal dynamics and endothelial cell self-assembly in lumen-like tubes. We show that pharmacological and genetic inhibition of ROCK rescues the functional defects in CCM and propose ROCK as a potential therapeutic target for CCM.

Using genetic, proteomic and functional approaches we also define that CCM1, 2 and 3 co-regulate the abundance and activity of the small GTPase Rap1, and demonstrate a novel interaction between CCM2 and the E3 ubiquitin ligase Smurf2. Smurf2 regulates the degradation of Rap1 in neurons and we propose that CCM1, 2 and 3 co-regulate Rap1 abundance and activity for the regulation of endothelial cell tube formation. The studies presented here provide evidence that CCM1,2 and 3 coordinately regulate RhoA and Rap1, two key signaling hubs for the maintenance of endothelial function and vascular repair.

To my incredible family for always supporting my every endeavor with absolute belief in my success. Mom and Dad, I would be grateful to achieve even half of what you managed to do.

ACKNOWLEDGEMENTS

Foremost I would like to thank Dr. Gary Johnson for his unwavering support for the duration of this project. Gary has created an outstanding intellectual environment for scientific growth, whether through establishing collaborations, providing the opportunity to learn state-of-the-art techniques or constantly encouraging independent thinking. I would like to thank the members of the Johnson lab for creating a collaborative spirit. I would especially like to thank Dr. Amy Abell for her ever-present willingness to provide help with experimental design and interpretation, troubleshooting techniques, reading manuscripts and grant proposals, and career advice.

I would also like to thank Dr. Richard Superfine for allowing me to use his lab instruments, resources, personnel and expertise for the experiments for the biomechanical properties of cells. I would like to thank Dr. Tim O'Brien for his training, help with data interpretation and for preparation of reagents. I would like to thank the rest of the Superfine lab for help with various experimental and instrumental questions. I would like to thank Dr. Klaus Hahn for letting me rotate

through his lab and learn the biosensor techniques, and for providing the RhoA biosensor.

I would like to warmly thank all the members of my thesis committee, who have provided excellent guidance with experiments and career choices. I would especially like to thank Dr. Keith Burridge for his intellectual support for various projects and allowing me to use many of the resources in his lab.

I would be amiss not to recognize the funding sources and exceptional training from the Lineberger Cancer Center Training grant for the duration of three years.

I am especially grateful to Nancy and Gary Johnson, and Amy Abell for driving me around town when I broke my leg. I quite literally could not have managed without their help.

Long overdue thanks go to my undergraduate research mentors Dr. Gary Nishioka and Dr. Charles Sokolik for actively encouraging me to apply to graduate school and providing all the necessary support to ensure that I am qualified to attend a top tier university.

Last but definitely not least I would like to thank my parents for creating a home filled with love, support and curiosity for learning, and for creating endless opportunities for intellectual and personal growth; my mother, sister and grandparents for their absolute love, support and belief in my success even at the lowest times, my friends from near and far, and to Tim Rice-Oxley for inspiring me to persevere during difficult times, for staying humble during the good times and reminding me of my own values when I forget them.

TABLE OF CONTENTS

LIST OF FIGURES

LIST OF ABBREVIATIONS

AC – Adenylyl Cyclase protein

APC – Anaphase promoting complex

CCM – Cerebral cavernous malformations disease

Ccm1 – Cerebral cavernous malformations 1 gene

CCM1 – Protein product of the cerebral cavernous malformations 1 gene; alternate names are OSM and malcavernin

Ccm2 – Cerebral cavernous malformations 2 gene

CCM2 – Protein product of the cerebral cavernous malformations 2 gene; alternate names is Krit-1

Ccm3 – Cerebral cavernous malformations 3 gene

CCM3 – Protein product of the cerebral cavernous malformations 3 gene; alternate name is PDCD10

CyPet – Cyan fluorescent protein for energy transfer

Dia – Diaphanous

Dpc – Days post coital

E – Embryonic developmental day

E-cadherin – Epithelial cadherin

E3 – Ubiquitin ligase

eCFP – Enhanced Cyan Fluorescent Protein

EPC – Endothelial progenitor cell

eYFP – Enhanced Yellow Fluorescent Protein

FERM domain – Band four point one, ezrin, radixin, moesin domain

FRET – F□rster resonance energy transfer

GAP – GTPase activating protein

GDP – Guanine diphosphate

GEF – Guanine exchange factor

GFP – Green fluorescent protein

GLUT1 - Glucose Transporter 1

GPCR – G-protein coupled receptor

GST – Glutathione S-transferase

GTP – Guanine triphosphate

Hpf – Hours post fertilization

HUVEC – Human Umbelical Vein Endothelial Cells

ICAP-1 – B1-integrin cytoplasmic associated protein -1

Krit – K-rev interaction trapped

LIMK – LIM Kinase

MEEC – mouse embryonic endothelial cells

MEKK3 – Mitogen activated protein kinase kinase protein 3

MLCK – Myosin Light Chain Kinase

MSH2 – MutS Homolog2 protein

MTC – Magnetic twisting cytometry

NES – Nuclear export sequence

NLS – Nuclear localization sequence

OSM – Osmosensing scaffold for MEKK3

PDCD10 – Programmed cell death protein 10

PKI – Protein Kinase Inhibitor

PTB domain – Phosphotyrosine binding domain

ROCK – Rho Kinase

RT PCR – Real Time Polymerase Chain Reaction

shRNA – Small hairpin RNA

siRNA – Small interfering RNA

Smurf1 – Smad ubiquitin regulatory factor 1

Smurf2 – Smad ubiquitin regulatory factor 2

VE-cadherin – Vascular Endothelial-cadherin

VEGF – Vascular Endothelial Growth Factor

YFP – Yellow Fluorescent Protein

YPet – Yellow fluorescent protein for energy transfer

CHAPTER I

INTRODUCTION

Definition, clinical manifestation and current standard of care

Cerebral Cavernous Malformations (CCM) is a genetic disease that causes dilated, hyper-permeable, fragile blood vessels along the central nervous system (Rigamonti et al., 1987; Zhang et al., 2000; Clatterbuck et al., 2001; Clatterbuck and Rigamonti, 2002). The primary location for CCMs is the brain(Porter et al., 1999; Zabramski et al., 1999), with less frequent occurrences in the spinal cord (Vishteh et al., 1999), retina (Couteulx et al., 2002), liver (Davenport et al., 2001) and skin (Eerola et al., 2000). Early-stage CCM lesions are single dilated vessels which can remain static in size for years (Rigamonti et al., 1988). Advanced CCM lesions appear ‘mulberry-like’ due to multiple intertwined dilated blood vessels (Rigamonti et al., 1987). Progression into a mulberry-like structure is not required for symptoms to develop and patients can present with single or multiple CCMs (Cavalcanti et al., 2012). While some patients never develop more than one lesion, others develop multiple lesions within months (Revencu and Vikkula, 2006). Progression into a symptomatic lesion is characterized by a slow, continuous extravasation of blood due to the hyperpermeability of the vessels, or by hemorrhage due to the dilated,

fragile lumens of CCM vessels (Boon et al., 2011). The accumulation of blood in the peri-lesion parenchyma leads to consistent inflammation and eventual necrosis of the surrounding tissue (Shi et al., 2007; 2009). Clinical symptoms include severe motor and sensory deficits, headaches, seizures and hemorrhagic stroke (Batra et al., 2009). The disease burden of CCM is further increased by multiple or recurrent lesions.

An estimated 1 in 200 people from the general population carry a heterozygous mutation for CCM. This frequency is increased to 1 in 70 for Hispanics. Of heterozygous carriers, an approximate 30% develop lesions and another 25% of lesion carriers present with symptoms (Otten et al., 1989). Once symptoms are present, the current standard of treatment is palliative and with limited success. Anti-epileptics are used to control seizures, however less than half of CCM patients report symptom improvement (Awad and Jabbour, 2006). Migraine headaches are controlled through high-dose narcotics which need to be rotated to prevent development of drug-dependency (Batra et al., 2009). In cases of debilitating symptoms, rapid lesion bleeding or patient request, lesions are surgically excised. However, surgery is a suboptimal treatment due to cost, high risk for complications, the chance for lesion recurrence, the presence of multiple asymptomatic lesions within a patient and the potential for surgical inaccessibility of the lesion (Lunsford et al., 2010). Because current therapy does not address the molecular causes of CCM, lesion growth and progression into symptom manifestation remain a major clinical challenge. Thus a preventative or curative therapy targeted specifically to the molecular discrepancies of CCM is direly needed.

Genetic causes for CCM and the two-hit hypothesis

CCM is linked with inactivating mutations in three genes: *cerebral cavernous malformations 1/k-rev interaction trapped (ccm1/krit1)* (Sahoo et al., 1999a)*, cerebral cavernous malformations 2/malcavernin/osmosensing scaffold for mekk3 (ccm2/malcavernin/osm)* (Liquori et al., 2003) and *cerebral cavernous malformations 3/programed cell death 10 (ccm3/pdcd10)* (Craig et al., 1998). Loss of function in just one gene is sufficient for pathogenesis and the clinical manifestation for *ccm1*, *2* or *3* patients is identical (Marchuk, 2003).

The three genes encode for scaffold-like proteins that lack catalytic domains (Francalanci et al., 2009). Between the three genes over one hundred different mutations have been recorded (Revencu and Vikkula, 2006). These are point mutations that lead to aberrant splicing, frame shift or premature stop codon insertions (Verlaan et al., 2002).

CCM is separated into two categories based on the pathological origins of the mutations. The familial form is defined by inherited heterozygous germline mutations, whereas the sporadic form is characterized by spontaneously acquired somatic mutations(Laberge et al., 1999). Among familial cases estimated 40-53% display mutations in *ccm1*, 15-20% in *ccm2*, and 10-40% in *ccm3* (Haasdijk et al., 2012).

Familial and sporadic patients display an identical set of symptoms. The most clinically distinguishable difference in the manifestation of the familial and sporadic forms is the age at symptomatic onset and the number of lesions present. Familial patients present between infancy and the third decade in life and develop multiple

lesions, whereas sporadic patients generally present after the sixth decade with prevalently single or few lesions (Revencu and Vikkula, 2006).

The discrepancy between the low frequency of clinical presentation relative to the frequency of heterozygous carriers in the population and the fact that not all familial mutation carriers develop lesions has raised the idea that lesion development requires a 'second-hit' or loss of heterozygosity due to mutational inactivation of the second allele (Akers et al., 2008). This idea has been validated by findings from two different studies. The first is a study of the factors contributing to mutations in the wildtype allele of heterozygous CCM knockout mice. Lesion development was assessed under conditions of overall genetic instability induced by homozygous deletion of the tumor suppressor p53 or the mismatch repair protein MutS Homolog2 (MSH2). Lesion penetrance in *Ccm1*$^{-/+}$/*Trp53*$^{-/-}$ and *Ccm2*$^{-/+}$/*Trp53*$^{-/-}$ mice was 83% and 62% respectively(Shenkar et al., 2008) and 47% for *Ccm1*$^{-/+}$/*Msh2*$^{-/-}$ mice (McDonald et al., 2011). *Ccm2*$^{-/+}$/*Msh2*$^{-/-}$ mice did not develop lesions (McDonald et al., 2011). While these findings failed to establish a role for MSH2 during CCM lesion development, they provided initial experimental evidence that lesion development is promoted under conditions of genetic instability. A subsequent study which used laser microdissection to extract individual endothelial cells from familial CCM patient lesions and then sequenced both alleles of the heterozygously mutated CCM gene identified somatic mutations in the inherited widltype allele (Akers et al., 2008). Somatic mutations were not found in all endothelial cells within a lesion suggesting that a mosaic loss of heterozygosity is sufficient for CCM progression.

The Blood Brain Barrier

In order for targeted molecular therapies to be created, the particular cell type affected by CCM had to be defined. Several cell types are important for the structural integrity and function of blood vessels in the brain (Figure 1.1). The main function of blood vessels in the brain is to maintain the blood brain barrier, or the passage of molecules from the blood to brain tissue. Larger blood vessels are composed of a tube-like inner monolayer of endothelial cells and an outer layer of smooth muscle cells. Capillaries are constituted of the monolayer of endothelial cells only and lack the smooth muscle layer (Abbott et al., 2006). The blood brain barrier is physically maintained by the permeability of the endothelial monolayer. Two mechanisms of permeability across the blood brain barrier have been described. These are paracellular traffic across dissociated junction proteins and transcellular traffic, by lipophilic-mediated transport directly through the endothelial cells (Wittchen et al., 2005). Endothelial cells are connected through adherens and tight junctions. These two types of junctions are strictly separated in epithelial cells, however they are highly intermingled in endothelial cells (Abbott et al., 2006). The dissociation of these junctions creates a physical gap between endothelial cells that allows the passage of molecules or other cells (Wolburg and Lippoldt, 2002). Junction dynamics and transcellular migration are regulated by intercellular mechanisms in response to changes in shear stress, cytokine, ion and nitric oxide abundance. Smooth muscle cells have been suggested to regulate the blood brain barrier by secreting nitric oxide (Abbott et al., 2006). Pericytes and astrocytes directly interact with endothelial cells and thus provide structural support for the

cerebrovasculature. Both pericytes and astrocytes have been shown to regulate the blood brain barrier indirectly through regulation of the permeability of the endothelial monolayer (Armulik et al., 2010). Astrocytes secrete Vascular Endothelial Growth Factor (VEGF), and regulate the perivascular concentration of ions, as well as regulate the expression and activity of the Pgp-1/CD44 and Glucose Transporter 1 (GLUT1) transmembrane transporters (Abbott et al., 2006). A deficiency in the number of pericytes around the cerebrovasculature leads to increased blood brain barrier permeability by regulation of the expression of blood brain barrier specific genes in endothelial cells and by regulating the interaction between astrocytes and endothelial cells (Armulik et al., 2010).

CCM blood vessels resemble capillaries in that they are composed only of an endothelial monolayer and lack smooth muscle cells. However, CCM vessels also lack pericytes and surrounding brain parenchyma (Marchuk, 2003). A nearly diagnostic characteristic of CCM lesions is the presence of extravasated blood in the tissue immediately surrounding the lesion, suggesting a focal increase in endothelial monolayer permeability (Yadla et al., 2010). Since the blood brain barrier is maintained by endothelial, smooth muscle and astrocyte cells, the specific cell type affected by CCM had to be experimentally defined.

Mice with conditional deletion of *Ccm1* or *2* in smooth muscle cells, glia and neurons are born normal and have a normal lifespan (Whitehead et al., 2009). Mice with conditional deletion of *Ccm 2* or *3* in the endothelium die between embryonic days E9.5 and E13.5 (Whitehead et al., 2009). Subsequent *in vitro* studies have confirmed that loss of CCM protein expression in endothelial cells impairs multiple

endothelial-specific functions including permeability of monolayers, migration and tube formation establishing the endothelial cell as the main cell type affected by CCM (Glading et al., 2007).

Recently, the involvement of other cell types in CCM has been investigated. He *et al*. (He et al., 2010) and Louvi *et al*. (Louvi et al., 2011) report two different outcomes for conditional deletion of *Ccm3* in neuronal and glial tissue. He *et al*. observed normal Mendelian ratios at birth, normal lifespan, no vascular lesions or other gross defects in mice when using the *Nestin-Cre* neuronal specific system to conditionally delete *Ccm3* in neuronal tissue. Louvi *et al*. observed lower than expected Mendelian ratios at birth, death at postnatal day 3 and larger brain size with dilated and simplified cerebral vasculature when *Ccm3* was deleted with the *Nestin-Cre* promoter. The group also found that deletion of *Ccm3* with a *Gfap-Cre* driver results in lower Mendelian ratios at birth, death at 4 weeks of age, enlarged brain, dilated ventricles and unsteady gait and circling. Gfap expression occurs in central nervous system neurons and glial astrocytes, oligodendroglia and ependymal cells. Finally, the group showed that when *Ccm3* is lost in neocortex and hippocampal glial astrocytes and oligodendrocytes using an *Emx-Cre* system, mice are born in normal Mendelian ratios, have a normal lifespan and no gross neurological or vascular deficits, however still have enlarged brain size. Astrocytes isolated from these mice, similarly to astrocytes from *Ccm3*$^{flox/flox}$*; Gfap-Cre* mice, displayed increased activation and proliferation and resistance to apoptosis, which can potentially impair normal endothelial cell function and the maintenance of the blood brain barrier. Overall the Louvi findings suggest a neuronal autonomous role

for *Ccm3* and implicate neuronal and glial cells in CCM pathogenesis. How the crosstalk between endothelial, neuronal and glial cells is impaired in CCM and the retributions from such impairment are unknown and the existing mouse models for CCM will help define the answers to these questions.

Animal models for CCM

In an effort to understand the pathogenesis of CCM, mouse and zebrafish disease models have been created. What has become apparent in these models is that similar to the disease phenotype in humans, loss of either *ccm1*, *2* or *3* leads to an identical phenotype suggesting that CCM1, 2 and 3 regulate a common endothelial cell function, although that function appears to be different during development of the vascular system and post-developmental maintenance of vessels.

Mus Musculus

Homozygous whole-animal and endothelium-specific deletion of *Ccm1*, *2*, or *3* in mice is embryonically lethal between E8.0 and E9.5 (Whitehead, 2004). This event points to an essential role for the three CCM proteins in endothelial function. At E8.5 knockout embryos display an enlarged left ventricular chamber of the heart, loss of branchial arch morphogenesis, enlargement of brain precursor vessels, and dilated aortic sac and pericardial cavity. By E9.5 the absence of aortic arch morphogenesis becomes fatal. Endothelial cells of the branchial arch arteries fail to organize an intact lumen, creating a gap in the circulatory system. This leads to failure to initiate bloodflow despite normal heartbeat and embryonic death. In *Ccm3*$^{-/-}$ embryos the myocardium and endocardium are also disconnected, indicating a loss

of interaction between the smooth muscle and endothelial cells (He et al., 2010). Based on these studies, loss of *Ccm1*, *2* or *3* is phenotypically identical and consistent with the clinically identical presentation of *ccm1*, *2* or *3* patients.

However, one group has presented data that embryos from endothelial specific *Ccm3*$^{-/-}$ mice created by the group establish normal circulatory system and bloodflow but die at E13.5 due to progressive enlargement and rupture of the cardinal vein (Chan et al., 2011). The authors interpreted these findings to mean that pathogenesis with loss of function in *ccm3* is unique from the pathogenesis with loss of function of *ccm1* or *2*. However, these studies were performed with only partial deletion of *Ccm3*, whereas the phenotype of the *Ccm3*$^{-/-}$ mice with complete *Ccm3* deletion created by (Louvi et al., 2011) and (He et al., 2010) fully overlap the phenotype of the *Ccm1* and *Ccm2* mice.

Vessel formation during development is divided into two stages, vasculogenesis and angiogenesis. Vasculogenesis is the *de novo* patterning of blood vessels from stem cells. Angiogenesis is the formation of branches from pre-existing vessels. In mice vasculogenesis begins at 7.0-7.5 dpc and angiogenesis begins at 9.0-9.5dpc (Uyttendaele et al., 2001). As lethality in *Ccm1*, *2* and *3* knockout mice occurs at 9.5 dpc, it has been hypothesized that the genes are activated during angiogenesis. More specifically, since patients display abnormal vascular morphology in pre-existing vessels rather than loss of vessel formation, the post-natal role of the genes is most likely in vessel remodeling. Indeed, studies with endothelial cells isolated from lesions of *ccm2* and *ccm3* patient lesions showed that upon short interfering RNA (siRNA) mediated knockdown of *ccm2* or *ccm3* mRNA

respectively (to compensate for the mosaic loss of heterozygosity), sprouting angiogenesis *in vitro* was not impaired but formed vessels eventually disintegrated more rapidly (Zhu et al., 2010; Zhu et al., 2011).

Several mouse models have failed to recapitulate the CCM pathogenesis. Homozygous whole animal knockout mice, as discussed above, die during development. Whole animal *Ccm1*$^{-/+}$ or *Ccm2*$^{-/+}$ mice survive to birth, however they also fail to develop lesions (Plummer et al., 2004; Whitehead et al., 2009). Lesion penetrance increased under conditions of genetic instability introduced by crossing *Ccm1*$^{-/+}$ and *Ccm2*$^{-/+}$ mice with *Trp53*$^{-/-}$ or *Msh2*$^{-/-}$ mice. Lesions developed in 83% of *Ccm1*$^{-/+}$*/Trp53*$^{-/+}$ mice, 62% of *Ccm2*$^{-/+}$*/Trp53*$^{-/+}$, 47% of *Ccm1*$^{-/+}$*/Msh2*$^{-/+}$ and in none of the *Ccm2*$^{-/+}$*/Msh2*$^{-/+}$ mice (Shenkar et al., 2008; (McDonald et al., 2011). These findings supported the hypothesis that loss of heterozygosity is a genetic mechanism for CCM. However, these genetically engineered mice are a poor disease model since there is currently no evidence that either p53 or MSH2 are ever mutated in CCM.

The most successful CCM disease model in mice utilizes postnatal drug-induced deletion of *Ccm2* or *3* in endothelial cells. An inducible conditional deletion mouse model for CCM1 has not been reported to date. With this approach, the CCM genes are allowed to express normally throughout development and embryos survive to birth. Cunningham *et al*., induced homozygous deletion of *Ccm2* at age 6-8 weeks, and observed seizures, ataxia and death at 7-8 months of age (Cunningham et al., 2011). Chan *et al*. induced *Ccm2* or *Ccm3* loss of heterozygosity in pups immediately following birth and observed lesion formation at

4 and 1 month respectively (Porter et al., 1999; Zabramski et al., 1999; Chan et al., 2011; 2011). Both groups reported 100% penetrance. Similarly to human lesions, mouse lesions could be detected by magnetic resonance imaging and were characterized by dilated vessels with erythrocyte enrichment within the lumen, and hemosiderin peri-lesion staining. Hemosiderin is an iron-bound complex enriched in erythrocyte and macrophages and its peri-vascular localization is indicative of lesion bleeding, hemorrhage and inflammation. Large clusters of macrophages were found in proximity to the lesions further indicating local inflammation. The dilated vessels lacked staining for smooth muscle cells, pericytes and astrocyte feet attachments similarly to human CCM. Chan *et al*. additionally reported on the difference in pathogenesis in *Ccm2* and *Ccm3* mice. In addition to the earlier onset of symptoms in *Ccm3* mice, the number of lesions formed was also greater in these mice. These findings parallel the disease progress in human CCM3 patients, who display symptoms earlier and with greater severity (Haasdijk et al., 2012).

In summary, normal embryonic development and lesion formation in adulthood define the inducible conditional mouse model as the approach that most faithfully recapitulates clinical CCM. This model holds great promise for use in future preclinical studies evaluating potential therapeutics, and in providing evidence for the molecular pathways responsible for loss of smooth muscle cells, pericytes and astrocyte attachments and lesion development.

Danio rerio

A zebrafish model for CCM has also been established and closely recapitulates the embryonic lethality phenotype observed in mice. Genetic silencing

of the zebrafish orthologs for *ccm1* and *ccm2*, *santa* and *valentine* respectively, is accomplished through injection of morpholino oligos in zebrafish embryos. *Santa* and *valentine* deficient embryos develop enlarged vessels of the brain, cardiac enlargement and occlusion of the branchial arch arteries that connect the heart to the aorta (Mably, 2006). This occlusion blocks the outflow of blood from the heart and leads to 95% lethality by 48 hours post fertilization (hpf). Morpholino knockdown of *ccm3* in zebrafish is embryonic lethal at 24 hpf which is prior to onset of cardiovascular patterning. However, expression of a morpholino which induces aberrant *ccm3* splicing in a manner identical to identified patient mutations causes thin-walled, dilated hearts, occlusion of the branchial arch arteries and embryonic death similarly to *santa* and *valentine* morpholino embryos (Zheng et al., 2010a).

Structure-function relationships in CCM1, 2 and 3 govern formation of the CCM complex

Sequence alignment and crystal structure studies of CCM1, 2 and 3 have shown that each of the proteins encode protein-protein interaction domains however lack catalytic domains (Béraud-Dufour et al., 2007a; Li et al., 2010). This suggests that CCM1, 2 and 3 perform scaffold or adaptor-like functions (Figure 1.2).

CCM1/KRIT1 (K-Rev Interaction Trapped 1)

CCM1/KRIT1 was initially identified in a yeast two-hybrid study for binding partners of the small GTPase Rap1/K-rev (Serebriiskii et al., 1997). *Ccm1* is located on chromosome 7q21.2 and contains 19 exons (Sahoo et al., 1999b). The N-terminal domain of the protein (aa1-207) encodes a functional nuclear localization sequence (K46-L58) and an NPXY motif ($_{192}$NPAY$_{195}$) which interacts with the

Phosphotyrosine Binding (PTB) domain of β1-integrin cytoplasmic associated protein -1 (ICAP-1) (Zawistowski et al., 2002; Zhang et al., 2001). ICAP-1 competes with talin for the NPXY motif in the β1-integrin cytoplasmic tail and is thus a negative regulator of β1 integrin activity (Bouvard et al., 2006). It has been hypothesized that this function of ICAP-1 is regulated by the competitive binding of CCM1 and the β1-integrin tail with ICAP-1 (Zawistowski et al., 2002; Zhang et al., 2001). However experimental evidence of the role of CCM1 in β1 integrin activity has not been published to date. Similarly, the biological significance of the nuclear localization of CCM1 also remains undefined.

The central region of CCM1 (aa208-417) encodes two additional NPXY motifs ($_{231}$NPLF$_{234}$ and $_{250}$NPYF$_{253}$) and three ankyrin repeats. The two NPXY motifs mediate CCM1-CCM2 binding which was first identified via mass spectrometry by Hilder *et al*. (Zhang et al., 2007a; Hilder et al., 2007). Ankyrin repeats are one of the most abundant domains and mediate protein-protein interactions (Mably, 2006; Li et al., 2006).

The C-terminal region of CCM1 (aa 418-736) is spanned by a Band-four-point-one-ezrin-radixin-moesin domain (FERM) domain. The domain is composed of three clover-like F lobes, where F1 has an ubiquitin-like fold, F2 has an acyl-coA-BP-like helix bundle, and F3 is PTB-like. The F3 domain interacts with the third NPXY motif ($_{250}$NPYF$_{253}$) in a head to tail interaction and maintains CCM1 in a closed conformation (Béraud-Dufour et al., 2007b). In this state, the nuclear import of CCM1 is inhibited and CCM1 is localized in the cytoplasm. The head to tail interaction is thought to be a regulatory mechanism for CCM1 activity. When in the

opened state, the F2 and F3 lobes mediate binding with Rap1, a master regulator of endothelial permeability and adherens junctions. This interaction favors the cytoplasmic localization of CCM1. Two isoforms of Rap1 have been identified to date, Rap1a and Rap1b, and both interact with CCM1 (Béraud-Dufour et al., 2007b). The cytoplasmic localization of CCM1 is also favored by interaction with CCM2, as co-expression of wildtype CCM1 and CCM2 leads to the cytoplasmic localization of both however co-expression of CCM1 and CCM2 with mutation at F217 to disrupt PTB-domain interactions leads to the nuclear localization of CCM1. When expressed alone CCM1 also localizes to the nucleus, suggesting that CCM2 regulates the subcellular localization of CCM1(Zawistowski, 2005; Zhang et al., 2007b).

CCM2/OSM (Osmosensing Scaffold for MEKK3)/malcavernin

To date only one functional domain has been identified in CCM2 and that is a phosphotyrosine binding domain (PTB) from Ser60 to Asp230 (Uhlik et al., 2003, Liquori et al., 2003). The domain was identified based on the primary sequence of CCM2. A high-resolution structure of CCM2, or for CCM1, has not been solved as of yet.

There are over 200 PTB domain proteins and the sequence motif recognized by this domain is classically defined as Asn-Pro-x-Tyr (NPxY) (Uhlik et al., 2005). The third position, indicated by x, can be occupied by any amino acid. Early studies had suggested that phosphorylation of the tyrosine was required for recognition by the PTB domain, however it is now recognized that a subclass of PTB domains do not require tyrosine phosphorylation for binding (Uhlik et al., 2005). Based on its

predicted crystal structure, the PTB domain of CCM2 belongs to the phosphotyrosine-independent Dab-like subclass (Uhlik et al., 2005).

In a seminal study Hilder *et al.* (Hilder et al., 2007) used full length CCM2 and CCM2 with a point mutation (F217A) predicted to disrupt the binding capacity of the PTB domain in a pull down assay followed by mass spectrometry-identification of the pulldown fraction. These experiments defined the PTB- dependent and PTB-independent binding partners of CCM2. CCM1 and CCM3 were found to bind full length, but not F217A CCM2, indicating that a PTB-dependent interaction occurs between CCM2 and CCM1 and a functional PTB domain is required for CCM3 to be in the complex. In a pulldown assay for CCM2, both CCM1 and CCM3 were simultaneously isolated indicating that CCM1 and CCM3 do not compete for binding with CCM2 and that the three proteins exist in a ternary complex. The CCM1-CCM2 interaction is maintained by the $_{231}$NPLF$_{234}$ and $_{250}$NPYF$_{253}$ motifs within CCM1. The CCM2-CCM3 interaction is maintained by a highly conserved hydrophobic patch within the FAT like domain of CCM3, however a specific NPxY-like motif within CCM3 has not been defined (Li et al., 2010; He et al., 2010).

CCM3/PDCD10 (Programmed Cell Death 10)

CCM3 is the only CCM protein for which a crystal structure has been solved (Li et al., 2010). Prior to the crystallization of CCM3, attempts to identify domains using sequence homology alignment, molecular modeling and secondary structure analysis had failed and the crystal structure defined the first ever identified domains within CCM3. The N terminal domain of the protein exhibits a unique structure that cannot be classified as any currently known fold (Li et al., 2010). In crystallography

structures this domain appeared in a homodimerized state. Pulldown experiments of overexpressed CCM3 confirmed the homodimerization of CCM3. Importantly the N terminal domain alone fails to interact with CCM2 in pulldown assays. The C terminal domain of CCM3 (M92-A212) exhibits a FAT-homology fold and when truncated from the N terminal domain is sufficient to mediate CCM3-CCM2 binding. The domain contains two alipathic helices of highly conserved sequence (HP1, after standard FAK domain nomenclature). The high sequence conservation within HP1 suggested an essential function for the region. The authors disrupted the overall negative charge of the helices by point mutations of four conserved lysines (Lys-132, Lys-139, Lys-172 and Lys-179), or a serine (Ser-175) and showed that these disrupted CCM3-CCM2 binding.

Defined molecular pathways for CCM1, 2 and 3

While a common molecular function for CCM1, 2 and 3 had not been defined prior to our findings the proteins had been individually defined in several cellular pathways.

CCM2-Smurf1-RhoA

In a seminal paper defining the first endothelial-relevant signaling pathway regulated by a CCM protein, Crose *et al.* demonstrated that CCM2 interacts with the Smad ubiquitin regulatory factor 1 (Smurf1) (Crose et al., 2009). Smurf1 is an E3 ubiquitin ligase that regulates the degradation of the small GTPase RhoA (Sahai et al., 2007; Cheng et al., 2011). The interaction between CCM2 and Smurf1 is mediated by the PTB domain of CCM2 and the HECT domain of Smurf1 (Crose et al., 2009). Knockdown of CCM2 expression by short hairpin RNA (shRNA) in the

brain endothelial cells bEND.3 resulted in two-fold increase in the total levels of RhoA protein. Overexpression of increasing amounts of CCM2 and wildtype Smurf1 led to gradual decrease in total RhoA levels, however overexpression of CCM2 and a catalytically inactive Smurf1 did not (Crose et al., 2009). These studies demonstrated that CCM2 is required for the Smurf1-dependent degradation of RhoA. The overexpression of CCM2 and Smurf1, and resultant depletion of RhoA, resulted in collapse of the actin cytoskeleton and decrease in cell size demonstrating that the interaction of CCM2 and Smurf1 is physiologically relevant (Crose et al., 2009). The particular role of CCM2 in Smurf1 function was defined by their co-localization at the cell edge, the site of active RhoA. Smurf1 localization to sites of active RhoA at the plasma membrane is mediated by the C2 domain of Smurf1 (Sahai et al., 2007). The localization of C2-truncated Smurf1 which contained just a HECT domain was cytoplasmic, due to the absence of the C2 domain (Crose et al., 2009). However, co-expression of the Smurf1 HECT domain with CCM2 led to the complete relocalization of the HECT domain to the plasma membrane. CCM2 thus functions in the localization of Smurf1 to the plasma membrane, where Smurf1degrades active RhoA. These studies showed that loss of CCM2 expression leads to increased total RhoA levels due to loss of Smurf1 localization to sites of active RhoA with the functional consequence of increased abundance of actin stress fibers, a well characterized RhoA-specific phenotype. shRNA mediated knockdown of CCM2 impaired bEND.3 migration in a wound healing assay, increased permeability of endothelial monolayers in Human Umbelical Vein Endothelial Cells (HUVECs), and impaired Mouse Embryonic Endothelial Cells (MEECs) formation of

lumen-like tube structures on matrigel, an *in vitro* assay of endothelial function (Crose et al., 2009). The authors proposed that these endothelial cell defects were due to the increased total RhoA protein levels and activity.

RhoA

RhoA is a small GTPase of the Rho family. It is activated downstream of multiple signals including but not limited to activated G-protein coupled receptors (GPCR)s, receptor tyrosine kinases and integrins. The main known function of RhoA is in regulation of the assembly and disassembly of the actin and microtubule cytoskeletons (Rossman et al., 2005). Regulation of the actin cytoskeleton occurs through two pathways activated by the RhoA effector Rho Kinase (ROCK). The first is activation of Myosin Light Chain Kinase (MLCK), which phosphorylates myosin light chain leading to the increased affinity of myosin for actin fibers and stabilization of the actin stress fibers (Shen et al., 2010). The second is activation of Lim Kinase (LIMK), which phosphorylates Coffilin. In its unphosphorylated state Coffilin binds and sequesters actin monomers thus inhibiting actin polymerization and favoring stress fiber degradation (Wiggan et al., 2012). Phosphorylation inhibits Coffilin and promotes stress fiber polymerization. The overall effect of increased RhoA activation is increased stress fiber abundance and stability. Regulation of microtubules occurs through Diaphanous (Dia) which is a scaffold protein that stabilizes the Anaphase Promoting Complex (APC) along microtubules and thus promotes microtubule assembly. Dia also functions in actin fiber assembly by regulating actin nucleation (Bishop and Hall, 2000; Jaffe and Hall, 2005; Watanabe et al., 1999).

Our understanding of small GTPase biology has greatly relied on F□rster resonance energy transfer (FRET)-based biosensor technology. In a FRET biosensor a small GTPase of interest is genetically coupled to cyan and yellow fluorescent proteins(Welch et al., 2011; Machacek et al., 2009). Activation of the small GTPase leads to a conformational shift and energy transfer from the cyan to yellow fluorescent protein and quantitative energy emission from the yellow fluorescent protein. This quantitative nature of the biosensors has made it possible to measure real time changes in the activation state of the small GTPase at particular cellular locations. Studies using RhoA biosensors have defined that RhoA regulates disassembly of the actin cytoskeleton at both the leading and retracting edge of migrating cells (Machacek et al., 2009; Pertz et al., 2006).

RhoA activity is essential for normal endothelial cell function. The dynamic changes in permeability during normal vessel function require dynamic changes in cell shape sufficient to increase or decrease adherens junction binding or to accommodate an inflammatory cell migrating between adjacent endothelial cells. Furthermore as a master regulator of cell migration, rapid on-off regulation of RhoA activity is essential during angiogenesis and vessel remodeling (Xu et al., 2009). Overexpression of constitutively active RhoA leads to impaired formation of lumen-like tubes on matrigel (Xu et al., 2011).

The essential nature of RhoA in endothelial and vascular biology is further evidenced by the vascular defect phenotypes observed in genetically engineered mice with knockout for RhoA or a RhoA regulatory protein. Knockout of the RhoGTPase activating protein (RhoGAP) Rasip leads to embryonic lethality at E7

due to failed patterning of the vascular tube (Xu et al., 2011). Knockout of Arap3, the RhoGAP encoding adapter protein activated by Rap1 leads to embryonic death at E11 due to endothelial cell autonomous defect in sprouting angiogenesis (Gambardella et al., 2010). The vascular plexus of *Arap3*$^{-/-}$ mice patterns correctly, however endothelial cells remain in enlarged, cavernous clusters with little vascular branching indicating a defect in vascular remodeling. Interestingly, this defect is most prominently observed in the cerebral vasculature.

The identification of CCM2 as an upstream regulator of RhoA abundance and possibly activity has raised the possibility of RhoA as a key factor in CCM pathogenesis with the potential of ROCK as a druggable therapeutic target for CCM.

CCM1-Rap1

The interaction between CCM1 and Rap1 was initially identified in a yeast-two-hybrid screen, and has been validated by several independent groups (Serebriiskii et al., 1997; Liu et al., 2011; Li et al., 2012).

While the phenotype of zebrafish treated with Rap1a or Rap1b morpholino does not phenocopy that of CCM zebrafish (see above), embryos injected with morpholinos for CCM1 and Rap1b at concentrations that alone yield 10% penetrance, when combined result in over 90% penetrance of the CCM-characteristic big heart and circulatory block phenotype and the Rap1b-characteristic cranial hemorrhage phenotype (Gore et al., 2008). These studies suggested that Rap1b and CCM1 genetically interact to regulate a physiological event relevant to CCM. The single event shown to be co-regulated by Rap1b and CCM1 is regulation of endothelial permeability (Liu et al., 2011; Glading et al., 2007). Consistent with the

increased permeability that characterizes CCM vessels, the permeability of monolayers of endothelial cells in which CCM1 expression has been silenced by siRNA is increased. Treatment of these cells with the Rap1 activating agent 8-pCPT-2'OMe-cAMP failed to rescue the increased permeability, demonstrating that CCM1 functions downstream of Rap1 (Glading et al., 2007). At present endothelial permeability is the only physiological significance demonstrated for the CCM1-Rap1 interaction however given the multiple cellular functions of Rap1 it is likely that the interaction has further physiological consequences. The role of the Rap1-CCM1 interaction in Rap1-regulated RhoA activity is of particular interest as CCM2 has been shown to regulate the degradation of RhoA as discussed.

Rap1

Rap1 is a small GTPase that functions in adherens junction formation, inside-out integrin activation and actin cytoskeletal regulation(Kooistra et al., 2006). Rap1 is ubiquitously expressed however its function has been most thoroughly studied in immune-response cells, endothelial cells and neurons (Wittchen, 2005; Bivona, 2004; Murphy et al., 2005). Two Rap1 splice varients have been identified, Rap1a and Rap1b. While the two exhibit 95% sequence conservation, Rap1a knockout mice are viable and fertile with no gross deficiencies, and Rap1b knockout mice display up to 75% embryonic lethality due to cranial, liver and gut hemorrhage between E8.5 and E13 (Lakshmikanthan et al., 2011). The surviving $Rap1b^{-/-}$ mice exhibit delay or complete loss of clotting. These studies have suggested that the two isoforms perform distinct molecular functions. The subcellular localization of Green Fluorescent Protein (GFP)-tagged Rap1a is primarily along adherens junctions at

the plasma membrane, whereas GFP-Rap1b is primarily found in the endoplasmic reticulum, Golgi and perinuclear region. However, because antibodies that distinguish between the isoforms do not currently exist studies in endothelial cells have either not distinguished between the isoforms or have targeted Rap1b due to the severe mouse phenotype. Thus, while several molecular functions are known for Rap1, the relative contribution of each isoform to these functions is not been well defined (Wittchen et al., 2011).

The best characterized physiological functions of Rap1 are in regulation of adherens-junction regulated endothelial permeability, i.e. vascular leak, cytoskeletal dynamics, cell polarity and integrin-mediated platelet-endothelium adhesion (Kooistra et al., 2006). Adherens junctions are composed of cadherins which are tethered to the actin cytoskeleton through a host of factors the best characterized of which are α- and β-catenin, p120-catenin, afadin6 (AF6) and zona occludin-1 (ZO-1). It has been now established that the homodimeric interactions of Vascular Endothelial cadherins (VE-cadherin) between adjacent endothelial cells are the primary mechanism for maintenance of endothelial monolayer permeability(Brunton et al., 2004; Davis et al., 2003; Dejana, 2004). As a small GTPase, Rap1 is activated by the exchange of Guanine Diphosphate (GDP) for Guanine Triphosphate (GTP) facilitated by Guanine Exchange Factors (GEFs) and inactivated by GTP to GDP hydrolysis catalyzed by GAPs. Knockdown of the Rap1 activating RapGEF DOCK4 results in loss of adherens junction formation, whereas introduction of wildtype DOCK4 or a mutationally activated form of Rap1 restores adherens junction formation (Yajnik et al., 2003). Pharmacological activation of Rap1 with 8-pCPT-

2`OMe-cAMP, an activating agent for the RapGEF Epac, decreases endothelial monolayer permeability, however this effect is lost in VE-cadherin null cells suggesting that Rap1 is a negative regulator of permeability in a manner that requires VE-cadherin expression (Kooistra et al., 2005). Overexpression of the Rap1 negative effector RapGAP inhibits adhesion of cells to Fc-VE-cadherin-coated plates, suggesting that Rap1 activity is required for VE-cadherin homodimerization. The mechanism through which Rap1 regulates VE-cadherin is not fully understood, however it is known that the RapGEF C3G competes with β-catenin for direct binding with the tail of Epithelial cadherin (E-cadherin), thus likely destabilizing and promoting its degradation (Hogan et al., 2004). Finally a recent study showed that Rap1a, but not Rap1b, regulates endothelial permeability as Rap1a but not Rap1b co-localized and immunoprecipitated with VE-cadherin, and knockdown of Rap1a but not Rap1b led to upregulation of permeability (Wittchen et al., 2011).

The role of Rap1 in integrin function was initially established in the context of lymphocyte, T-cell and platelet adhesion to the endothelium which is mediated through integrins. Knockdown of Rap1a and Rap1b expression in these cells resulted in decreased $\alpha_{IIb}\beta 3$ integrin activation, and decreased adhesion to the endothelium (Zhang et al., 2011). Physiologically, loss of Rap1b but not Rap1a in mice leads to delay or loss of clotting following injury (Lakshmikanthan et al., 2011). A role for Rap1 in integrin activation in non-inflammatory response cells has also been established, suggesting a broader importance of Rap1 in integrin activation. Overexpression of constitutively activated Rap1 in chinese hamster ovary cells leads to the recruitment of the Rap1 effector RIAM, actin, and talin to the cytoplasmic tail

of the β-subunit of α4β1 integrins and integrin activation (Lee et al., 2009). While Rap1 regulation of integrin signaling in non-inflammatory cells appears to bear no physiological consequences as the phenotype in Rap1b knockout mice is hemorrhage during development (likely due to impaired adherens junction integrity) and delayed clotting in surviving pups, Rap1 is actively investigated in the regulation of epithelial to mesenchymal transition during tumor metastasis.

Rap1 regulates RhoA

Regulation of cytoskeletal dynamics by Rap1 is mediated through indirect regulation of RhoA, Rac1 and cdc42 (Hogan et al., 2004; Arthur et al., 2004). Initial studies into the role of Rap1 in cytoskeletal dynamics were prompted by the observation that treatment of endothelial cells with thrombin increased permeability and actin stress fiber formation (Kooistra et al., 2005). These studies suggested that cytoskeletal rearrangement may regulate the degradation and reformation of adherens junctions during permeability. Regulation of stress fiber dynamics is a function of the small GTPase RhoA (Jaffe and Hall, 2005). The activity of RhoA and Rap1 are both upregulated in endothelial cells treated with thrombin, however introduction of constitutively active Rap1 prevents thrombin-induced RhoA (Kooistra et al., 2005) activation suggesting that Rap1 is a negative upstream regulator of RhoA. The mechanism through which Rap1 signals to RhoA is that active Rap1 recruits the adaptor protein Arap3 which encodes a RhoGAP domain(Gambardella et al., 2010; Moon and Zheng, 2003). In addition to regulating endothelial permeability, this Rap1-RhoA switch is important not only for regulating endothelial permeability but also axon formation in neurons (Jeon et al., 2010a; Yamada et al.,

2005). Arap3 additionally encodes a GAP domain for the small GTPase Arf6, which is an upstream effector of Rac1 (Donaldson and Jackson, 2011). The main molecular role for Arf6 is regulation of vesicular trafficking. Arf6 is required for VE-cadherin localization to the plasma membrane and recycling as knockdown of Arf6 or introduction of a dominant negative mutant results in the accumulation of VE-cadherin in vesicles and loss of VE-cadherin localization at the plasma membrane.

CCM2-HEG1

CCM2 has been shown to genetically and biochemically interact with the orphan seven transmembrane receptor Heart of Glass 1 (HEG1). The enlarged heart phenotype and circulatory block observed in *ccm1* and *ccm2*-morphant zebrafish is duplicated in *heg1*-morphant fish(Mably, 2006). Whole mouse knockout of *Heg1* produces viable offspring, however 50% of the pups die due to pulmanory hemorrhage prior to weaning(Kleaveland et al., 2009a). Evidence for the genetic interaction of *Heg1* and *Ccm2* comes from genetically engineered mice. $Heg1^{-/-}$; $Ccm2^{lacz/+}$, but not $Ccm2^{lacz/+}$, mice phenocopy $Ccm2^{-/-}$ animals and die at E9.5 due to failure of the endothelial cells to organize the lumens of the dorsal aorta and branchial arch arteries despite the cells homing to the proper location (Kleaveland et al., 2009b; Zheng et al., 2010a).

HEG1 and CCM2 interact biochemically as CCM2 is immunoprecipitated with the cytoplasmic tail of HEG1 (Kleaveland et al., 2009a). This interaction is enhanced upon co-expression of CCM2 and CCM1, and is lost with a CCM2 L197R mutation, which was originally identified in a CCM patient and has been shown to disrupt

CCM1-CCM2 binding. The cytoplasmic tail of HEG1 also immunoprecipitated CCM1 alone, and CCM1 and CCM2 when co-expressed.

To date neither a ligand nor a specific downstream pathway has been defined for the HEG1 receptor. How HEG1 regulates normal endothelial cell function or CCM protein function thus remain unknown.

CCM3-VEGFR2

Evidence for the interaction of CCM3 with VEGFR2 comes from studies of the CCM3 knockout mouse (Li et al., 2010; (Zheng et al., 2010a). Due to the impaired vascular formation phenotype of *Ccm3*$^{-/-}$ mice the authors performed a small QRT PCR screen for well-established vascular regulatory factors. The mRNA levels of *Vegfr2*, *Gata-1*, and *Scl1* were reduced(Zheng et al., 2010b; Louvi et al., 2011). This reduction in VEGFR2 expression also led to a decrease in downstream signaling as evidenced by decreased levels in phospho-PLC-γ, and phospho-Akt. In cultured endothelial cells the levels of CCM3 protein bound to the cytoplasmic tail of VEGFR2 increased in a time course treatment with VEGF suggesting that CCM3 is recruited to VEGRF2. Finally, the authors showed that co-expression of VEGFR2 and three unique patient identified mutations of CCM3 led to lower overall levels of VEGFR2 than when the receptor was coexpresed with wildtype CCM3, suggesting that the stability of VEGFR2 is decreased in the absence of wildtype CCM3. Furthermore, loss of CCM3 was defined to upregulate VEGFR2 endocytosis and degradation. However, the authors reported that they failed to observe an interaction between CCM2 and VEGFR2 or decreased VEGFR2 expression or signaling in CCM2 knockdown cultured endothelial cells. Thus whether dysregulated VEGFR2 signaling

is a general defect in CCM due to loss of any of the three CCM genes or specific to CCM due to loss of CCM3 alone is currently not known.

Objectives of this project

Formation of the CCM complex

There are over 100 unique mutations in *ccm1*, *2* and *3* identified in patients(Revencu and Vikkula, 2006). The vast majority of these lead to premature truncations or internal deletions with just several non-truncating point mutations identified to date(Verlaan et al., 2002; Akers et al., 2008; Couteulx et al., 2002).

The most frequent mutations within CCM2 lead to alternative splicing and subsequent deletion of the N-terminal portion of the PTB domain, or to premature truncation and deletion of the C-terminus of the PTB domain thus likely resulting in disrupted or weakened PTB binding interactions (Verlaan et al., 2004). The single non-truncating CCM2 point mutation (L198R) which has been repeatedly identified in familial patients occurs within the PTB domain (Denier et al., 2004). This mutation is predicted to disrupt PTB domain interactions and has been experimentally shown to disrupt binding of CCM2 with CCM1 or CCM3 (Hilder et al., 2007; Zawistowski, 2005). The big heart phenotype of *ccm2*-morphant zebrafish is rescued by expression of wildtype ccm2 but is not rescued by expression of ccm2L198R (Kleaveland et al., 2009b). Overall these findings point toward the physiological requirement for a functional PTB domain in CCM2. As a physiological function of the CCM2 PTB domain is in organization of the CCM1/2/3 complex, we hypothesized that loss of organization of the CCM complex is a pathological event for CCM.

The events that govern the formation of the CCM complex however remain unknown. A common mechanism for governing protein complex formation and function is regulated subcellular localization. Regulation of subcellular localization has been proposed to be a mechanism that governs the formation of the CCM complex(Zawistowski, 2005; Faurobert and Albiges-Rizo, 2010). The endogenous localization of the three CCM proteins remains unknown due to the lack of immunofluorescence grade antibodies. When overexpressed alone in the monkey kidney fibroblast line COS-7 CCM1 localizes to the nucleus and CCM2 is found in the cytoplasm (Zawistowski, 2005). However, when CCM1 is overexpressed with CCM2 the localization of CCM1 shifts to the cytoplasm, where CCM1 and CCM2 co-localize. Co-expression of CCM1 with the PTB mutated F217A CCM2 fails to relocalize CCM1 to the cytoplasm (Zawistowski, 2005), suggesting that the cytoplasmic localization of CCM1 is mediated by CCM2. **We hypothesized that this co-regulation may occur by CCM2 directly recruiting CCM1 from the nucleus thus serving as a nuclear export adaptor for CCM1. We proposed to experimentally define the signals that govern the nuclear import and export of CCM2 and whether CCM2 encodes a functional nuclear import or export sequence required for a shuttling activity.**

CCM1, 2 and 3 regulate a common signaling pathway

A successful therapy for CCM requires the identification of the molecular pathway(s) disrupted during CCM pathogenesis. Several clinical observations and experimental findings have suggested that CCM1, 2 and 3 regulate a common signaling pathway. The clinical symptoms, lesion morphology and pathology are

indistinguishable between *ccm1*, *ccm2* and *ccm3* patients. There is complete phenotypic overlap - enlarged heart, cardiac block and death by 48 hours post fertilization, for *ccm1*, *ccm2*, and *ccm3*-morphant zebrafish(Mably, 2006)' (Zheng et al., 2010a). Mice with whole-tissue or endothelial specific deletion of *Ccm1*, *Ccm2* or *Ccm3* display mortality at E9.5 due to incomplete lumen formation of the dorsal aorta and branchial arch arteries (He et al., 2010; Whitehead, 2004; Whitehead et al., 2009; Kleaveland et al., 2009b).

The biochemical evidence for a common signaling pathway comes from the triple complex between CCM1, 2 and 3 where complex formation depends on a functional PTB domain within CCM2 (Zawistowski, 2005; Hilder et al., 2007). The most frequent mutations within CCM2 lead to alternative spicing and subsequent deletion of the N-terminal portion of the PTB domain, or to premature truncation and deletion of the C-terminus of the PTB domain. The single non-truncating point mutation (L198R) identified in a *ccm2* patient occurs within the PTB domain and has been experimentally shown to disrupt binding of CCM2 with CCM1 or CCM3 (Denier et al., 2004; Zawistowski, 2005; Zheng et al., 2010a). The big heart phenotype of *ccm2*-morphant zebrafish is rescued by expression of wildtype ccm2 but is not rescued by expression of ccm2L198R, suggesting that loss of formation of the CCM complex is pathogenic (Kleaveland et al., 2009b). When co-expressed CCM1 and CCM2 co-localize to the cytoplasm whereas co-expression of CCM1 and the PTB mutated F217A CCM2 or expression of CCM1 alone result in the nuclear localization of CCM1 (Zawistowski, 2005). While the functional significance of the nuclear

localization of CCM1 has not been experimentally defined, these findings suggest that the subcellular localization of CCM1 is regulated by CCM2.

Based on the common phenotype with loss of function in any of the three genes, disease progression which requires loss of just one CCM gene, and the formation of a CCM complex where the interaction of CCM2 with CCM1 and CCM3 is impaired with patient-identified mutations, **we hypothesized that CCM proteins regulate a common signaling pathway required for lumen formation, function and maintenance of endothelial cells.**

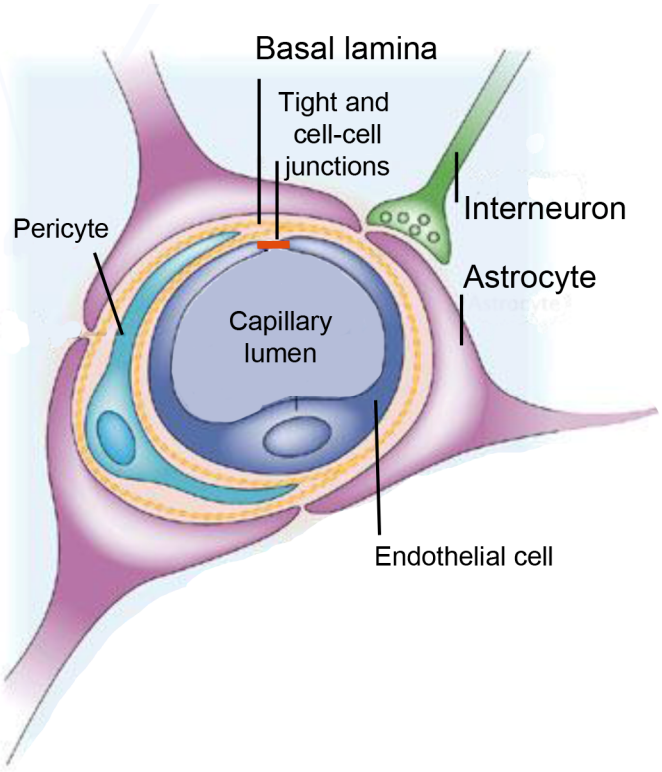

Figure 1.1: Structure of a cerebrovascular capillary. The endothelial monolayer is structurally supported by pericytes and astrocytic feet. Tight and cell-cell junctions regulate paracellular permeability. Paracrine signaling from astrocytes, pericytes and interneurons regulate the blood brain barrier (adapted from Abbot NJ *et al*. 2006).

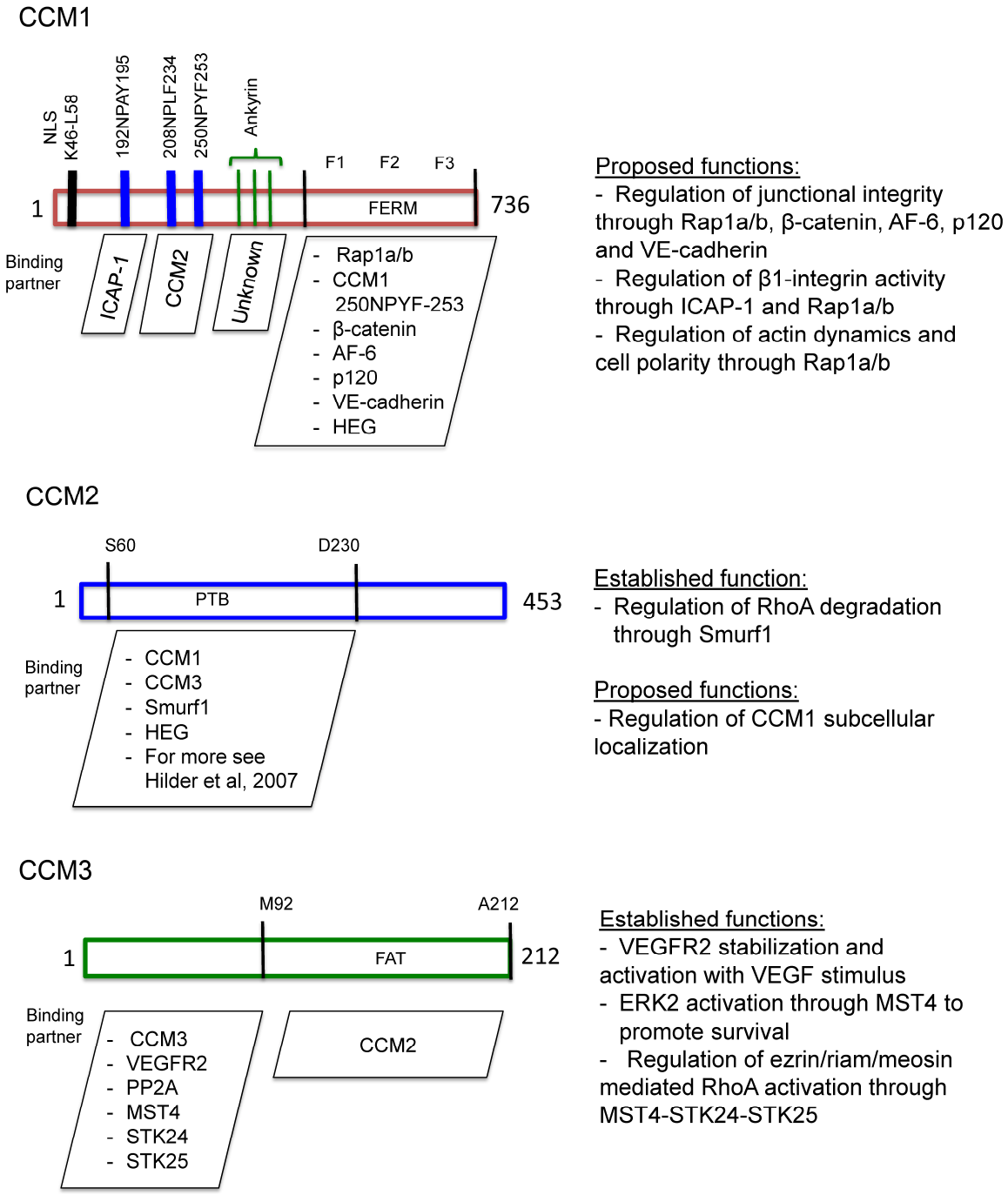

Figure 1.2: The known structure function relationships for CCM1, 2 and 3. All three proteins lack catalytic domains suggesting an adaptor-like function for the CCM1/2/3 complex. Underneath each binding domain are listed known binding partners. The established or proposed function of binding interactions is listed on the right.

CHAPTER II

MATERIALS AND METHODS

Methods employed in Chapter III

Cell Culture

MEECs were maintained in Dulbecco's Modified Eagle medium (DMEM, Gibco)/3% fetal bovine serum (FBS, Invitrogen)/1% penicillin/streptomycin (pen-strep, Invitrogen). HEK 293T and COS-7 cells were maintained in DMEM/10% FBS/1% pen-strep.

shRNA knockdown and addback cell lines

For knockdown of CCM2 in MEECs two different shRNA sequences (labeled shRNA#3 and shRNA#4) were used. Clone pLKO.1 shRNA moCCM2 TRCN# RMM3981-99230368 (Open Biosystems) was labeled shRNA #3 and clone TRCN# RMM3981-99230200 was labeled shRNA#4. To prepare shRNA lentivirus an 80% confluent 10cm plate of HEK293T cells were transfected with lentiviral cDNA and the packaging vectors pMDG.2 and pax2 in a ratio of 2:1:2 using Lipofectamine Reagent (Invitrogen). The virus-loaded media from the cells was collected 24 and 48 hrs post-transfection and filtered through a 0.48um filter. Virus media was mixed with 1.5ug/ml Sequabrene (Sigma) and placed on top of the endothelial cells. Forty-eight

hours later the media on the endothelial cells was replaced with standard cell media supplemented with 4ug/ml Puromycin (Promega) to select for cells infected with the puromycin-encoding pLKO shRNA vector. Knockdown was assessed using QRT-PCR.

For addback of wildtype and nuclear export deficient CCM2, the retroviral vector pLNCx2 was used. To prevent knockdown of wildtype CCM2 once added back to MEECs with shRNA from CCM2, the sequence for CCM2 was mutated at the six independent residues recognized by shRNA#3. The mutations altered the codon but not amino acid sequence of CCM2. The CCM2 sequence recognized by shRNA #3 is 430WDRMISDISSDIEALGCSMDQDSA453. For addback of wildtype CCM2, the codon sequence for the following residues was changed as follows: Iso434 ATT to ATA, Iso437 ATC to ATA, Ser438 AGT to TCA, Iso441 ATT to ATA, Leu444 CTA to TTG, and Ser447 AGC to TCA. The nuclear export sequence of CCM2 is encoded between Iso434 and M448 and the nuclear export deficient CCM2 sequence contains Alanine substitutions at Iso434, Iso437, Iso441 and Leu444 which provide sufficient mismatch with the target sequence of shRNA#3 and the nuclear export deficient CCM2 was predicted to be resistant to shRNA #3-targeted degradation without further codon substitutions. Codon-substituted Yellow fluorescent Protein for energy transfer (YPet)-CCM2 and nuclear export deficient YPet-CCM2 were cloned into pLNCx2 using HindIII and NotI. The HindIII site between YPet and CCM2 was mutationally ablated prior to cloning into pLNCx2. To generate pLNCx2 retrovirus, pLNCx2 DNA was transiently transfected in HEK 293 Phoenix cells which already encode the packaging vectors for retroviral infection of

mouse cells. Virus was collected as described above for lentiviral virus production. pLNCx2 positive cells were selected with FACS sorting for the YPet fluorescent marker.

Plasmids

Full-length CCM1, 2 and 3 were fused N-terminally with YPet or Cyan Protein for energy transfer (CyPet) by cloning into the mammalian expression vectors pYPet-C1 and pCyPet-C1 (Clontech). Rev1.4-YFP was obtained courtesy of Dr. Beric Henderson, Westmead Millenium Institute, Switzerland.

Cell transfection

MEECs were transfected with Amaxa Nucleofector electroporation using 1x10^6 cells and 1ug DNA in 100ul suspension in the 'MEF electroporation solution' from Amaxa and electroporation program M37. Cells were immediately plated in full serum media at the needed concentration.

Leptomycin B nuclear export assay and cell fixation

Glass coverslips were coated with 0.0005% Fibronectin/PBS (Sigma) for 1hr at 37C in a 6-well dish. 50,000 cells were seeded in each well and allowed to adhere overnight. Cells were treated with 2ug/ml of Leptomycin B for 1-3hr prior to imaging as indicated. The media was aspirated and without washing the cells were fixed in 3% paraformaldehyde/PBS for 20min. The cells were washed three times for 5min with PBS with gentle rocking. Cells were mounted in 90%glycerol/10% 1M Tris pH 8.5 and imaged on a Zeiss Axiovert 200M microscope.

Rev1.4 nuclear export assay

One microgram of Rev1.4-eYFP DNA was transfected in 50,000 COS-7 cells using Lipofectamine 2000 (Invitrogen) using the recommended protocol from the manufacturer. Glass coverslips were coated for 1hr at 37˚C with 1:200 fibronectin/Phosphate Buffered Saline (PBS; Invitrogent) and washed twice with PBS. The transfected cells were seeded onto the coverslips and incubated overnight. Cells were treated with 5μg/ml Actinomycin D (Invitrogen) for 3hrs at 37˚C prior to fixation as described above.

Beta-galactosidase nuclear localization assay

The vectors pHM830 Yellow Fluorescent Protein (YFP)-beta-galactosidase and pHM840 YFP-NLS-beta-galactosidase were obtained from Addgene. Full length CCM2 or CCM2 1-230 and 231-453 were cloned using standard cloning techniques between the NheI and SacII restriction sites. For imaging experiments 0.25 x 10^6 COS7 cells were transiently transfected with 250ng DNA using Lipofectamine 2000 (Invitrogen) and plated on fibronectin coated coverslips. Cells were fixed and imaged 18-24 hours after plating.

Statistical analysis

All statistical analysis was performed using Student's t-test in Excel.

Methods employed in Chapter IV

Cell Culture

MEECs were maintained in Dulbecco's Modified Eagle medium (DMEM, Gibco)/3% fetal bovine serum (FBS, Invitrogen)/1% penicillin/streptomycin (pen-

strep, Invitrogen). HEK 293T and COS-7 cells were maintained in DMEM/10% FBS/1% pen-strep.

Generation of knockdown cell lines

Knockdown of CCM2 in MEECs was achieved with pLKO.1 shRNA moCCM2 TRCN# RMM3981-99230368 (Open Biosystems). To prepare shRNA lentivirus an 80% confluent 10cm plate of HEK293T cells were transfected with lentiviral cDNA and the packaging vectors pMDG.2 and pax2 in a ratio of 2:1:2 using Lipofectamine Reagent (Invitrogen). The virus-loaded media from the cells was collected 24 and 48 hrs post-transfection and filtered through a 0.48um filter. Virus media was mixed with 1.5ug/ml Sequabrene (Sigma) and placed on top of the endothelial cells. Forty-eight hours later the media on the endothelial cells was replaced with standard cell media supplemented with 4ug/ml Puromycin (Promega) to select for cells infected with the puromycin-encoding pLKO shRNA vector. Knockdown was assessed using QRT-PCR.

QRT PCR

Cells were cultured to 70% to 80% confluence in 10cm plates. Total RNA was extracted with RNEasy Plus Kit (Qiagen). Three micrograms of total RNA were converted to cDNA using SMARTer cDNA synthesis kit (Clontech). Standard Real Time PCR reactions were prepared using the manufacturer's recommended TaqMan probes and 2x Universal Master Mix (Applied Biosystems).

RhoA Biosensor

Viral particles of the single chain eYFP-eCFP RhoA biosensor encoded in the adenoviral vector pAd/CMV/V5-GW/*lacZ* were a kind gift from Dr. Klaus Hahn (UNC-

CH). To expand the viral particles the ViraPower Adenoviral Expression System (Invitrogen) was used. Fifty thousand MEECs were plated on 1:200 fibronectin coated coverslips. The following day, cells were infected with 30ul of adenovirus. Cells were imaged 18-24 hours later and images were processed exactly as described(Pertz et al., 2006).

Tube formation assay

A 24-well plate was coated on ice with 300ul of growth-factor reduced matrigel basement membrane (BD Biosciences). The matrigel was allowed to polymerize at 37C for 30min. Each well was seeded with 75,000 cells and the assay was allowed to continue for 18-22hrs at 37C/7% CO2. For drug treatments 10uM Y27632 (Cell Signaling) were added at the time the cells were plated on Matrigel. Cells were fixed with 3% paraformaldehyde/PBS for 20min, washed in PBS, permeabilized in 0.1% Triton X-100/PBS for 1hr, washed with PBS two times and incubated overnight with 1:200 Rhodamine Phalloidin solution at 4C. Cells were washed one time with PBS and imaged with BD Pathway confocal microscope (BD Biosciences). To accommodate for variation in matrigel thickness images were obtained as a multi-layer stack. Images were analyzed with ImageJ software by creating a maximum intensity projection image from the Z-stack command.

Western blotting

Cells were rinsed twice in ice-cold PBS and lysed on ice in 125mM Tris-HCl, pH8, 375mM NaCl, 25mM $MgCl_2$, 2.5mM EDTA, 2.5% Triton X-100 supplemented with NaF, sodium orthovanadate, aprotinin and PMSF (all from Sigma). Protein concentration was quantitated with a Bradford assay. For total RhoA blots were

probed with mouse anti-RhoA (26C4, 1/1000) from Santa Cruz Biotechnologies, for phosphomyosin light chain blots were probed with rabbit anti-phosphoMLC2 (3671, 1/1000) from Cell Signaling and for phosphor-coffilin (3313, 1/3000), Cell Signaling.

3D force microscopy (3DFM)Magnetic Twisting Cytometry

3DFM assays were performed as previously described(Guilluy et al., 2011). A 10x10mm cloning cylinder (Sigma) was attached to a glass coverslips using silicone grease. The area within the cloning cylinder was coated in fibronectin (1/100, Sigma). 10x10^5 cells were plated in each cylinder for 80-90% confluency 18-24hrs prior to assaying. 2.8mm tosyl-activated magnetic dynabeads (Invitrogen) were incubated with Tris-free human fibronectin (Invitrogen) for 24hrs at room temperature. Beads were rinsed three times in PBS, sonicated and incubated on cells for 45min. Cell-bound beads were subjected to perpendicular tensile pullforces generated using the UNC 3D Force Microscope as previously described(Tim O'Brien et al., 2008). The poletip was placed 15um above the surface of the glass coverslips with cells. Pullforces were generated at 1V for 5sec in three consecutive pulls with 10sec recovery time at 0V between pulls. Movies of the bead displacement were recorded using a Pulnix high speed video camera (JAI, Ca). The trajectory of the bead movement during each pull was tracked with Video Spot Tracker (Center for Computer Integrated Systems for Microscopy and manipulation, www.cismm.cs.unc.edu). Spring constants were calculated by fitting the bead displacement trajectory and applied force during each pull to Jeffrey's model of viscoelastic fluids.

The force applied at each pull was calculated based on standard curve of the distance traveled by a bead in a viscoelastic fluid of known density when force is applied by a poletip at 15um above the glass coverslip surface.

Statistical analysis

All statistical analysis was performed using Student's t-test in Excel.

Methods employed in Chapter V

Cell Culture

HUVECs (ATCC) were cultured in EBM-2 media (Lonza). MEECs were maintained in Dulbecco's Modified Eagle medium (DMEM, Gibco)/3% fetal bovine serum (FBS, Invitrogen)/1% penicillin/streptomycin (pen-strep, Invitrogen). HEK 293T cells were maintained in DMEM/10% FBS/1% pen-strep.

For knockdown in HUVECs shRNA clones from Open Biosystems were used. To prepare shRNA lentivirus an 80% confluent 10cm plate of HEK293T cells were transfected with lentiviral cDNA and the packaging vectors pMDG.2 and pax2 in a ratio of 2:1:2 using Lipofectamine Reagent (Invitrogen). The virus-loaded media from the cells was collected 24 and 48 hrs post-transfection and filtered through a 0.48um filter. Virus media was mixed with 1.5ug/ml Sequabrene (Sigma) and placed on top of the endothelial cells. Forty-eight hours later the media on the endothelial cells was replaced with standard cell media supplemented with 4ug/ml Puromycin (Promega) to select for cells infected with the puromycin-encoding pLKO shRNA vector. Knockdown HUVECs were cultured for minimum of 72hrs post initial exposure to puromycin prior to assaying. Knockdown was assessed using QRT-PCR.

QRT PCR

Cells were cultured to 70% to 80% confluence in 10cm plates. Total RNA was extracted with RNEasy Plus Kit (Qiagen). Three micrograms of total RNA were converted to cDNA using SMARTer cDNA synthesis kit (Clontech). Standard Real Time PCR reactions were prepared using the manufacturer's recommended TaqMan probes (CCM1 HS00184988_m1, CCM2 HS00230191_m1, CCM3 HS00200578_m1, Arap3 Hs01078405_m1) and 2x Universal Master Mix (Applied Biosystems).

RhoA and Rap1 pulldowns

For all pulldowns cells were grown to 70-80% confluency and lysed as for Western blotting. Where indicated cells were treated with 5uM Forskolin/DMSO (Calbiochem) for 3hrs or 18-22hrs. Pulldowns were performed as described previously (Wittchen, 2008) with modifications as described below.

Pulldowns for active RhoA were performed with mouse anti-GTP-RhoA from New East Biosciences. For each sample, 1ul of the antibody was coupled to 60ul of 50/50 bead slurry of Sepharose-G beads (GE Healthcare). Pulldowns for active Rap1 were performed using the purified and Glutathione S-transferase (GST)-tagged Rap1-binding domain RalGDS coupled to Glutathione Sepharose 4G beads (GE Healthcare). RalGDS-GST transformed bacteria were a kind gift from Dr. Keith Burridge (UNC-CH). RalGDS beads were prepared as described(Wittchen, 2008).

Following incubation with anti-GTP-RhoA-coupled beads, cell lysates were incubated with RalGDS-coupled beads. To demonstrate that pulldowns were performed from equal amount of total protein across all samples 50ug of total protein

was removed from each sample before the sample was loaded onto the anti-GTP-RhoA-coupled beads. The removed aliquots were separated on western blot and blotted for total RhoA or Rap1 and total ERK1/2.

Tube formation assay

A 24-well plate was coated on ice with 300ul of growth-factor reduced matrigel basement membrane (BD Biosciences). The matrigel was allowed to polymerize at 37C for 30min. Each well was seeded with 75,000 cells and the assay was allowed to continue for 18-22hrs at 37C/7% CO2. For drug treatments 5uM Forskolin/DMSO (Calbiochem), 200uM 8-(4-chlorophenylthio)-cAMP/MeOH (C010, Biolog) or 200uM N6-Benzoyl-cAMP/DMEM (B009, Biolog) were added at the time the cells were plated on Matrigel. Cells were fixed with 3% paraformaldehyde/PBS for 20min, washed in PBS, permeabilized in 0.1% Triton X-100/PBS for 1hr, washed with PBS two times and incubated overnight with 1:200 Rhodamine Phalloidin solution at 4C. Cells were washed one time with PBS and imaged with BD Pathway confocal microscope (BD Biosciences). To accommodate for variation in matrigel thickness images were obtained as a multi-layer stack. Images were analyzed with ImageJ software by creating a maximum intensity projection image from the Z-stack command.

Western blotting

Cells were rinsed twice in ice-cold PBS and lysed on ice in 125mM Tris-HCl, pH8, 375mM NaCl, 25mM $MgCl_2$, 2.5mM EDTA, 2.5% Triton X-100 supplemented with NaF, sodium orthovanadate, aprotinin and PMSF (all from Sigma). Protein concentration was quantitated with a Bradford assay. For total or active RhoA blots

were probed with mouse anti-RhoA (26C4, 1/500) from Santa Cruz Biotechnologies. For total or active Rap1 blots used was mouse anti-Rap1 from BD Biosciences (1/1000). Rabbit anti-ERK 1/2 (C-14, 1/10000) was from Santa Cruz Biotechnologies.

Statistical analysis

All statistical analysis was performed using Student's t-test in Excel.

CHAPTER III

THE ROLE OF THE SUBCELLULAR LOCALIZATION OF CCM2 IN REGULATION OF THE NUCLEOCYTOPLASMIC DISTRIBUTION OF CCM1 AND ENDOTHELIAL CELL FUNCTION

Introduction

Cerebral Cavernous Malformations is caused by loss of function mutations in *ccm1*, *ccm2*, and *ccm3* in endothelial cells. CCM1, 2 and 3 form a ternary complex (CCM complex) dependent on a functional PTB within CCM2. The *ccm2* point mutation L198 identified from patients occurs within the PTB domain and disrupts formation of the CCM complex (Zawistowski, 2005; Zheng et al., 2010a; Kleaveland et al., 2009b). In addition to mediating the formation of the CCM complex, the CCM2 PTB domain regulates the localization of CCM1. YFP-CCM1 localizes to the nucleus when overexpressed alone in the monkey kidney fibroblast cells Cos7. Co-expression with wildtype but not a PTB mutated CCM2 redistributes CCM1 to the cytoplasm, suggesting that the nucleocytoplasmic distribution of CCM1 is regulated by binding with CCM2 (Zawistowski, 2005). The particular mechanism that governs this redistribution has not been defined. Change in subcellular localization is a common mechanism for the regulation of protein activity. Thus defining the mechanism through which CCM2 regulates the nucleocytoplasmic distribution of

CCM1 can provide evidence for the yet undefined mechanism for the regulation of CCM protein activity. We hypothesized that by exchanging between the cytoplasm and nucleus, CCM2 exports CCM1 from the nucleus.

Exchange of molecules between the cytoplasm and nucleus occurs across the nuclear pore complex embedded within the nuclear envelope. Proteins smaller than 25kD utilize passive diffusion, whereas proteins larger than 25kD utilize facilitated diffusion. Proteins targeted for the nucleus encode a nuclear localization sequence (NLS) which is a 5-10 residue stretch of consecutive positively charged amino acids, Argenine (R), Histidine (H), Lysine (K). The sequence is recognized by the nuclear pore machinery and facilitates import into the nucleus (Mekhail et al., 2007; Leung, 2003). Nuclear export is facilitated by recognition of a nuclear export sequence (NES) which has the canonical sequence of $LeuX_{1-3}$ $LeuX_{2-3}$ LeuXLeu, where X can be any amino acid and the Leucine can be substituted with other hydrophobic residues such as Isoleucine and Valine (Henderson and Percipalle, 1997). The particular nuclear localization or nuclear export sequence can directly regulate the relative distribution of a protein with both a NLS and a NES (Henderson, 2000; Li, 2006; Bhattacharya, 2003). A greater the number of positively charged residues within a NLS or hydrophobic residues within a NES results in a ‘stronger’ nuclear import or nuclear export signal (Henderson and Percipalle, 1997). Thus the steady-state localization of a protein with a strong NLS but weak NES can be predicted to be in the nucleus, whereas the steady-state localization of a protein with a weak NLS and a strong NES would be in the cytoplasm. The nuclear import and export of proteins is further regulated by binding partners which may mask the NLS

or NES, or themselves encode a NLS or NES, and by posttranslational modifications that induce conformational changes to expose or conceal a NLS or NES (Henderson, 2000; Thompson, 2005; Casar et al., 2007; Costa et al., 2006; Trotman et al., 2007).

Here, we report that the total CCM2 population within a cell exchanges between the cytoplasm and nucleus. We identify a functional NES at the C-terminus of CCM2. The majority of identified patient mutations in CCM2 lead to premature truncations and the truncated species are thus predicted to lack the NES. We failed to define a nuclear localization sequence in the primary structure of the protein. When CCM1 was co-expressed with the nuclear export deficient CCM2, CCM1 was equally distributed between the cytoplasm and nucleus, suggesting that CCM2 regulates the localization of CCM1 by both exporting CCM1 from the nucleus and by blocking the nuclear import of CCM1 likely by blocking the nuclear localization sequence of CCM1. We show that endothelial cells in which endogenous CCM2 expression has been silenced through shRNA but which express the nuclear export deficient CCM2 fail to self-assemble into vascular lumen-like structures *in vitro*. These data suggest that the partial population of CCM1 and nuclear export deficient CCM2 that remain in cytoplasm is insufficient to maintain endothelial cell functions or fails to function properly due to the absence of a binding partner that the CCM1-CCM2 complex deliver from the nucleus or due to lack of a post-translation modification that the CCM1-CCM2 complex acquire in the nucleus.

Results

CCM2 translocates between the cytoplasm and nucleus

Based on the finding that co-expression with CCM2 leads to the re-distribution of CCM1 from the nucleus to the cytoplasm in the fibroblast cells COS7, we hypothesized that CCM2 is a nucleocytoplasmic shuttle for CCM1. First we defined the subcellular localization of CCM1 and CCM2 when expressed alone or together in endothelial cells. When overexpressed alone YPet-CCM1 or YPet-CCM2 in wildtype MEECs, CCM1 localizes strongly to the nucleus and CCM2 localizes almost exclusively to the cytoplasm. When the two proteins are co-expressed CCM1 co-localizes strongly with CCM2 in the cytoplasm (Figure 3.1).

To define whether CCM2 exchanges between the cytoplasm and nucleus of endothelial cells YPet-CCM2 transfected MEECs were treated with the small molecule Leptomycin B which inhibits nuclear export by blocking the target recognition site of the CRM1 protein from the nuclear export machinery(Henderson, 2000; Henderson and Percipalle, 1997). If Ypet-CCM2 translocates between the cytoplasm and nucleus, then treatment with Leptomycin B is expected to result in the accumulation of YPet-CCM2 in the nucleus. In a timecourse treatment with Leptomycin B the nuclear population of YPet-CCM2 steadily increases, with the majority of YPet-CCM2 becoming trapped inside the nucleus by 3hrs after drug treatment (Figure 3.2). These findings indicate that CCM2 continuously translocates between the cytoplasm and nucleus. While localization studies are best performed on the endogenous protein population as overexpression can disrupt the stoichiometry of the endogenous rate of exchange between the cytoplasmic and

nuclear populations, the lack of an immunofluorescence grade antibody for endogenous CCM2 precludes such studies.

CCM2 encodes a functional nuclear export sequence

In order to define the role of CCM2 in the nucleocytoplasmic localization of CCM1, we first needed to define a method to disrupt the nucleocytoplasmic translocation of CCM2. Drugs such as Leptomycin B that inhibit the nuclear export machinery would produce insufficiently specific results as the drug will inhibit the nuclear export of CCM2 and all other proteins that exchange between the nucleus and cytoplasm. The primary sequence of CCM2 contains thirteen putative NESs (Figure 3.3). To define which of these are functional we utilized a nuclear export assay in which the Human Immunodeficiency Viral envelope protein Rev is fused with a putative NES and YFP (Henderson, 2000; Henderson and Percipalle, 1997). The assay has been successfully used by several independent groups (Rodriguez et al., 2004; Bhattacharya, 2003; Li, 2006). The wildtype Rev protein encodes both a NLS and a NES and consistent with published reports(Henderson and Percipalle, 1997) appears in the cytoplasm and nucleoli when transfected in cells (Figure 3.4A*i* and *ii*). The nucleoli accumulation of Rev is due to its binding to newly translated ribosomal mRNA. The RNA polymerase inhibitor Actinomycin D depletes the ribosomal mRNA pool, and the nuclear binding partners of Rev(Henderson, 2000)'(Henderson and Percipalle, 1997). When cells transfected with Rev-YFP are treated with Actinomycin D, Rev-YFP that enters the nucleus fails to becomes sequestered by binding with ribosomal mRNA, the nucleoli localization of Rev-YFP is lost and Rev-YFP appears cytoplasmic (Figure 3.4A *iii* and *iv*). To validate that

Actinomycin D only prevents the retention of Rev-YFP in the nucleus and does not inhibit the nuclear import of Rev-YFP and to validate the presence of a functional nuclear export sequence in Rev-YFP, cells transfected with Rev-YFP were treated with Leptomycin B (Figure 3.4B). Under these conditions, Rev-YFP accumulates in the nucleus consistent with the presence of a functional NLS and nuclear export dependent on a NES recognized by the nuclear export complex. Importantly, Rev-YFP does not localize in the nucleoli indicating that the nuclear population is a result of the inhibited nuclear export of Rev-YFP rather than its retention in nucleoli.

A mutated species of Rev, referred to as Rev1.4, contains point mutations within the NES to disrupt its nuclear export capacity. Rev1.4-YFP alone localizes exclusively in the nucleoli (Figure 3.4C*i* and *ii*). Fusion of Rev1.4-YFP with a previously defined functional NES such as that from the Protein Kinase Inhibitor protein (PKI; NSNE**L**A**L**K**L**AG**L**D**I**NKTE) leads to the export of the chimera, named Rev1.4-YFP-PKI (NES), from the nucleus to the cytoplasm (Figure 3.4D). It is well established that nuclear localization and nuclear export sequences vary in 'strength,' i.e. the extent to which they can redirect subcellular localization (Henderson, 2000; Henderson and Percipalle, 1997). This strength is imparted by the number of basic or hydrophobic residues within the NLS or NES respectively. The primary sequence alone is sufficient to predict the relative strength of two nuclear localization or two nuclear export sequences, however the primary sequence alone is not sufficient to predict the relative strength between a nuclear localization and nuclear export sequence. The relative strength of a nuclear localization and export sequences within a protein is defined by the subcellular localization of the protein at steady

state(Henderson, 2000; Henderson and Percipalle, 1997). As exemplified by the strongly cytoplasmic localization of wildtype Rev or Rev1.4-YFP-PKI (NES), a protein can appear cytoplasmic despite the presence of a functional NLS(Henderson, 2000; Henderson and Percipalle, 1997). To reduce the accumulation of false positive fluorescent signal in the cytoplasm due to newly translated protein, cells were treated with the translation inhibitor cyclohexamide. The molecular role of Rev is to export newly transcribed ribosomal mRNA from the nucleus to the cytoplasm (Henderson and Percipalle, 1997). The relative abundance of Rev in the nucleus or cytoplasm is dynamically regulated by the overall abundance of ribosomal mRNA. Consistent with this function, wildtype Rev appears both in the cytoplasm and nucleoli (Figure 3.4A*i* and *ii*). Using Rev1.4-YFP as an assay for the nuclear export capacity of putative sequences can produce false negative outcomes if the putative nuclear export sequence tested is 'weaker' relative to the NLS in Rev1.4 and the Rev1.4-YFP-NES chimera appears in the nucleoli similarly to the control Rev1.4-YFP(Henderson, 2000; Henderson and Percipalle, 1997). Addition of Actinomycin D reduces the nucleoli localization of Rev-YFP (Figure 3.4A *iii* and *iv*) as the native NES exports the protein from the nucleus. In the absence of a functional NES, Rev1.4-YFP remains in the nucleoli (Figure 3.4C*i* and *ii*). Actinomycin D treatment was used in all subsequent assays for putative nuclear export sequences as indicated.

To define whether CCM2 encodes a functional NES, full length CCM2 (1-453) was fused with Rev1.4-YFP and the chimera was transfected in COS7 cells. Rev1.4-YFP-CCM2 (1-453) localizes in the nucleoli and cytoplasm similarly to wildtype Rev-

YFP and Rev1.4-YFP-PKI (NES) indicating that CCM2 encodes a functional NES (Figure 3.5A*i*). Furthermore, the nucleoli population of Rev1.4-YFP-CCM2 (1-453) is depleted upon the addition of Actinomycin D (Figure 3.5A*ii*).

To narrow down the portion of CCM2 that encodes the NES and to define whether CCM2 encodes a single or multiple functional nuclear export sequences, the N and C terminus of CCM2 were separately tested for nuclear export capacity. The N terminus was defined as residues 1-230 and the C terminus was defined as residues 231-453. The N terminus failed to relocalize Rev1.4-YFP to the cytoplasm even in the presence of Actinomycin D (Figure 3.5B), indicating that the N terminus does not encode a nuclear export sequence. The chimera encoding the C terminus relocalizes to the cytoplasm when cells are treated with Actinomycin D (Figure 3.5C), suggesting that the NES of CCM2 is encoded between residues 231-453. The C terminus was further truncated and each serial truncation was fused with Rev1.4-YFP and tested for nuclear export capacity (Figure 3.6). The sequence 428DEWDRMISDISSDIEALGCSMDQDSA453 was found to be sufficient to export the Rev1.4-YFP chimera to the cytoplasm (Figure 3.6). The consensus sequence for a nuclear export sequence is $Lx_{1-3}Lx_{2-3}LxL$, where the leucine can be substituted by a valine or isoleucine(Mekhail et al., 2007). Within the sequence D428 to A453, the sequence 433M**I**SD**I**SSD**I**EA**L**444 most closely matches the consensus sequence for a NES and a peptide with this sequence was fused with Rev1.4-YFP. This sequence was sufficient to cause the cytoplasmic localization of Rev1.4-YFP in the presence of Actinomycin D (Figure 3.6) demonstrating that it has nuclear export capacity. The nuclear export sequence is within the last 20 residues of the C

terminus of CCM2 and the majority of CCM2 mutations lead to premature truncation of the protein, which would lead to the loss of the nuclear export sequence.

To define whether 433M**I**SD**I**SSD**I**EA**L**444 is a functional nuclear export sequence in CCM2, Iso434, Iso437, Iso441 and Leu444 in full length YPet-CCM2 were simultaneously mutated to alanine (YFP-CCM2-NESm). The construct was transiently expressed in MEECs and its subcellular localization was examined by fluorescent microscopy. YPet-CCM2-NESm accumulated in the nucleus similarly to the extent of YPet-CCM2 accumulation observed when cells are treated with the nuclear export inhibitor Leptomycin B (Figure 3.7A). Furthermore, point mutations of as few as two of the isoleucine residues are sufficient to disrupt the nuclear export of CCM2 (Figure 3.7B). This suggests that if loss of the nuclear export function of CCM2 is important for CCM pathogenesis, a nuclear export defect occurs with mutation of just two of the four residues required for export.

CCM2 mediates the nuclear export of CCM1 and blocks its nuclear import

To define the role of the dynamic nucleocytoplasmic translocation of CCM2 in the assembly of the CCM complex, wildtype CCM2 (CCM2wt) or CCM2 with mutationally inactivated nuclear export sequence (CCM2-NESm) was conjugated to the blue fluorescent protein CyPet and transiently co-expressed with YPet-CCM1 in MEECs. When expressed alone CCM1 localizes almost completely in the nucleus (Figure 3.8). While co-expression of wildtype CCM2 with CCM1 leads to the redistribution of CCM1 from the nucleus to the cytoplasm, co-expression with CCM2-NESm results in an almost equal distribution of CCM1 between the nucleus and cytoplasm (Figure 3.8). These results suggest that the nuclear export of CCM1 is

regulated by the nuclear export sequence of CCM2. While a molecular function for the CCM1-CCM2 interaction in the cytoplasm and nucleus is not currently known, the patient mutation L198R in CCM2 disrupts the formation of the CCM1-CCM2 complex (Zawistowski, 2005; Liu et al., 2011), indicating that the interaction is required for endothelial cell function. The data presented here are consistent with a molecular role of CCM2 in the regulation of the subcellular localization of CCM1 and regulation of the assembly of the CCM1-CCM2 complex at the differential subcellular localizations.

To define whether the CCM1 population that remains in the cytoplasm is retained by the cytosolic fraction of CCM2-NESm, or due to a CCM2-independent binding partner or posttranslational modification, the subcellular localization of CCM1 was defined when CCM2 was genetically targeted to the nucleus. Two canonical nuclear localization sequences were fused with CyPet-CCM2-NESm (CyPet-CCM2-NESm-NLS-NLS) and the protein was transiently co-expressed with YPet-CCM1 in Cos7 cells. Both CCM1 and CCM2-NESm-NLS-NLS appear entirely in the nucleus (Figure 3.8C), suggesting that the cytosolic fraction of CCM1 observed when the nuclear export of CCM2 is disrupted is due to the CCM2-NESm remaining in the cytoplasm. Previous findings using mass spectrometry and immunoprecipitation (Hilder et al., 2007) have shown that CCM1 and CCM2 form a complex, however these studies could not provide evidence for what proportion of the protein population exists in a complex or remains unbound by a CCM partner. Our finding that the subcellular localization of CCM1 duplicates that of CCM2 when the subcellular localization of CCM2 is genetically manipulated suggests that the

subcellular localization of CCM1 is regulated by CCM2. These data also validate the existence of the CCM1-CCM2 complex and provide strong evidence that the majority of the CCM1 and CCM2 populations exist as part of the CCM complex.

The nuclear import of CCM2 is not mediated by a nuclear localization sequence encoded in the primary sequence

Our findings defined that CCM2 regulates the subcellular localization of CCM1 however the mechanism through which the nuclear import of CCM2 is mediated remains unknown. To define whether CCM2 encodes a nuclear localization sequence the protein was threaded in the NucPred program (Brameier et al., 2007). The program scans the primary sequence for consecutively positively charged residues. The program failed to identify a nuclear localization sequence within a 37% margin of error (Figure 3.10).

CCM2 contains three regions with several positively charged residues that appear in close proximity in the primary sequence. These are K6, K7, K9, K10 and K23, K26, R28, K29, K30, H32, K34, K38, K39 and 396RHRR399 (Figure 3.10). To define the role of these residues in the nuclear import of CCM2, the residues 2-40 were deleted and 396RHRR399 was independently mutationally modified to 396AHAA399. Each of these two CCM2 variants were independently expressed in endothelial cells and the cells were treated with the nuclear import inhibitor Leptomycin B. CCM2 lacking residues 2-40 and CCM2 396AHAA399 accumulated in the nucleus similarly to wildtype CCM2 (Figure 3.11 and 3.12). These results indicate that none of the three Lys, Arg, His-rich regions are functional nuclear import sequences for CCM2.

As an independent assay for putative nuclear localization sequences we used a nuclear localization assay based on the beta-galactosidase enzyme. The assay is designed similarly to the Rev1.4 nuclear export assay (Sorg and Stamminger, 1999). Proteins smaller than 50kD migrate across the nuclear pore by passive diffusion. Proteins larger than 50kD require a nuclear localization sequence to be actively imported into the nucleus (Mekhail et al., 2007; Lange et al., 2006' Leung, 2003). The molecular weight of CCM2 is ~54kD. When the beta-galactosidase protein, which has a molecular weight of 116kD, is fused with YFP (molecular weight of 25kD) the resultant chimera (labeled YFP-b-gal) localizes exclusively in the cytoplasm (Figure 3.13A). When a nuclear localization sequence PKKKRKV from the SV-40 large T antigen is inserted between YFP and beta-gal, the chimera redistributes strongly to the nucleus (Figure 3.13B) in agreement with previous citations of the assay (Sorg and Stamminger, 1999). Insertion of wildtype full length CCM2 between YFP and beta-gal results in the complete cytoplasm localization of the chimera (Figure 3.13C) similarly to YPet-CCM2 (Figure 3.1). However, when fused with the nuclear export deficient CCM2-NESm the YFP-b-gal chimera become strongly nuclear (Figure 3.13D), suggesting that CCM2 encodes a NLS or binds a partner with a functional NLS. CCM2-NESm was truncated in half as for the Rev1.4 assay and the halves were fused with YFP-b-gal. Neither the N (defined as residues 1-230) nor the C terminus of CCM2-NESm (230-453) was sufficient to import the YFP-b-gal chimera (Figure 3.14). These results suggest that CCM2 does not encode a nuclear localization sequence but that the protein may be imported into the nucleus by a binding partner.

To experimentally define whether CCM2 is imported into the nucleus by a binding partner that binds to the PTB domain, the phosphotyrosine binding domain of CCM2 was disrupted by a point mutation of F217A. The mutation has been previously validated by mass spectrometry and immunoprecipitation assays to severely abrogate the interactions of CCM2 and its known binding partners (Hilder et al., 2007). The nuclear import capacity of YPet-CCM2 F217A was defined by a transient transfection in endothelial cells followed by treatment with the nuclear export inhibitor Leptomycin B. The F217A CCM2 accumulates in the nucleus similarly to wildtype CCM2 (Figure 3.15) suggesting the nuclear import of CCM2 is not mediated by a binding partner that utilizes the PTB domain to associate with CCM2. Using mass spectrometry over ten different CCM2 binding partners have been identified whose binding is only partially disrupted by the F217A mutation (Hilder et al., 2007).

Endothelial cell self-assembly into tube-like structures is disrupted by inhibition of the nuclear export of CCM2

To define the functional significance of the nucleocytoplasmic translocation of CCM2 we used an *in vitro* assay for endothelial cell self-assembly in lumen-like tubes on a three-dimensional collagen matrix. The expression of endogenous CCM2 was silenced in endothelial cells by shRNA and the nuclear export deficient variant of CCM2 was stably expressed. The cells were allowed to self-assemble into lumen-like tubes. Loss of CCM2 impairs the formation of lumen-like tubes, whereas addback of wildtype CCM2 rescues tube formation. Addback of CCM2-NESm fails to

rescue tube formation suggesting that it is the cytoplasmic localization of CCM2 that is important for CCM2-regulated tube formation (Figure 3.16).

Discussion

The discovery of a complex between CCM1, 2 and 3 and the identification of a patient mutation in CCM2 (L198R) which disrupts its binding with CCM1 and 3 suggests that the formation of the CCM1-2-3 complex is essential for the function of CCM1, 2 and 3. The molecular events which govern the formation of the CCM1-2-3 complex however remain unknown. Based on previous findings that the nucleocytoplasmic distribution of CCM1 is altered upon co-expression with CCM2 (Zawistowski, 2005), we hypothesized that the nucleocytoplasmic translocation of CCM2 regulates the formation of the CCM1-2 complex.

To this effect we first defined that CCM2 can localize in the nucleus by treating CCM2-transfected cells with Leptomycin B, a drug that inhibits the nuclear export machinery. The accumulation of CCM2 in the nucleus of drug-treated cells demonstrated that CCM2 can localize to the nucleus. Furthermore, the finding suggested that the rate at which CCM2 exchanges between the nucleus and cytoplasm is rapid and biased toward a cytoplasmic localization as CCM2 is found almost entirely in the cytoplasm of quiescent cells.

The nucleocytoplasmic exchange of proteins is governed by nuclear export and nuclear localization sequences. These are a consecutive stretch of hydrophobic or basic residues respectively, which are encoded in the primary sequence of the translocating protein or that of a binding partner(Lange et al., 2006; Mekhail et al., 2007; Chuderland et al., 2008). In order to define the role of CCM2 in the

nucleocytoplasmic distribution of CCM1, a method to manipulate the nucleocytoplasmic distribution of CCM2 was necessary.

Using a Rev1.4 nuclear export assay we identified a functional nuclear export sequence in CCM2 within residues Iso434, Iso437, Iso441 and Leu444. Alanine substitutions at these residues in full length CCM2 lead to the strong nuclear localization of CCM2, suggesting that the protein becomes ‘trapped’ inside the nucleus in the absence of a functional nuclear export sequence. The nuclear export sequence of CCM2 occurs in the final 30 amino acids of the C-terminal tail of the protein and outside the single-encoded domain within CCM2, a phosphotyrosine binding domain. The vast majority of patient mutations lead to premature truncation of the protein which would lead to the deletion of the nuclear export sequence located at the very C-terminus.

To define the role of CCM2 in the subcellular distribution of CCM1, nuclear export deficient CCM2 was co-expressed with CCM1. Previous observations had demonstrated that the subcellular distribution of CCM1 shifts from the nucleus to the cytoplasm when co-expressed with wildtype but not F217A CCM2 suggesting that CCM2 either inhibits the nuclear import of CCM1 by blocking the nuclear localization sequence in CCM1 (Zawistowski, 2005) or serves to export CCM1 from the nucleus. Our current findings showed that CCM1 completely overlaps the nuclear localization of nuclear export deficient CCM2. Despite the nuclear export mutation of CCM2, a small portion of CCM2-NESm remains in the cytoplasm. A portion of CCM1 is also observed in the cytoplasm of CCM2-NESm cells. To define whether this cytoplasmic population of CCM1 and 2 exists in a complex or is due to newly translated protein,

CCM2-NESm was tagged with two copies of the nuclear localization sequence from PKI. The nuclear localization sequences are expected to target CCM2 to the nucleus regardless of the endogenous factors that regulate the nuclear import of CCM2. CCM2-NESm-NLS-NLS localizes exclusively in the nucleus together with CCM1, suggesting that the nuclear import of CCM1 is regulated by CCM2 possibly through the import of the CCM1-CCM2 complex. These findings suggest that CCM1 is imported and exported from the nucleus as a complex with CCM2.

We used the beta-galactosidase assay to test for a nuclear localization sequence within CCM2 (Sorg and Stamminger, 1999). When CCM2 is truncated in two, neither half targets the beta-gal chimera to the nucleus suggesting that the nuclear import of CCM2 is not governed by a nuclear localization encoded in the primary sequence of the protein. We also demonstrate that the nuclear import of CCM2 is not mediated by a binding partner dependent on F217 in the phosphotyrosine binding domain. However the F217A mutation in CCM2 does not fully disrupt the binding of CCM2 with every one of its binding partners, suggesting that the nuclear import of CCM2 may be mediated by a binding partner not dependent on F217. Alternatively, the nuclear import of CCM2 may be mediated by a nuclear localization sequence created by the three dimensional fold of the protein rather that a sequence encoded in the primary sequence. The nuclear import of proteins is still poorly understood with the alpha and beta importins as the primary known proteins to recognize primary sequence basic residues. However multiple proteins have been shown to be imported into the nucleus in a manner independent

of alpha and beta importin (Lange et al., 2006) suggesting that other nuclear import machinery exists.

Finally, we show that the molecular function of the nucleocytoplasmic translocation of CCM2, in addition to regulating the subcellular localization of CCM1 and thus the CCM1-2 complex, is to regulate the self-assembly of endothelial cells in lumen-like tube structures *in vitro*. Consistent with the disease phenotype, shRNA-mediated deletion of CCM2 in endothelial cells impair their ability to self-assemble into tubes. Addback of the wildtype but not nuclear export deficient CCM2 rescues this defect, suggesting that the cytoplasmic localization of CCM2 is required for CCM2-regulated tube formation and that the nuclear localization of CCM2 is not sufficient to drive tube formation in endothelial cells.

Overall, our findings report for the first time the exact nuclear export sequence in CCM2, show that CCM2 does not encode a canonical basic-residue nuclear localization sequence and that the cytoplasmic localization of CCM2 is required for CCM2-driven lumen assembly of endothelial cells.

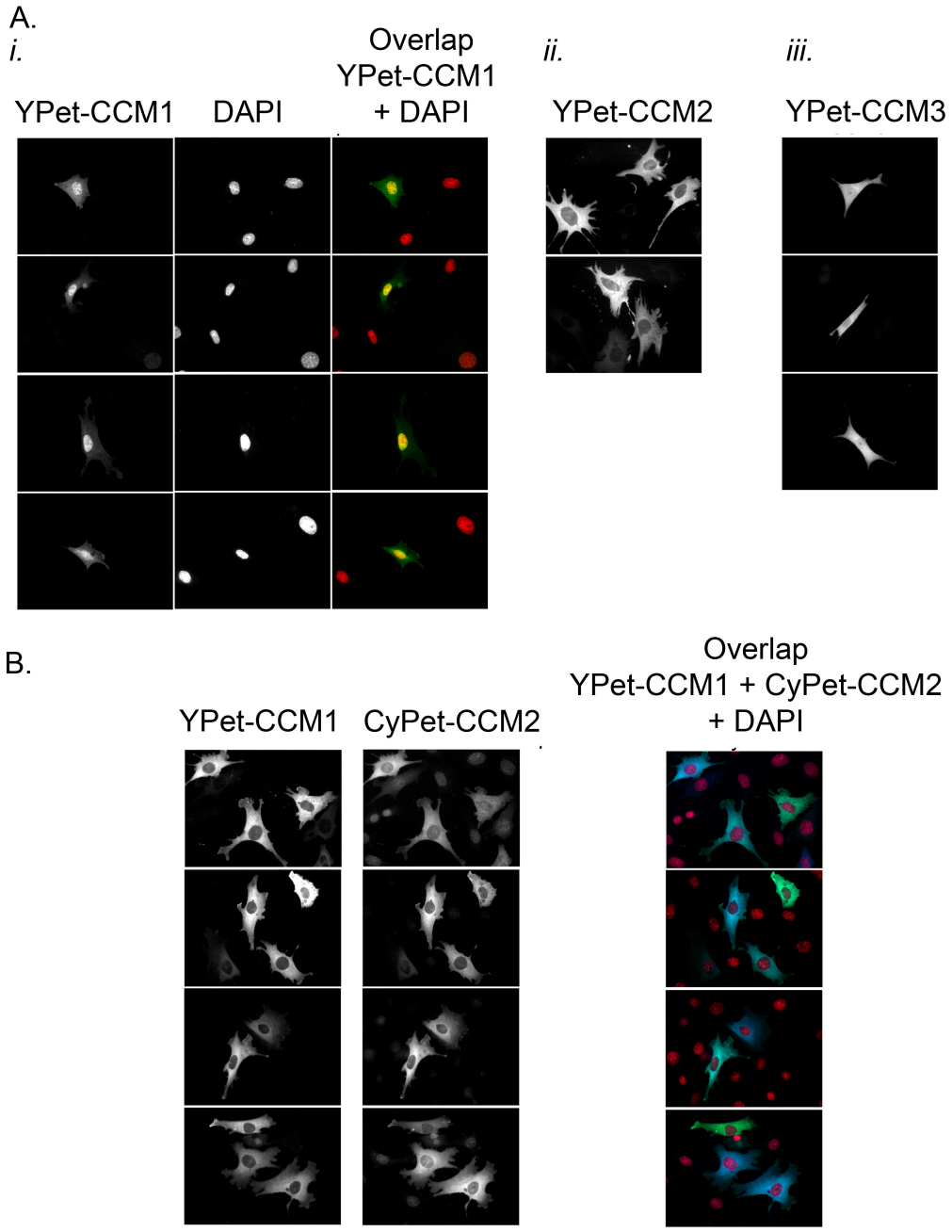

Figure 3.1: The subcellular localization of CCM1 is regulated by CCM2 expression. MEECs were transiently transfected with YPet-tagged CCM1, 2 or 3. CCM1 localizes almost exclusively in the nucleus (Ai; YPet-CCM1 is in green, DAPI staining in red and DAPI demarcates the nucleus), whereas CCM2 localizes in the cytoplasm (Aii.) and CCM3 distributes equally between the cytoplasm and nucleus (Aiii). When CCM1 is transiently co-expressed with CCM2, the subcellularlocalization of CCM1 shifts from the nucleus to the cytoplasm (B; YPet-CCM1 in green, CyPet-CCM2 in blue, DAPI in red).

A.

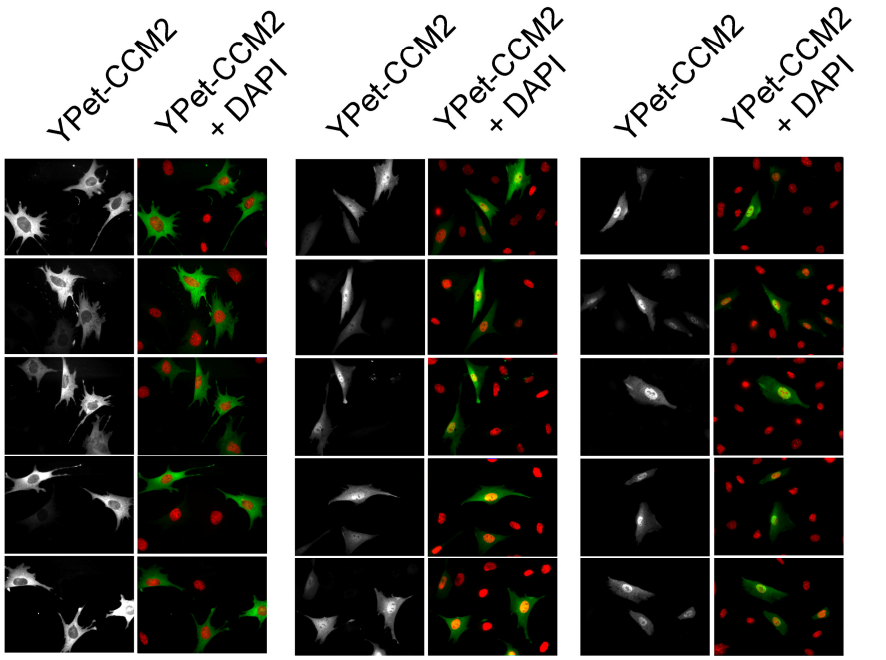
i. No Treatment
ii. 1hr Leptomycin B
iii. 3hr Leptomycin B
YPet-CCM2
YPet-CCM2 + DAPI
YPet-CCM2
YPet-CCM2 + DAPI
YPet-CCM2
YPet-CCM2 + DAPI

B.

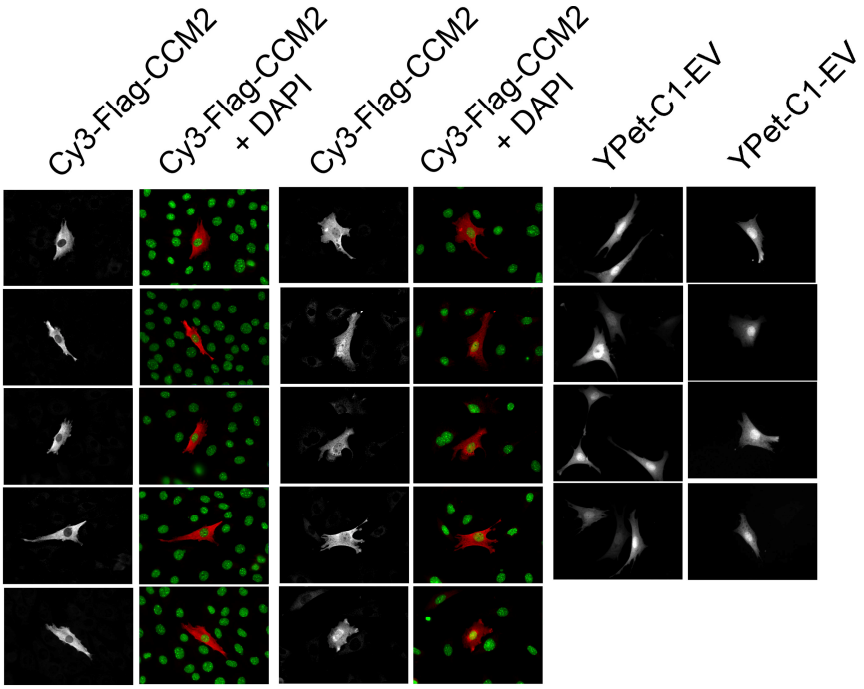
Leptomycin B
i. –
ii. +
Cy3-Flag-CCM2
Cy3-Flag-CCM2 + DAPI
Cy3-Flag-CCM2
Cy3-Flag-CCM2 + DAPI

C.

Leptomycin B
i. –
ii. +
YPet-C1-EV
YPet-C1-EV

Figure 3.2: CCM2 translocates between the cytoplasm and nucleus. MEECs were transiently transfected with YPet-CCM2 and treated with the nuclear export machinery inhibitor Leptomycin B for 1 or 3hr. In untreated cells YPet-CCM2 appears strongly in the cytoplasm (A*i*). With continuous treatment with Leptomycin B, a population of YPet-CCM2 progressively accumulates in the nucleus indicating that CCM2 translocates between the cytoplasm and nucleus (A*ii* and A*iii*). YPet-CCM2 in green, DAPI is red and DAPI demarcates the nucleus. The translocation of CCM2 is recapitulated with Flag-CCM2 (B*i* and B*ii*, Flag-CCM2 was immunofluorescently stained with Cy3 anti-Flag and appears in red. DAPI is green). The subcellular localization of the YPet protein alone in untreated MEECs (C*i*) is different from that of YPet-CCM2 (A*i*) and does not respond to treatment with Leptomycin B (C*ii*) suggesting that the subcellular localization of the YPet-CCM2 chimera is governed by CCM2 and not YPet.

MEEEGKKGKKPGIVSPFKRVFLKGEKSRDKKAHEKVTERRPLHTVVLALPERVEPDRLLSDYIEKEVKYL
GQLTSIPGYLNPSSRTEILHFIDKAKRSHQLPGHLTQEHDAVLSLSAYNVKLAWRDGEDIILRVPIHDIA
AVSYVRDDAAHLVVLKTAQDPGISPSQSLCAESSRGLSAGSLSESAVGPVEACCLVIMATESKVAAEELC
SLLSQVFQIVYTESTIDFLDRAIFDGASTPTHHLSLHSDDSSTKVDMKDSYDADASTFCFPDSGDVGGLP
PLPFCMQTSPHSKTVSESELSTSATELLQDYMLTLRTKLSSQEIQQFAALLHEYRNGASIHEFCISLRQL
YGDSRKFLLLGLRPFIPEKDSQHFENFLETIGVKDGRGIITDSFGRHRRALSTTSTSTINGNRTTGSPDD
RSAPSEGDEWDRM**ISDISSDIEAL**GCSMDQDSA

Figure 3.3: CCM2 encodes thirteen putative nuclear export sequences. All Iso, Leu and Val residues are highlighted in yellow. Clusters of residues similar to the consensus nuclear export sequence $Lx_{1-3}Lx_{2-3}LxL$, where L is Leu, Iso or Val and x is any residue, are underlined. For reference, the first and last residues of the PTB domain (S60 and D230) are shown in blue. The experimentally defined nuclear export sequence in CCM2 is shown in bold.

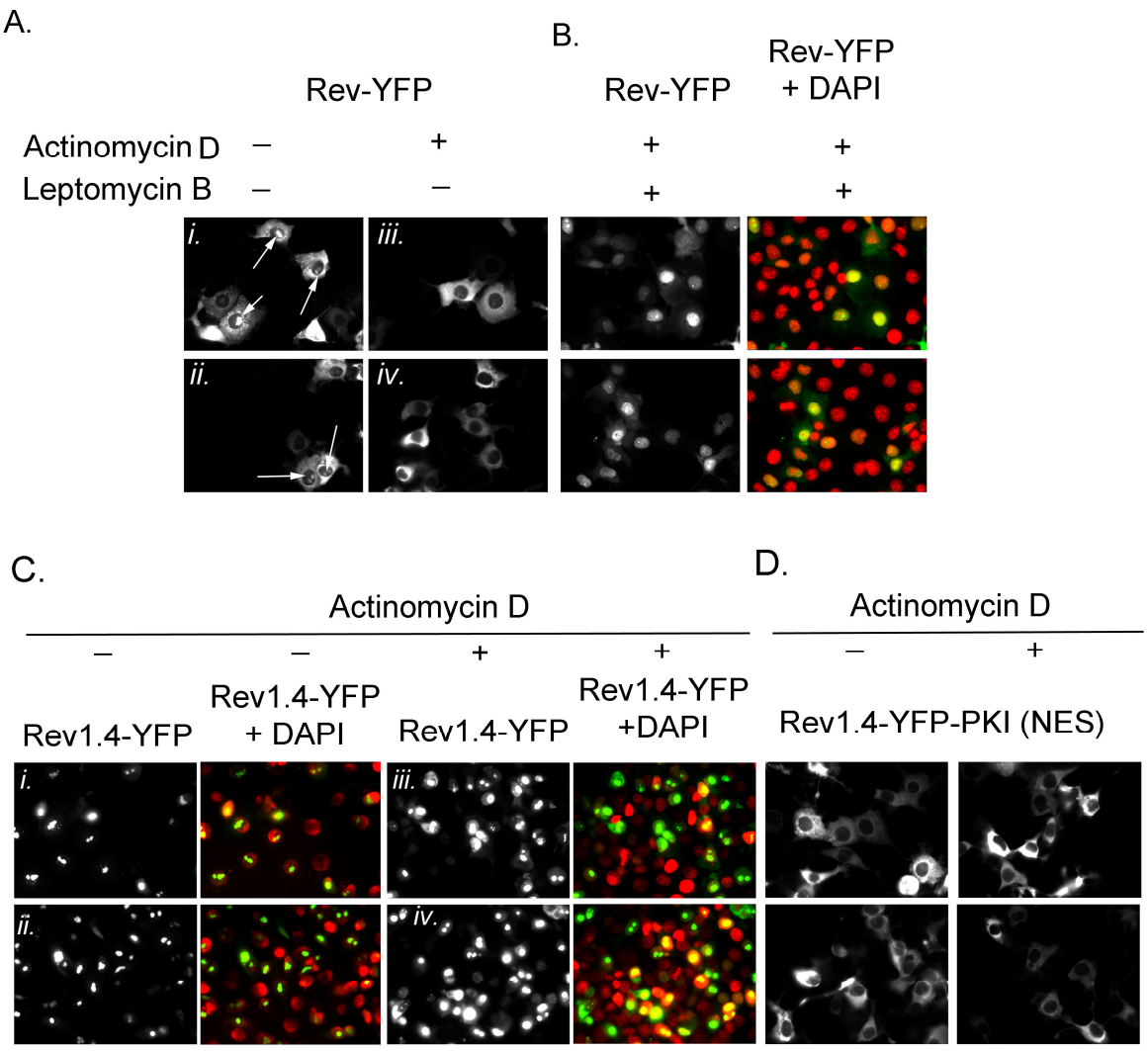

Figure 3.4: Validation of the Rev1.4-YFP assay for nuclear export sequences. When transiently expressed in Cos7 cells Rev-YFP wildtype localizes in the cytoplasm and nucleoli (A*i* and *ii*, arrows). Treatment with Actinomycin D blocks the Rev-YFP accumulation in the nucleoli and Rev-YFP appears cytoplasmic (A*iii* and *iv*). Treatment with Leptomycin B causes the nuclear accumulation of Rev-YFP due to the presence of a functional NLS and NES in Rev (B). Rev1.4-YFP lacks a NES and localizes exclusively in the nucleoli (Ci and ii) even in the presence of Actinomycin D (C*iii* and *iv*). When the NES from PKI is clones in Rev1.4-YFP, the chimera localizes in the cytoplasm (D), demonstrating that addition of a NES to Rev1.4-YFP causes a shift in subcellular localization. Rev-YFP is in green, DAPI in red.

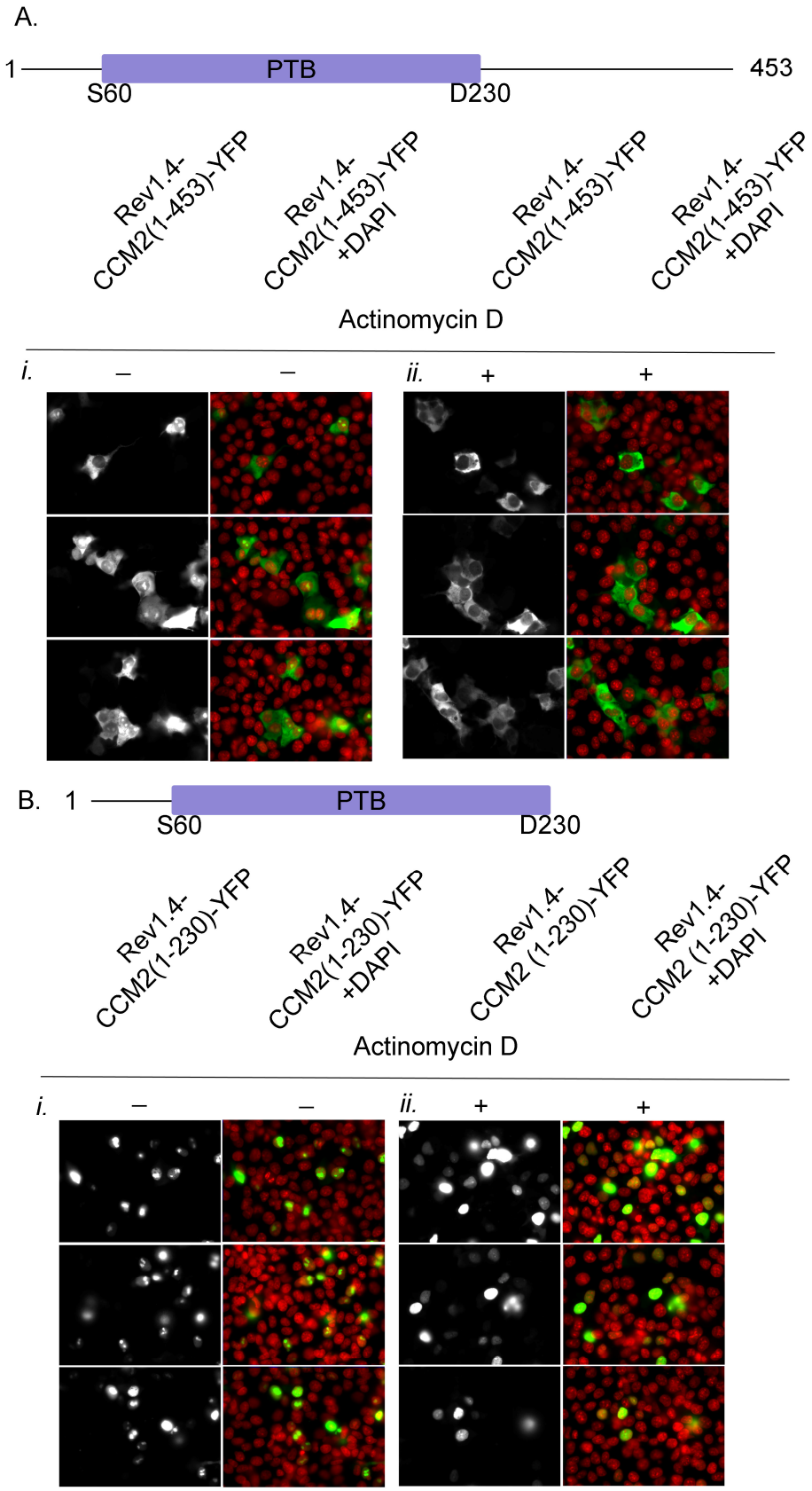
A.
1
PTB
453
S60
D230
Rev1.4-CCM2(1-453)-YFP
Rev1.4-CCM2(1-453)-YFP +DAPI
Rev1.4-CCM2(1-453)-YFP
Rev1.4-CCM2(1-453)-YFP +DAPI
Actinomycin D
i.
–
–
ii.
+
+
B.
1
PTB
S60
D230
Rev1.4-CCM2(1-230)-YFP
Rev1.4-CCM2(1-230)-YFP +DAPI
Rev1.4-CCM2 (1-230)-YFP
Rev1.4-CCM2 (1-230)-YFP +DAPI
Actinomycin D
i.
–
–
ii.
+
+

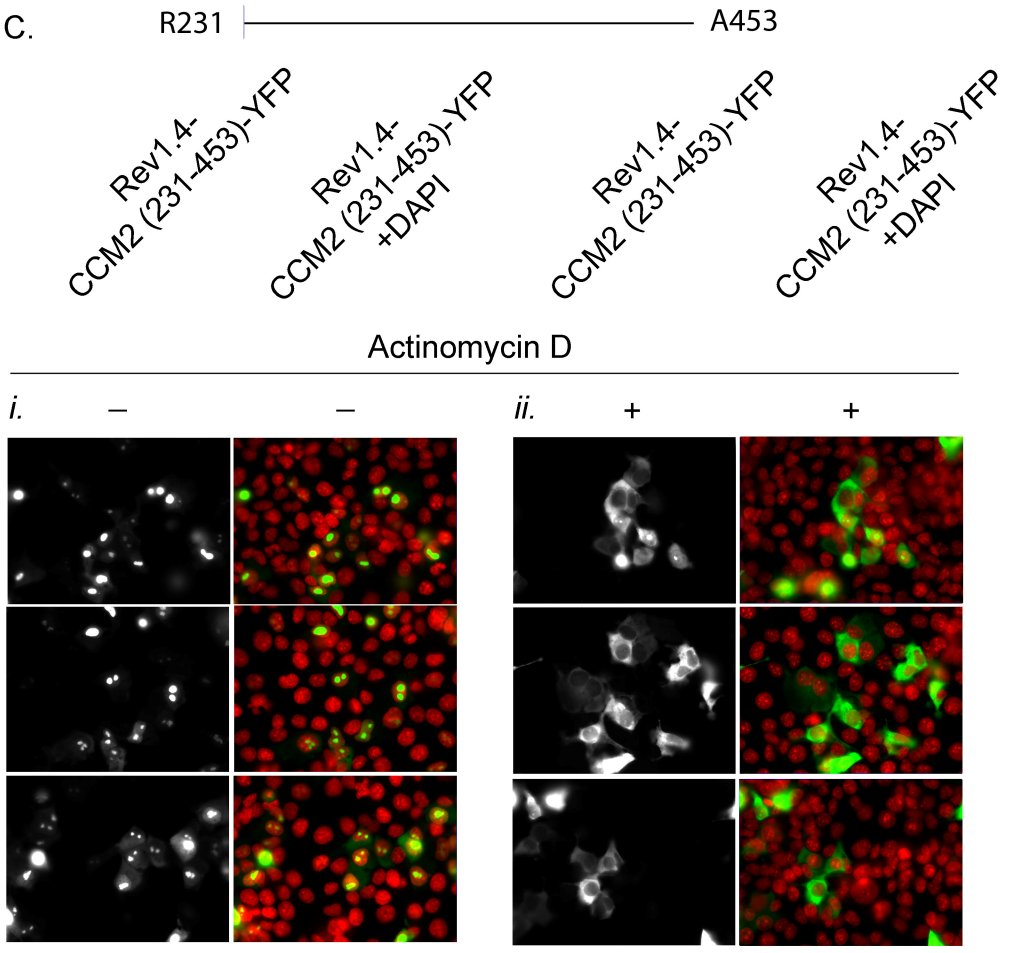

Figure 3.5: CCM2 residues 230-453 encode a functional NES.Cos7 cells were transiently transfected with full length CCM2 or CCM2 1-230 or CCM2 231-453 fused with Rev1.4-YFP and treated with Actinomycin D as indicated. Full length and 230-453 CCM2 Rev1.4-YFP localize to the cytoplasm in Actinomycin D treated cells (A*ii* and C*ii*) suggesting that the C terminal half of CCM2 encodes a functional NES. Rev1.4-YFP chimeras are in green, and DAPI in red.

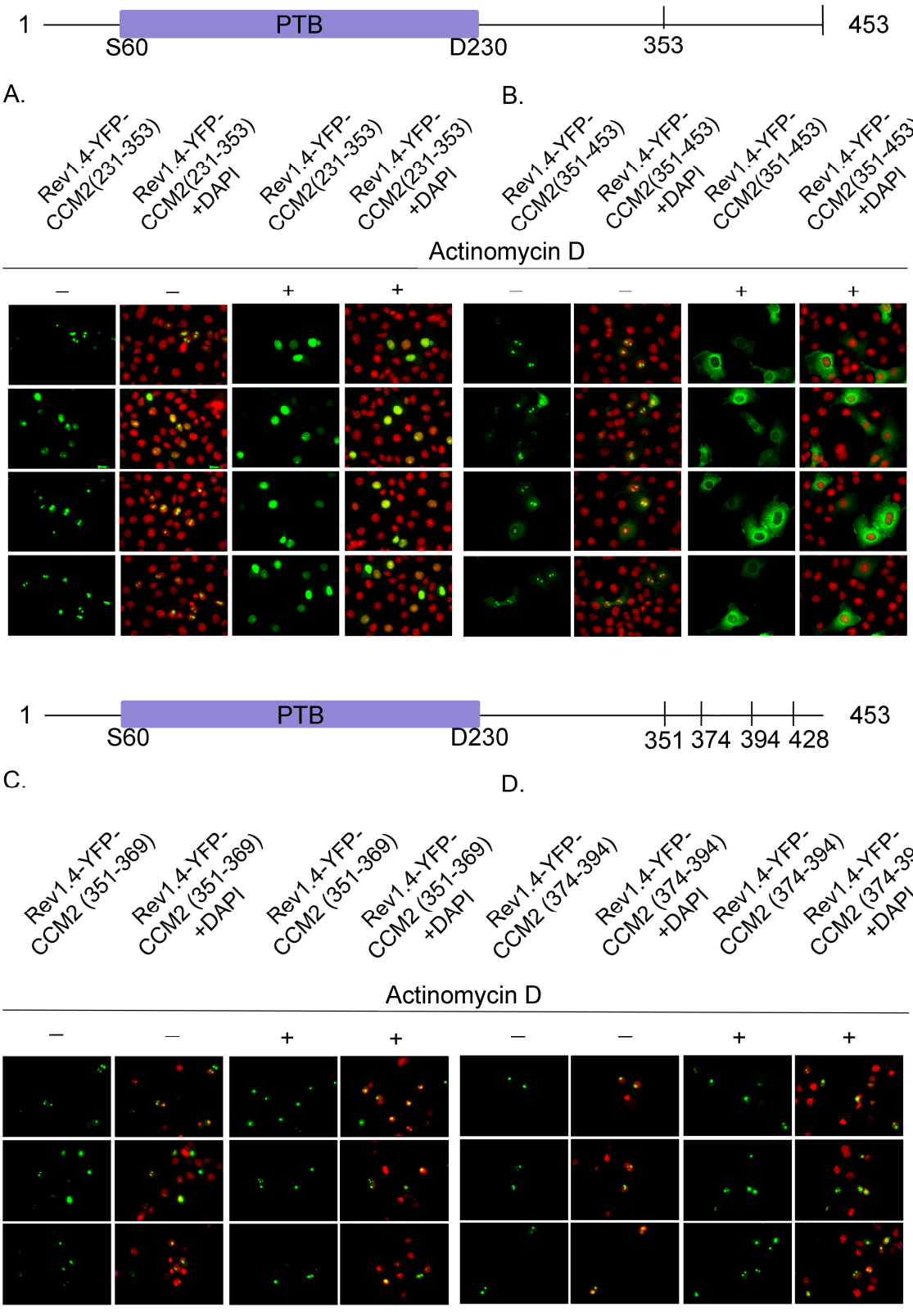
1
PTB
S60
D230
353
453
A.
B.
Rev1.4-YFP-CCM2(231-353)
Rev1.4-YFP-CCM2(231-353)+DAPI
Rev1.4-YFP-CCM2(231-353)
Rev1.4-YFP-CCM2(231-353)+DAPI
Rev1.4-YFP-CCM2(351-453)
Rev1.4-YFP-CCM2(351-453)+DAPI
Rev1.4-YFP-CCM2(351-453)
Rev1.4-YFP-CCM2(351-453)+DAPI
Actinomycin D
– – + + – – + +
1
PTB
S60
D230
351 374 394 428
453
C.
D.
Rev1.4-YFP-CCM2 (351-369)
Rev1.4-YFP-CCM2 (351-369)+DAPI
Rev1.4-YFP-CCM2 (351-369)
Rev1.4-YFP-CCM2 (351-369)+DAPI
Rev1.4-YFP-CCM2 (374-394)
Rev1.4-YFP-CCM2 (374-394)+DAPI
Rev1.4-YFP-CCM2 (374-394)
Rev1.4-YFP-CCM2 (374-394)+DAPI
Actinomycin D
– – + + – – + +

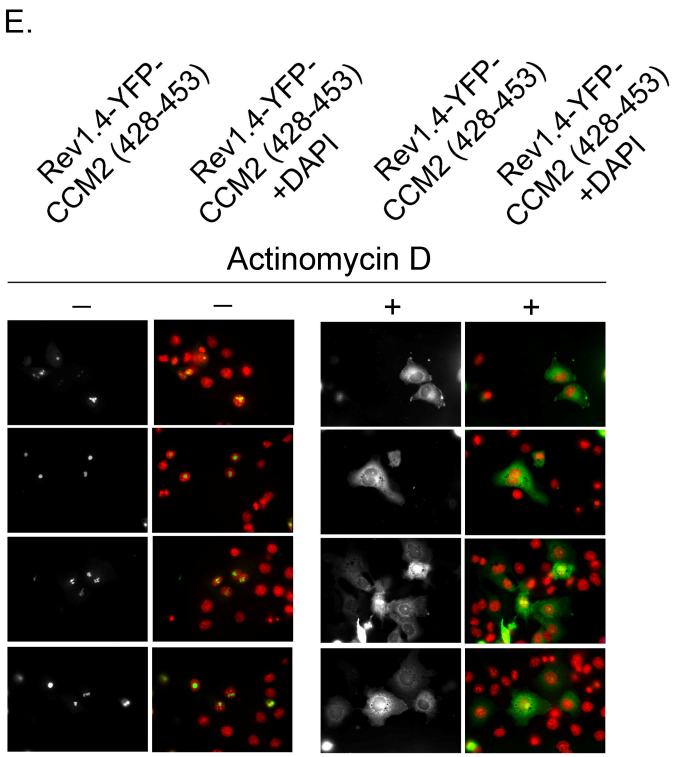

Figure 3.6: Residues 428-453 in CCM2 encode a NES. Serial truncations of CCM2 were fused with Rev1.4-YFP and tested for nuclear export capacity. The region 428-453 was the minimally required sequence for nuclear export (E). Rev1.4-YFP signal is in green and DAPI in red.

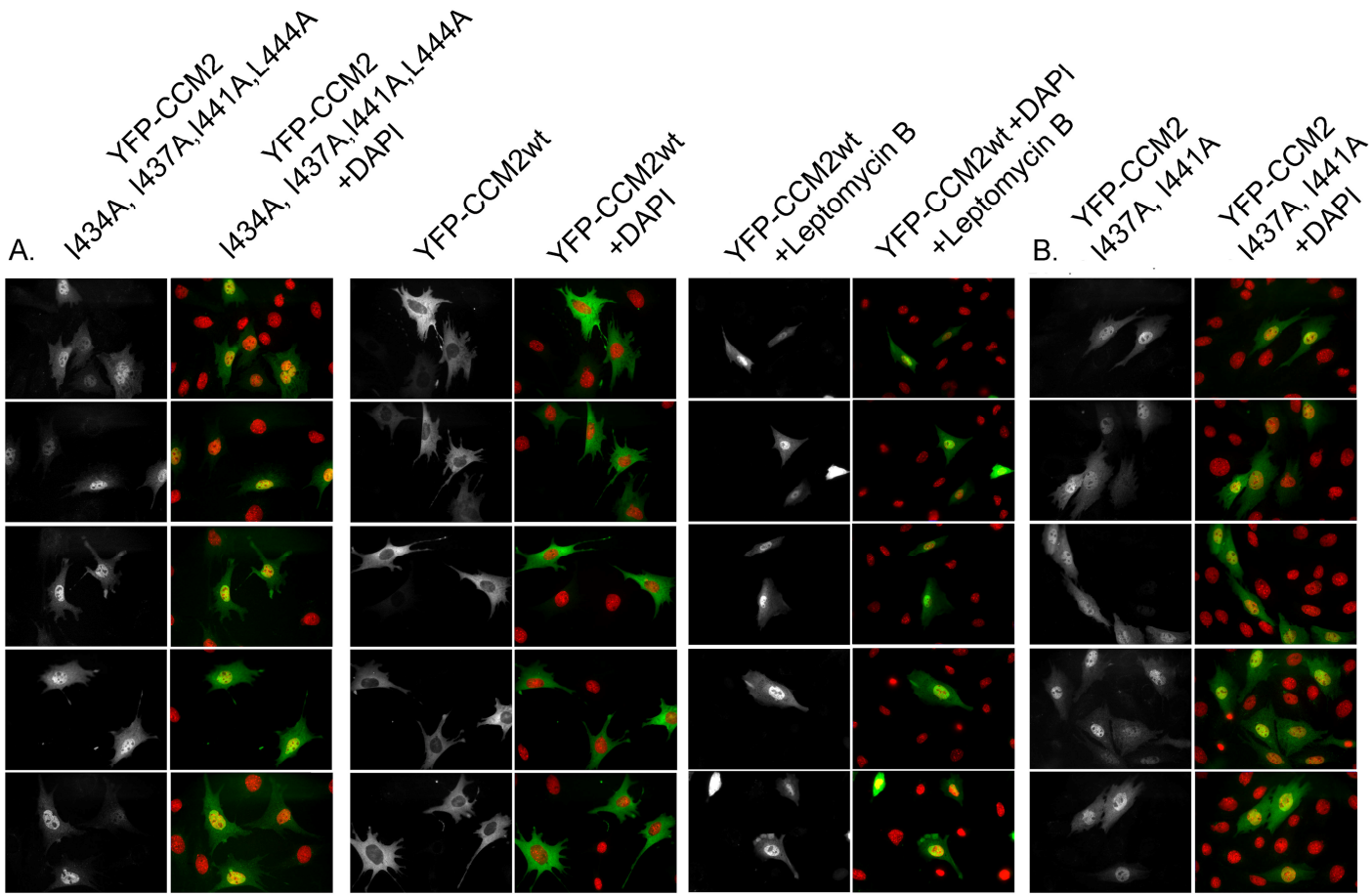

Figure 3.7: Residues I434, I437, I441 and L444 encode the NES in CCM2. Simultaneous mutagenesis of I434, I437, I441 and L444 to alanine in full length YFP-CCM2 leads to the nuclear accumulation of YFP-CCM2 to a similar extend as the nuclear accumulation of wildtype YFP-CCM2 following treatment with Leptomycin B (A). Mutagenesis of just two of the four residues, I437 and L444 is sufficient to abrogate the nuclear export of CCM2 (B). YFP fusion proteins are in green, DAPI in red.

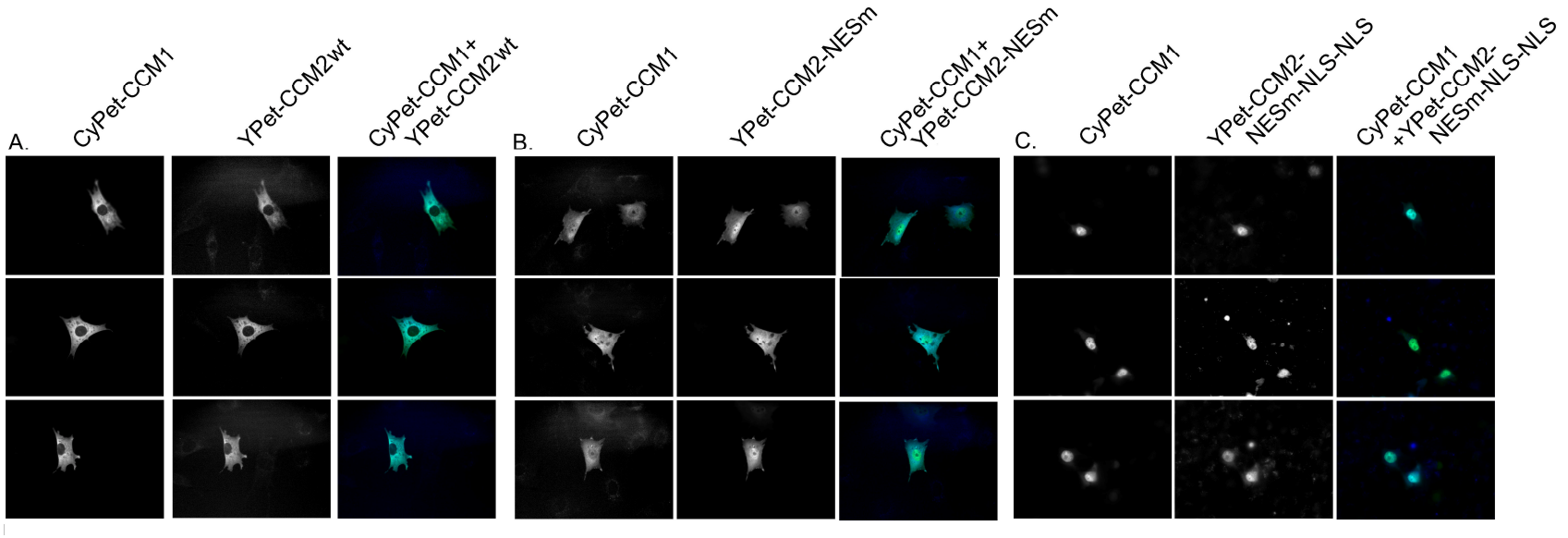

Figure 3.8: The subcellular localization of CCM1 mimics that of CCM2. CyPet-CCM1 (in blue) and YPet-CCM2 (in green) were transiently co-expressed in MEECs. CCM1 appears cytoplasmic when co-expressed with wildtype CCM2 (A), but relocalizes partially to the nucleus when co-expressed with CCM2-NESm (B) and becomes fully trapped in the nucleus when co-expressed with a CCM2-NESm fused with two consensus NLS (C) to force the nuclear import of the cytoplasmic population of CCM2-NESm as observed in B.

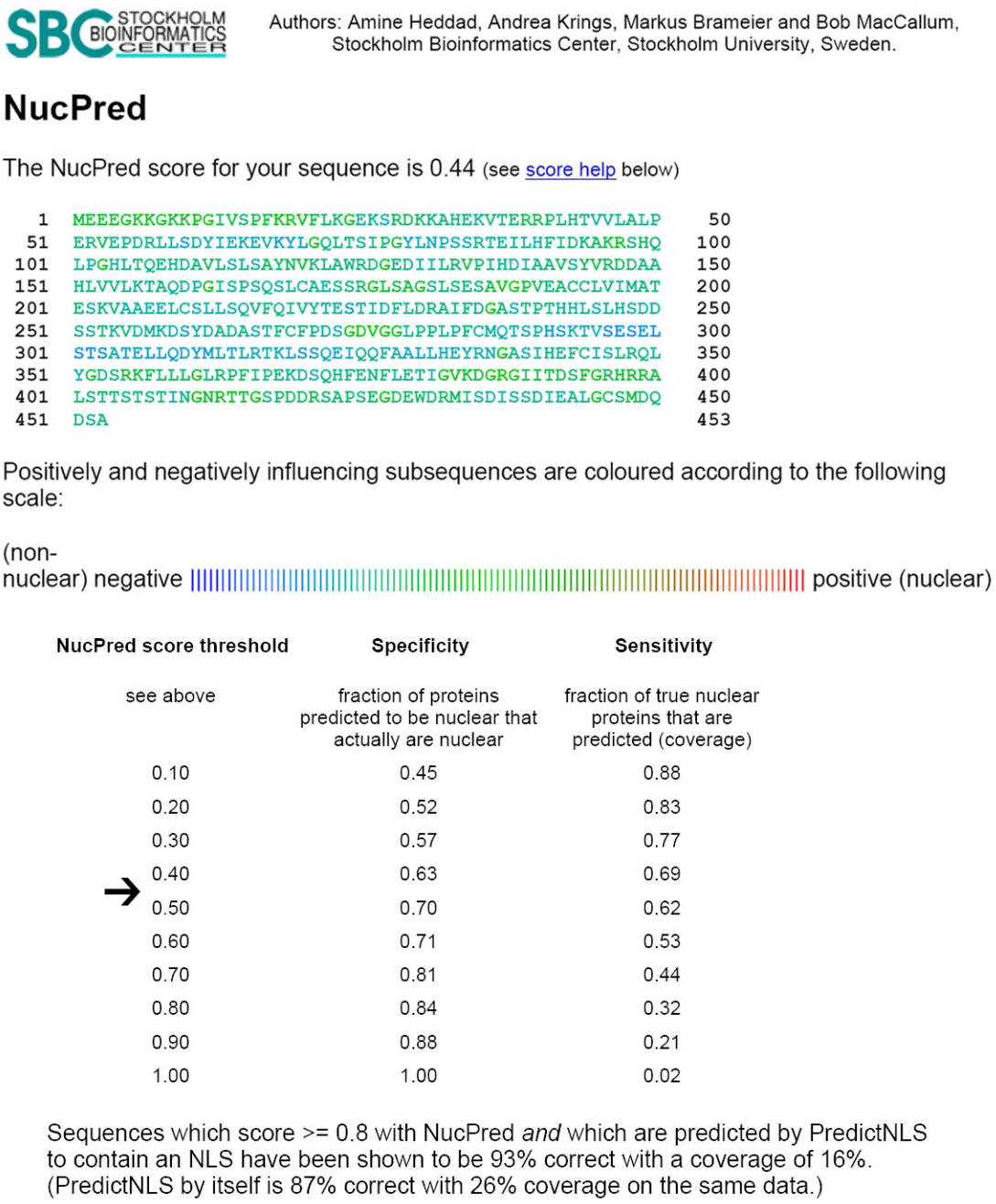

Authors: Amine Heddad, Andrea Krings, Markus Brameier and Bob MacCallum,
Stockholm Bioinformatics Center, Stockholm University, Sweden.

NucPred

The NucPred score for your sequence is 0.44 (see score help below)

```
  1  MEEEGKKGKKPGIVSPFKRVFLKGEKSRDKKAHEKVTERRPLHTVVLALP   50
 51  ERVEPDRLLSDYIEKEVKYLGQLTSIPGYLNPSSRTEILHFIDKAKRSHQ  100
101  LPGHLTQEHDAVLSLSAYNVKLAWRDGEDIILRVPIHDIAAVSYVRDDAA  150
151  HLVVLKTAQDPGISPSQSLCAESSRGLSAGSLSESAVGPVEACCLVIMAT  200
201  ESKVAAEELCSLLSQVFQIVYTESTIDFLDRAIFDGASTPTHHLSLHSDD  250
251  SSTKVDMKDSYDADASTFCFPDSGDVGGLPPLPFCMQTSPHSKTVSESEL  300
301  STSATELLQDYMLTLRTKLSSQEIQQFAALLHEYRNGASIHEFCISLRQL  350
351  YGDSRKFLLLGLRPFIPEKDSQHFENFLETIGVKDGRGIITDSFGRHRRA  400
401  LSTTSTSTINGNRTTGSPDDRSAPSEGDEWDRMISDISSDIEALGCSMDQ  450
451  DSA                                                  453
```

Positively and negatively influencing subsequences are coloured according to the following scale:

(non-nuclear) negative positive (nuclear)

NucPred score threshold	Specificity	Sensitivity
see above	fraction of proteins predicted to be nuclear that actually are nuclear	fraction of true nuclear proteins that are predicted (coverage)
0.10	0.45	0.88
0.20	0.52	0.83
0.30	0.57	0.77
→ 0.40	0.63	0.69
0.50	0.70	0.62
0.60	0.71	0.53
0.70	0.81	0.44
0.80	0.84	0.32
0.90	0.88	0.21
1.00	1.00	0.02

Sequences which score >= 0.8 with NucPred *and* which are predicted by PredictNLS to contain an NLS have been shown to be 93% correct with a coverage of 16%. (PredictNLS by itself is 87% correct with 26% coverage on the same data.)

Figure 3.9: An NLS cannot be predicted based on the primary sequence of CCM2. The sequence of CCM2 was threaded in a NLS prediction software, where residues color-coded in blue and green are less likely to encode for a NLS and residues in red are more likely. No NLS sequences can be predicted in CCM2.

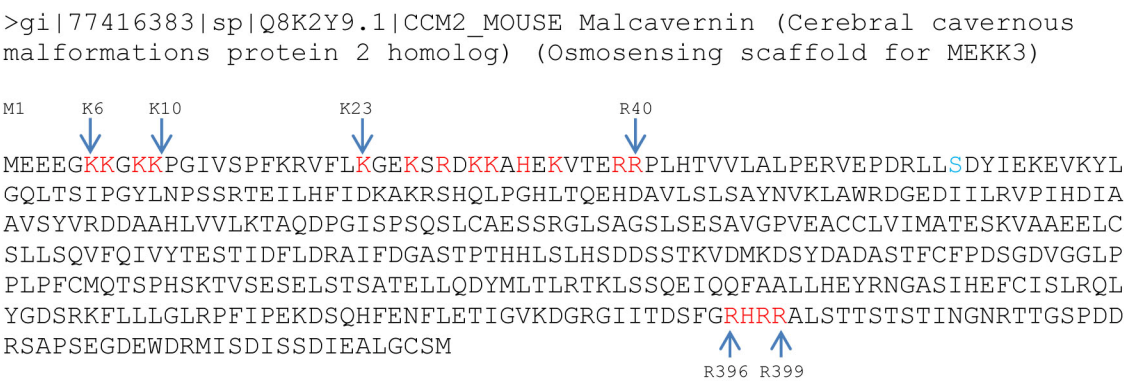

Figure 3.10: Putative NLS residues in CCM2 predicted on consensus sequence. The consensus definition for a NLS is a cluster of basic residues. Three clusters of basic residues were found in CCM2 and appear in red here.

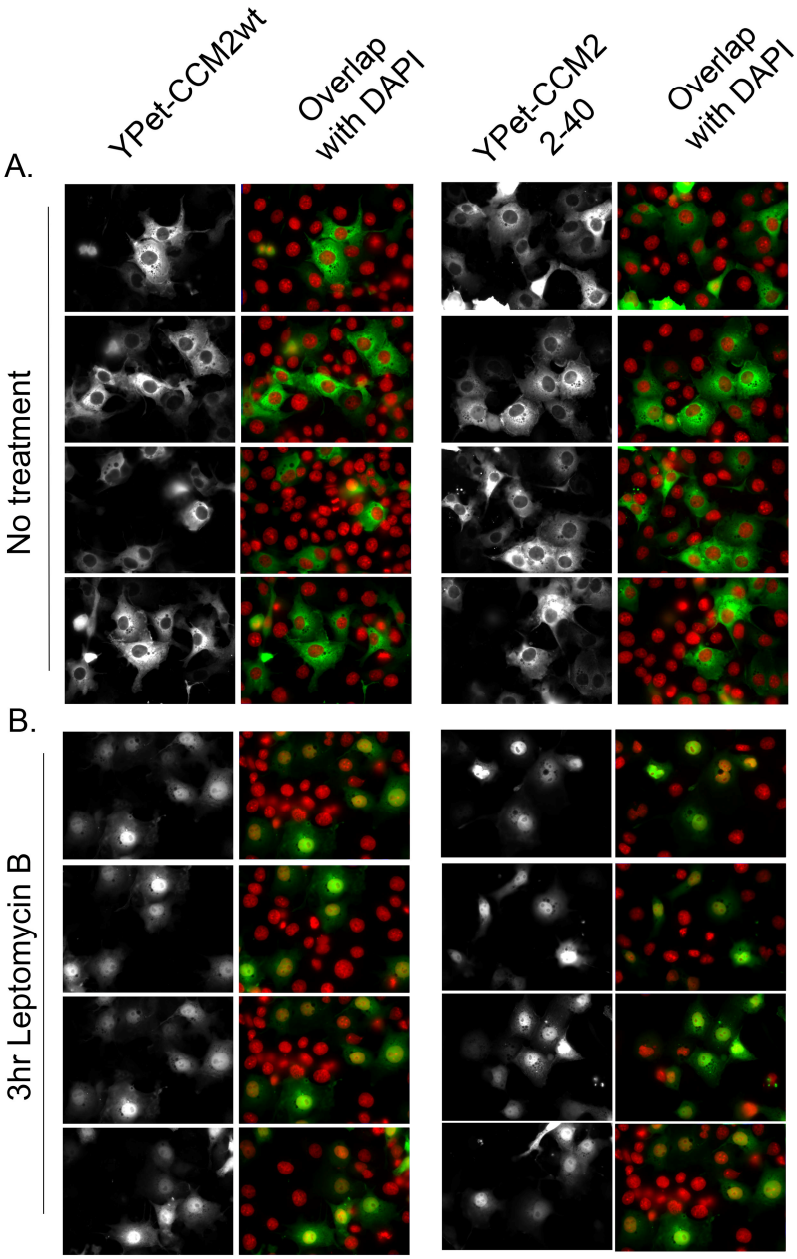

Figure 3.11: Deletion of the first 40 residues in CCM2 fails to abrogate the nuclear import of CCM2. Residues 2-40 were deleted in wildtype YFP-CCM2 and the construct was transiently expressed in Cos7 cells. Despite the lack of the first two clusters of putative NLS residues in YFP- CCM2 2-40, the protein still accumulates in the nucleus following treatment with Leptomycin B (B), indicating the YFP-CCM2 2-40 translocates from the cytoplasm to the nucleus and a NLS is not encoded in residues 2-40. YFP fusion proteins are in green, DAPI in red.

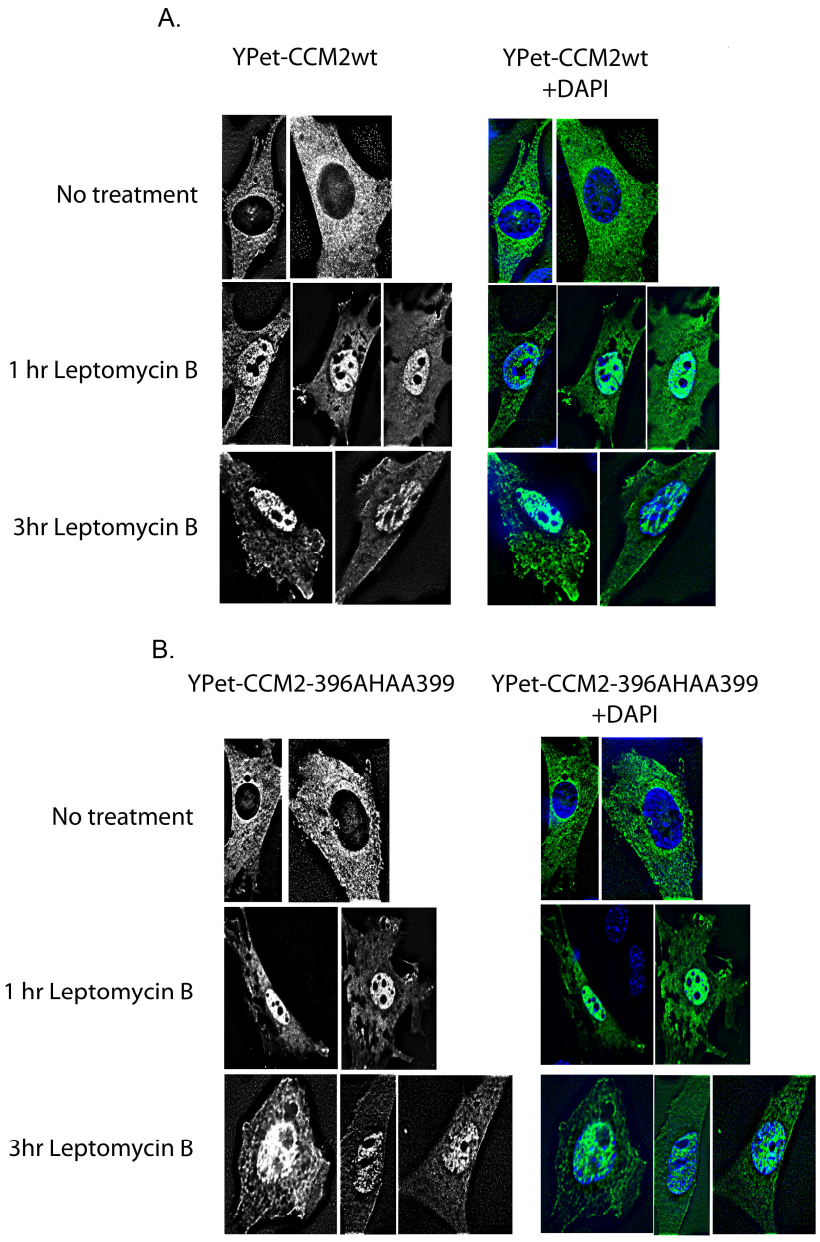

Figure 3.12: Residues 396RHRR399 do not encode a NLS in CCM2. The sequence was modified to AHAA by PCR and YPet-CCM2-396AHAA399 was transiently expressed in MEECs. To directly examine the nucleus for fluorescence signal, serial sections along the z-axis were generated and deconvolved to eliminate background fluorescence. Disruption of the 396AHAA399 sequence did not inhibit the nuclear import of CCM2 and YPet-CCM2-396AHAA399 (A) is still observed in the nucleus similarly to wildtype YPet-CCM2 (B) following treatment with Leptomycin B. YPet fusion protein in green, DAPI in blue.

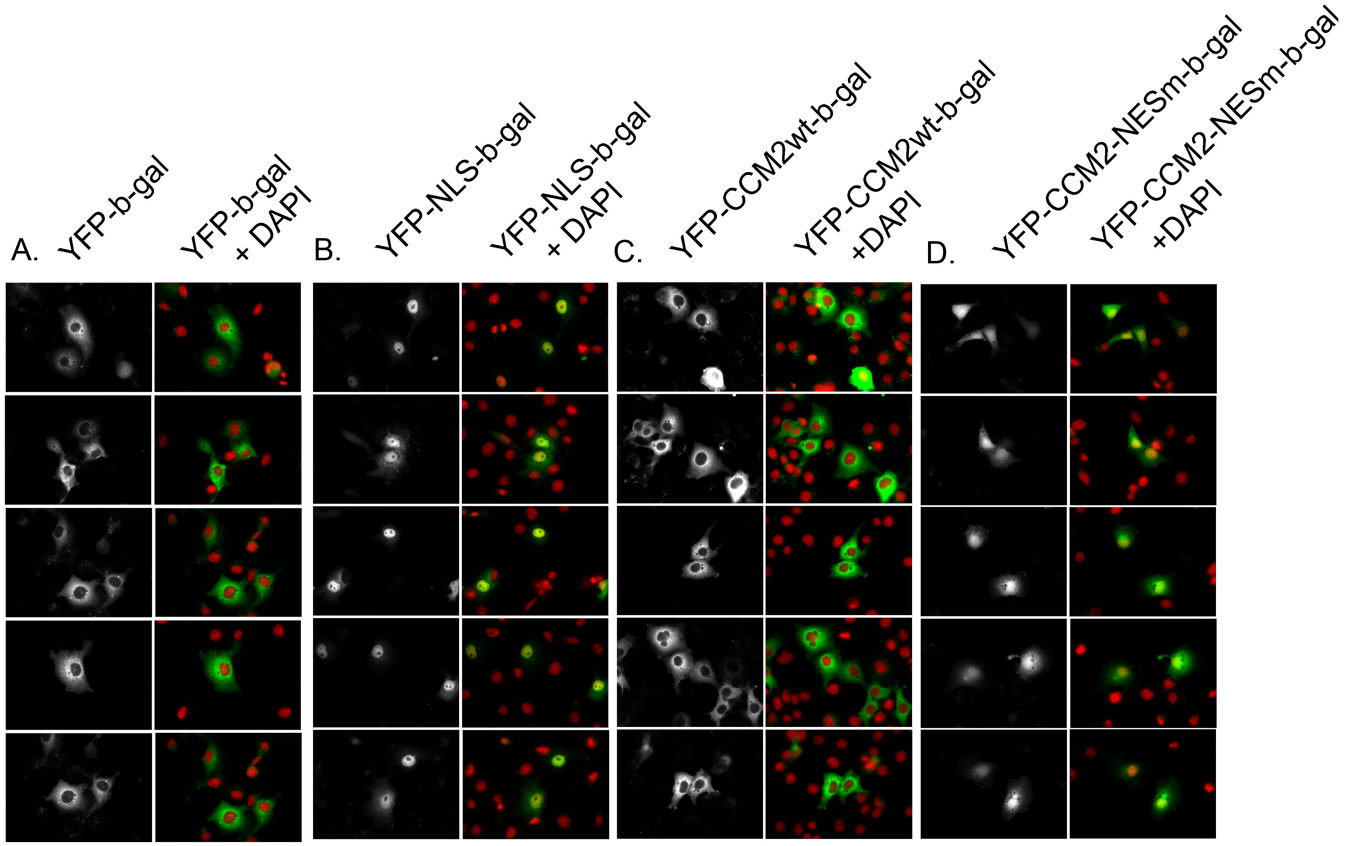

Figure 3.13: Validation of the β-galactosidase assay for putative NLS. YFP-β-gal localizes in the cytoplasm (A) due to the larger than 50kD size of YFP-β-gal and the absence of a NLS in β-gal. Fusion of β-gal with a canonical NLS leads to the complete localization to the nucleus (B). Fusion of YFP-β-gal with wildtype CCM2 fails to relocalize the chimera to the nucleus (C) however fusion of YFP-CCM2-NESm with β-gal leads to the nuclear accumulation of the chimera (D), demonstrating that CCM2 translocates to the nucleus, YFP-CCM2-NESm appears cytoplasmic due to the functional NES, and that fusion with β-gal does not impair the nucleocytoplasmic translocation of CCM2. DAPI pseudocolored in red.

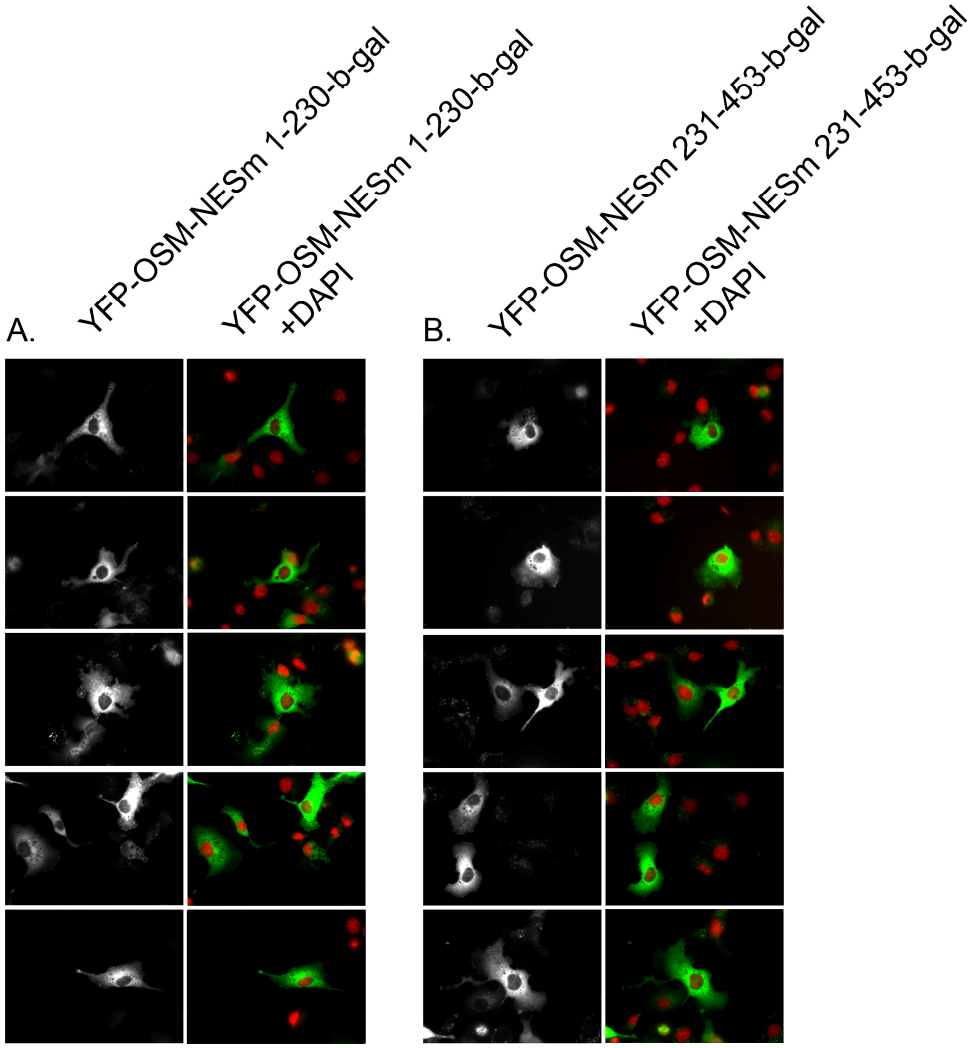

Figure 3.14: Neither residues 1-230 nor 231-453 NESm of CCM2 encode a NLS. CCM2 truncations 1-230 and 231-453NESm were fused with YFP-β-gal and transiently expressed in MEECs. Neither sequence causes the nuclear import of the YFP-CCM2 truncation- β-gal chimera. YFP fusion proteins are in green and DAPI in red.

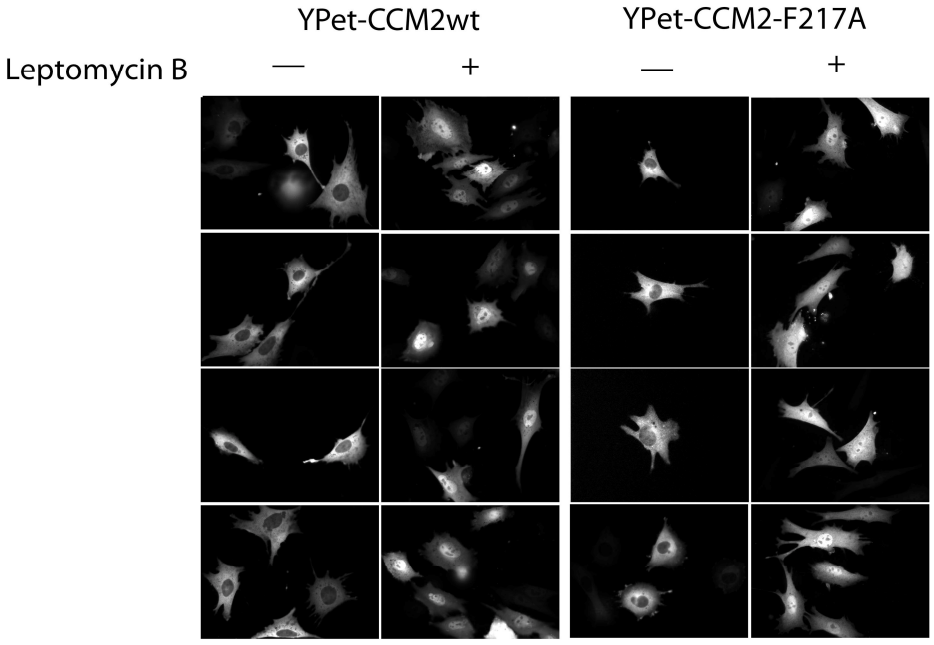

Figure 3.15: The nuclear import of CCM2 is not mediated by a binding partner. The nucleocytoplasmic translocation of YPet-CCM2-F217A mutant expressed in MEECs is similar to that of wildtype YPet-CCM2 following treatment with Leptomycin B.

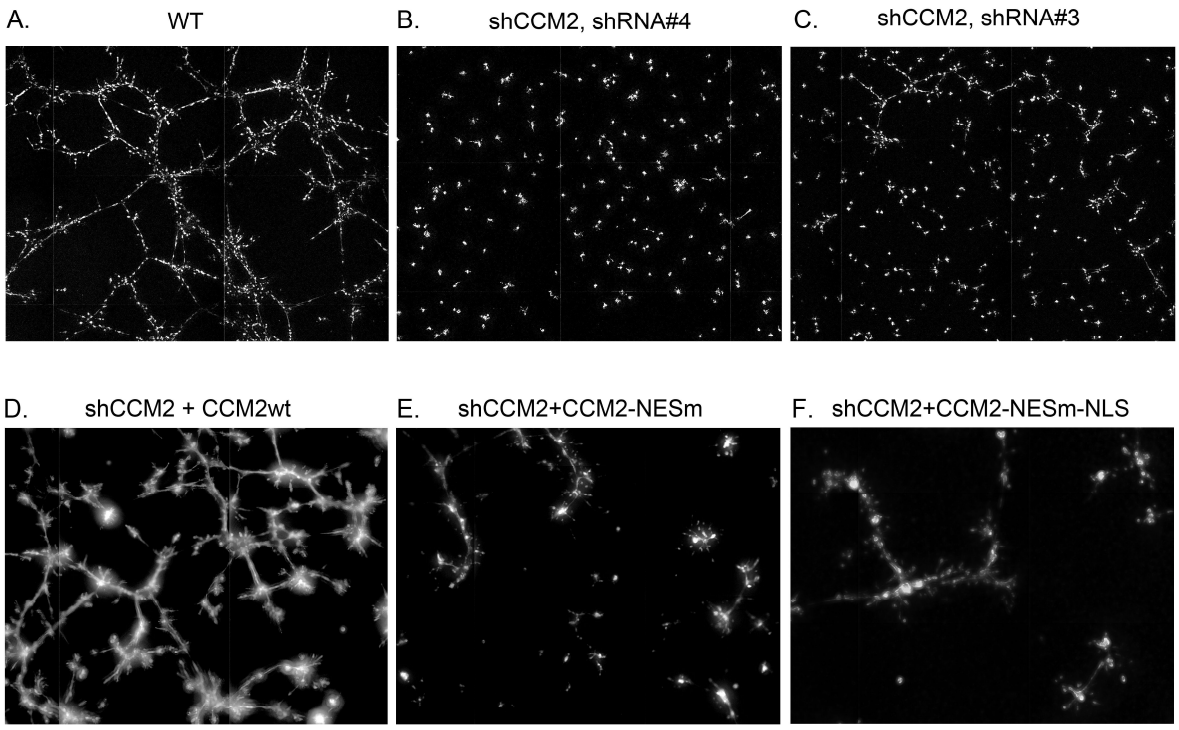

Figure 3.16: The cytoplasmic localization and nuclear translocation of CCM2 are required for the molecular function of CCM2 in endothelial cell self-assembly in lumen-like tubes. Wildtype MEECs self-assemble in lumen-like tube structures when plated on matrigel (A). Loss of CCM2 expression by two different shRNA sequences disrupts the ability of MEECs to form tube like structures (B and C). Addback of wildtype CCM2 in the shCCM2 MEECs rescues tube formation (D). However addback of CCM2-NESm or CCM2-NESm-NLS fails to rescue the tube formation of shCCM2 cells (E and F).

CHAPTER IV

RHO KINASE INHIBITION RESCUES THE ENDOTHELIAL CELL CEREBRAL CAVERNOUS MALFORMATION PHENOTYPE

Introduction

It was recently shown that loss of endothelial cell expression of CCM2 resulted in activation of the GTPase RhoA (Crose et al., 2009). Crose *et al*. 2009 demonstrated that CCM2 knockdown in brain microvascular endothelial cells resulted in defective RhoA degradation because of the dysregulation of Smurf1, a CCM2 binding partner and an E3 ubiquitin ligase that controls RhoA degradation. RhoA overabundance induced by loss of CCM2 was shown to increase cytoskeletal stability, inhibit vessel-like tube formation, and increase endothelial cell monolayer permeability. Herein, we show that loss of CCM1, 2 or 3 expression results in a common phenotype associated with RhoA overexpression and activation. We use a single-cell live-cell assay to define the cytoskeletal biomechanical phenotype resulting from loss of CCM expression in human endothelial cells. We define Rho Kinase (ROCK) as a critical RhoA effector for the pharmacological manipulation of the RhoA phenotype in CCM cells. ROCK is activated by RhoA and phosphorylates several substrates, including myosin light chain, myosin light chain phosphatase, and LIM kinase for the regulation of actin cytoskeletal

dynamics(Jaffe and Hall, 2005). ROCK has also been shown to regulate vascular permeability and has been a drug discovery target for regulation of vascular bed diseases (Chrissobolis and Sobey, 2006). Our findings show the increased RhoA abundance and activity in CCM cells leads to increased cytoskeletal stiffening which leads to aberrant invasion and tube formation. We demonstrate that ROCK inhibition rescues extracellular matrix invasion and vessel-like tube formation, two endothelial cell functions disrupted by the loss of CCM protein expression.

Results

Knockdown of CCM1, 2 or 3 induces RhoA overexpression and persistent RhoA activity

Stable knockdown of CCM1, 2 or 3 in Human Umbelical Vein Endothelial Cells (HUVECs) each resulted in 4.58, 5.11 and 3.78 average fold increases in RhoA expression relative to WT cells (p values were respectively 0.0009, 0.013 and 0.0018; Figure 4.1A and B). Knockdown was achieved with targeted shRNA for each *ccm1*, *ccm2* and *ccm3* mRNA and was on average 76, 93 and 96% respectively for shCCM1, 2 and 3 relative to wildtype (p values 0.00028, 1.11e-8, 1.82-e7 respectively; Figure 4.1D and E). The finding that inhibition of CCM1, 2 or 3 protein expression similarly caused marked increases in RhoA expression demonstrates for the first time that the three CCM proteins function coordinately to regulate RhoA protein levels; loss of any one CCM protein causes an increase in RhoA expression. Analysis of the mRNA transcript levels for RhoA in shCCM1, 2 and 3 cells revealed no significant increase in RhoA message levels (Figure 4.1F). An increase in the abundance but not transcription levels of RhoA is consistent with a dysregulation in RhoA degradation caused by loss of

CCM1, 2 or 3, although we have not excluded aberrant post-translational regulation of RhoA.

Previously, we showed that CCM2 knockdown resulted in dysregulated Smurf1-mediated degradation of RhoA (Crose et al., 2009). The overlapping phenotype of increased RhoA abundance for all three CCM knockdown cell lines is consistent with a requirement of a functional CCM1/2/3 protein complex for the regulation of RhoA degradation.

To assess whether the increase in total RhoA results in an increase of active RhoA, the levels of active, GTP-bound RhoA were assayed in shCCM1, 2 and 3 HUVECs. The levels of active RhoA in shCCM1, 2 and 3 cells were respectively 3.78, 2.40 and 4.83 fold higher than in wildtype cells (p values 0.001, 3.95e-6, 0.049 respectively Figure 4.1A). These data provide direct evidence that loss of not only CCM2, but CCM1 or CCM3 results in the increased activation of RhoA, and establishes the first identified common pathway for CCM1, 2 and 3.

To validate that loss of CCM1, 2 or 3 leads to increased RhoA abundance and activity, the RhoA protein and activation levels were assayed in a second endothelial cell line using an independent assay for RhoA activity. Loss of CCM1, 2 or 3 expression by shRNA in mouse embryonic endothelial cells (MEECs) was 70, 96 and 95% respectively relative to control cells treated with the pLKO.1 shRNA empty vector (Figure 4.2A). Loss of CCM2 protein expression was also validated by western blot with a mouse antibody raised against full-length CCM2 (Figure 4.2B). Antibodies for CCM1 and CCM3 are not currently available through commercial sources.

Similarly to the phenotype observed in human endothelial cells with shRNA for CCM1, 2 or 3, loss of CCM protein expression in mouse endothelial cells also resulted in the 3.8, 8.6 and 2.1 fold increase in RhoA relative to wildtype cells (p values are 0.034, 0.0044, 0.017 respectively; Figure 4.2C and 4.2D). To define the RhoA activity in shCCM1, 2 and 3 MEECs the spatial distribution of active RhoA was assayed using a single-chain RhoA biosensor based on Förster Resonance Energy Transfer (FRET). The biosensor has been extensively characterized for measurement of RhoA activity in live cells (Pertz et al., 2006). The overexpression of RhoA observed in CCM knockdown cells results in a persistent activation of RhoA (Figure 4.2E). In WT endothelial cells, RhoA activity is low and observed primarily at the cell edge as previously described for fibroblasts. With shRNA knockdown of CCM2 or CCM3 there is a significant increase in RhoA activity not only at the cell edge but also in the cytoplasm and nucleus. When a population of approximately 50 single cells is imaged and averaged for FRET intensity of the RhoA biosensor at the cell edge, cytoplasm or nucleus, the CCM1, 2 and 3 knockdown cells each have a highly statistically significant increase in RhoA activation relative to control cells (Figure 4.2F). Strikingly, RhoA activity is extremely high in CCM1 knockdown cells relative to control, CCM2 or CCM3 knockdown cells (Figure 4.2E). Statistical analysis of a population of individual CCM1 knockdown cells indicates an average of 1.62, 2.33, and 1.48-fold increase in FRET intensity relative to WT cells for the cytoplasm, nucleus, and cell edge, respectively (Figure 4.2F).

These results show regulation of RhoA protein expression is consistent in two independent endothelial cell lines and is common to the loss of any of the three CCM proteins. However, the pronounced RhoA activity in CCM1 knockdown cells compared

to CCM2 or CCM3 knockdown indicates the CCM proteins are not simply in a common pathway but have specific functions. Whereas CCM2 binds Smurf1 for control of RhoA degradation, CCM1 appears to have a functional role as a negative regulator of RhoA activity and loss of CCM1 has a pronounced effect on RhoA activity, which is different from the regulation of RhoA protein expression. Thus, the CCM proteins organize a signaling network, not simply a pathway for control of RhoA function.

ROCK2 is required for increased phosphorylation of myosin light chain 2 and cofilin in CCM 1, 2 or 3 knockdown cells

ROCK1 and ROCK2 are closely related kinases with overlapping but also distinct functions. Both ROCK1 and ROCK2 bind activated GTP-RhoA. ROCK1/2 phosphorylates MLC2 and phosphorylates and activates LIM Kinase, which consequently phosphorylates Cofilin. Phospho-MLC2 and phospho-Cofilin are a measure of ROCK1/2 activity in cells. MLC2 is required for the control of actin cytoskeletal dynamics, induction of stress fiber formation, and cell contraction, whereby ROCK1/2 phosphorylation of MLC2 and MLC phosphatase leads to increased cytoskeletal stability. Cofilin is an adaptor that binds and sequesters away actin monomers to promote actin stress fiber degradation. Phosphorylation is an inhibitory modification for Cofilin and thus increased phosphorylation of Cofilin also leads to increased cytoskeletal stability.

We previously showed that stress fiber-associated phospho-MLC2 was increased in brain microvascular endothelial cells upon knockdown of CCM2 (Crose et al., 2009). Given the increased RhoA activity observed in CCM1, 2 or 3 knockdown

endothelial cells (Figures 4.1 and 4.2), we predicted that stress fiber formation and phosphorylation of MLC2 and Cofilin would be increased with knockdown of each of the CCM proteins.

The levels of phospho-MLC2 in shCCM1, 2 and 3 human endothelial cells were increased 3.1, 2.1 and 1.8 fold relative to pLKO.1 control cells (Figure 4.3A). Phospho-Cofilin levels in shCCM1, 2 and 3 cells were increased 2.4, 3.4 and 3.1 fold relative to pLKO.1 control cells (Figure 4.3B-D). Consistent with an increase in phospho-MLC2 and phospho-Cofilin, shCCM1, 2 and 3 cells displayed increased formation of stress fibers and increased cell size (Figure 4.3C, E,F). However, there is not a linear relationship with the RhoA activity measured in Figure 4.1 with knockdown of CCM1, 2 or 3 and the relative levels of phospho-MLC2 and phospho-Cofilin or stress fiber formation. This is consistent with dysregulation of a regulatory network differentially controlled by each CCM protein. Nonetheless, control of RhoA expression is a convergent regulatory function requiring each CCM protein.

In endothelial cells ROCK2 is the functionally predominant ROCK form and was targeted for shRNA knockdown. Loss of ROCK2 expression reversed the increase in phospho-MLC2 observed in each of the CCM protein knockdown MEEC lines, and treatment with the small molecule ROCK inhibitor Y-27632 reversed the increased phospho-Cofilin in shCCM1 HUVECs (Figure 4.4). These data demonstrate that ROCK2 stimulates the phosphorylation of MLC2 and Cofilin in endothelial cells.

The cytoskeleton of CCM deficient endothelial cells shows increased stiffening in response to external mechanical force

To define the functional consequence of the increased RhoA with loss of CCM a biomechanical assay that measures the cytoskeletal response to applied mechanical force was used. Magnetic twisting cytometry (MTC) is a well established biophysical approach for the profiling of the mechanical phenotype of the cell cytoskeleton(Tim O'Brien et al., 2008; Guilluy et al., 2011; Kasza et al., 2009). Several decades of study of the biomechanical properties of cells have established that in response to a series of external applied force pulses the actinomyosin cytoskeleton remodels and this cytoskeletal response is mathematically described as a viscoelastic spring(Hoffman and Crocker, 2009; Koenderink et al., 2009; Kasza et al., 2009).

MTC was used as an independent, single-cell assay to define the cytoskeletal dynamics in human endothelial cells with loss of CCM proteins. For MTC, beads were coated with fibronectin and allowed to adhere to integrins on the surface of plated wildtype or shCCM1 or 2 HUVECs. The cell-bead interaction was imaged by Scanning Electron Microscopy which demonstrated that beads are attached directly to the surface of the cell and that the bead-cell interaction between wildtype and shCCM1 cells bears no gross differences (Figure 4.5A). A series of short magnetic pulses were introduced to create a mechanical pullforce on the integrin-bound beads and the displacement of the bead in the x and y direction was recorded. The displacement of beads on wildtype HUVECs progressively decreased with consecutive pulls due to the progressive stiffening spring-like response of the underlying cytoskeleton (Figure 4.5B). CCM1

deficient HUVECs also responded by cytoskeletal stiffening with progressive applications of magnetic pullforce, however the difference in the distance traversed by the bead following the first and consecutive pulls was greater for shCCM1 cells than for wildtype cells (Figure 4.5B). The displacement of the bead can be related to the stiffness of the underlying cytoskeleton by Jeffrey's modulus. Briefly, the stiffening response of the cytoskeleton is modeled as a spring, where the stiffness of the cytoskeleton is the product of the predefined magnitude of the pullforce applied to the beads divided by the distance traveled by the bead for the duration of the force (Tim O'Brien et al., 2008; Guilluy et al., 2011).

The difference in the relative stiffness of the cytoskeleton during the first and second pull was measured for 38 independent beads over four independent experiments in wildtype cells, 37 independent beads for four independently derived shCCM1 HUVEC cell lines and 9 independent beads for three independently derived shCCM2 HUVEC cell lines. No significant cytoskeletal stiffening occurred between the first and second pulls for wildtype cells for which the average fold change in first to second pull stiffness was 0.99 (p value 0.85; Figure 4.5C). Stiffening in wildtype cells was observed during the third pull (Figure 4.5B). The fold increase in cytoskeletal stiffness between the first and second pulls for shCCM1 and shCCM2 cells was respectively 1.21 (p value 0.0026) and 1.37 (p value 0.033; Figure 4.5C).

The molecular mechanisms that are described by the cytoskeletal stiffening measured with MTC of fibronectin coated beads on fibroblasts were recently defined (Guilluy et al., 2011). In response to a mechanical force on β1integrins, the RhoGEFs

LARG and GEF-H1 are activated leading to the activation of RhoA. When RhoA was knocked down by siRNA the stiffening response was abrogated and no significant difference in stiffness was observed between the first and second pulls of RhoA-depleted cells (Guilluy et al., 2011). These studies established that the stiffening response in cells is mediated by the activation of RhoA, where the amplitude of the stiffening response is proportional to the concentration of active RhoA. In line with the Guilluy findings, the increased stiffening response in CCM depleted HUVECs suggests a greater abundance of total or active RhoA or an increase in the total abundance of the LARG and GEF-H1 RhoGEFs leading to the rapid activation of a greater population of RhoA molecules. Indeed, as demonstrated by western blot, immunoprecipitation for active RhoA and with the RhoA biosensor, the abundance of total and active RhoA is increased in CCM deficient cells. The relative mRNA levels of GEF-H1 in wildtype or shCCM1 endothelial cells were assessed independently of MTC experiments and were found to be equivalent between wildtype and shCCM1 cells (data not shown). MTC provides an independent, single-cell validation of the RhoA phenotype with loss of CCM.

To unequivocally establish whether RhoA activation causes the increased cytoskeletal stiffening in CCM depleted cells, the stiffening response was measured in shCCM1 cells treated with Y-27632. The stiffening response in shCCM1 cells was abrogated upon ROCK inhibition with a 1.05 fold increase in stiffening between the first and second pulls (p value 0.61; Figure 4.5D). In short, the MTC studies in shCCM1 and 2 cells provided an independent assay for the functional consequence of the loss of

CCM proteins. The biomechanical phenotype of shCCM1 and 2 cells is one of increased RhoA activation following mechanical deformation of the cell resulting in increased cytoskeletal stiffness relative to the stiffness observed in wildtype cell subjected to similar mechanical stress.

Filamin A is an actin cross-linking adaptor protein whose expression has been shown to correlate positively with an increase in cytoskeletal stiffness (Coughlin et al., 2006; Kasza et al., 2009). The levels of Filamin A in shCCM1, 2 and 3 HUVECs were increased relative to wildtype cells (Figure 4.5E and F). Knockdown in these cell lines was verified by RT PCR (data not shown) and as an additional marker for knockdown cells were also stained for actin stress fibers which were shown to be increased in shCCM1, 2 and 3 cells above. Filamin A crosslinks actin filaments and thus reinforces the stability of the cytoskeleton. When a pullforce is applied, the underlying cytoskeleton rapidly reorganizes to counteract the force and to reinforce the linkage of the integrins to which the bead is coupled. An increase in Filamin A abundance can be predicted to increase the resistance of the cytoskeleton to deformation created by a pullforce. The observed increase in the levels of Filamin A is consistent with the increase in cytoskeletal stiffness resulting from increased RhoA-P-MLC2/P-Cofilin signaling.

The bead-coupled integrins are tethered to the underlying cytoskeleton and to define this interaction in CCM deficient cells, passive movement rheology measurements were obtained for the passive diffusion of bead-coupled integrins across the plasma membrane. For passive movement rheology the displacement of fibronectin-coated beads in the x and y directions was recorded in the absence of applied external

force. The passive diffusion coefficient was calculated for each bead and was 1.51, 2.02, and 1.79 fold higher in shCCM1, 2 or 3 HUVECs respectively (p values 0.012, 2.94e-11, 2.34e-10 respectively; Figure 4.5G and H). This increased diffusion of integrin-coupled beads in CCM deficient cells suggest a disrupted coupling of the integrins to the cytoskeleton consistent with the disrupted RhoA activity and cytoskeletal dynamics demonstrated here.

Combined these biophysical studies define that the biomechanical profile in CCM deficient HUVECs is increased RhoA/ROCK activation in response to external force on integrin such as during cell migration and cell-cell or cell-matrix adhesion required during vascular remodeling in three dimensions. Furthermore, these data define that the functional consequence of the elevated RhoA/ROCK leads to increased cytoskeletal stiffness in response to mechanical cues consistent with CCM as a disease of disrupted RhoA/ROCK signaling and cytoskeletal dynamics.

*Knockdown of CCM1, 2 or 3 inhibits endothelial cell vessel-like tube formation and invasion of extracellular matri*x

Knockdown of CCM1, 2 or 3 in endothelial cells results in the inhibition of extracellular matrix invasion and vessel-like tube formation (Figure 4.6, Figure 4.7A*i-iv* and 4.7B). The findings define a common phenotype for loss of each of the three CCM proteins with inhibition of invasion and vessel-like tube formation providing quantitative assays to define treatments to rescue the CCM pathology. Based on the common inhibition of invasion and vessel-like tube formation, and the increased ROCK2-

dependent increase in phospho-MLC2 with knockdown of each CCM protein, we reasoned that ROCK2 was a therapeutic target to reverse the CCM phenotype.

CCM1, 2 or 3 knockdown pathology is rescued by inhibition of ROCK.

Relevant to rescue of the CCM pathology, we previously demonstrated that the small molecule ROCK inhibitor Y-27632 rescued the inhibition of endothelial cell migration resulting from shRNA knockdown of CCM2 in a scrape wound healing assay with brain microvascular endothelial cells (Crose et al., 2009). Y-27632 was used to test the role of ROCK in rescuing the loss of endothelial cell invasion of extracellular matrix (Figure 4.7iv-viii and 4.7B). The inhibition of extracellular matrix invasion resulting from CCM1, 2 or 3 knockdown was rescued by either loss of ROCK2 expression or treatment of cells with Y-27632 (Figure 4.7). CCM1 knockdown cells were only weakly rescued by Y-27632 but strongly rescued by shRNA knockdown of ROCK2. This may in part be due to the time-dependent reversal of the strong CCM1 knockdown phenotype with Y-27632 (Figure 4.2E, Figure 4.6 and see below).

Discussion

The three CCM genes are scaffold or adaptor proteins capable of forming a CCM1-2-3 protein complex for organization of proteins involved in regulating the cytoskeleton(Hilder et al., 2007). Thus, the molecular basis of CCM is fascinating in that the loss of function of a scaffold or adaptor protein is sufficient to develop the pathology (Uhlik et al., 2003; Kleaveland et al., 2009b; Whitehead et al., 2009). The function of CCM proteins was further elucidated by the discovery that RhoA becomes overexpressed with loss of CCM2 expression, and that CCM2 regulates RhoA protein

level by controlling its degradation (Crose et al., 2009, Whitehead et al., 2009). We have now shown that CCM1 and 3 proteins in addition to CCM2 are required for regulation of RhoA protein levels, and loss of CCM1, 2 or 3 each results in the pronounced increase in expression of RhoA. This result supports the critical role of the CCM protein complex in controlling RhoA expression. The RhoA biosensor allowed measurement of live cell images for RhoA activity in control and CCM1, 2 and 3 knockdown cells. Clearly, RhoA activity is increased with loss of CCM1, 2 or 3 proteins and the increased RhoA activity results in changes in regulation of ROCK and the cytoskeleton. We propose a model of CCM as a disease of disrupted cytoskeletal stability through deregulation of RhoA abundance and activity (Figure 4.8). The pronounced RhoA activity with CCM1 knockdown strongly suggests that CCM1 has a function controlling a Rho guanine nucleotide exchange factor or Rho GTPase activating protein. This difference suggests a function specific for CCM1 relative to CCM2 or 3. However, the effect of CCM1 loss of expression was not generally different than what was observed with loss of CCM2 or 3 expression for changes in phospho-MLC2 and phospho-Cofilin levels or dysregulation of invasion or vessel-like tube formation. The dysregulated RhoA/ROCK-control of cytoskeleton remodeling defined by MTC, increased Filamin A and passive rheology provide a comprehensive single-cell profile of the cytoskeleton in shCCM1,2 and 3 HUVECs and independently demonstrate a consistent similarity in the disrupted cytoskeleton response with loss of all three CCM proteins.

These findings indicate there is not simply a linear pathway of RhoA expression-ROCK activation-phosphorylation of MLC2 and Cofilin. Rather, the CCM proteins

represent a dynamic regulatory network where they are sometimes in a complex but other times found in different cellular locations (Zawistowski, 2005; Uhlik et al., 2003), consistent with common but also distinct functions. We have proposed that CCM proteins localize signaling complexes to specific cellular locations associated with actin reorganization(Crose et al., 2009; Hilder et al., 2007). This would suggest CCM proteins spatially control RhoA degradation for regulating specific physiological functions. Interestingly, activation of Rho GTPases and ROCK has also been observed in Smith-Lemli-Opitz syndrome (Jiang et al., 2010), suggesting that dysregulation of this signaling axis has major pathophysiological implications in different human diseases.

Surgical resection is currently the standard treatment for symptomatic CCM, a highly invasive procedure with significant risk to the patient (Awad, 2005). In addition, lesions located in critical areas such as the brainstem or basal ganglia are more likely to exhibit a poor natural history, yet no treatment exists because they are surgically inaccessible. The discovery that inhibition of ROCK, a kinase activated by RhoA, is able to rescue dysregulated endothelial cell physiology resulting from loss of CCM1, 2 or 3 expression provides, for the first time, a pharmacological approach using a small molecule kinase inhibitor for treatment of CCM. The function of RhoA and ROCK in promoting vascular permeability is consistent with the dysregulated RhoA-ROCK signaling axis being important in promoting CCM pathology. Thus, ROCK inhibitors are clearly potential therapeutics for the treatment of CCM. Studies have shown that two ROCK inhibitors, Fasudil and Y-27632, are reasonably well tolerated in animals (İnan and Büyükafşar, 2008). In fact, Fasudil has been used in Japan for treatment of

cerebral vasospasm following subarachnoid hemorrhage since 1995 (Yamazaki et al., 2009), indicating ROCK inhibitors can be tolerated in humans.

Given that the RhoA-ROCK signaling network is clearly dysregulated in CCM, there is still much to learn about the RhoA activation and inactivation cycle and how it is dysregulated in CCM endothelial cells. Questions also remain regarding the CCM protein complex and control of signaling networks including the potential involvement of additional kinases that could contribute to the CCM pathology and be pharmacologically targeted for treatment of CCM. For example, mitogen activated protein kinase kinase 3 (MEKK3), a MAP3K that regulates ERK5, JNK and NF□B, is in the CCM protein complex and is important for regulating responses to inflammatory cytokines such as IL-1 (Hilder et al., 2007; (Yamazaki et al., 2009). Significantly, it appears a pharmacological small molecule treatment to control CCM is a real possibility.

A.

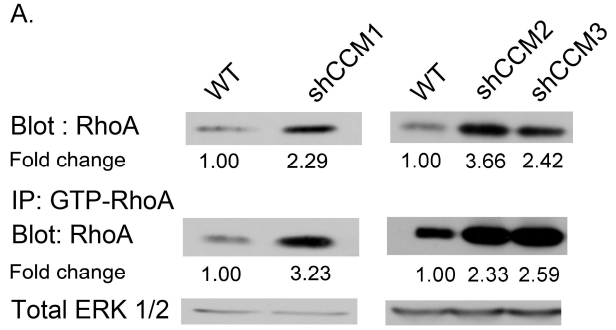

B.

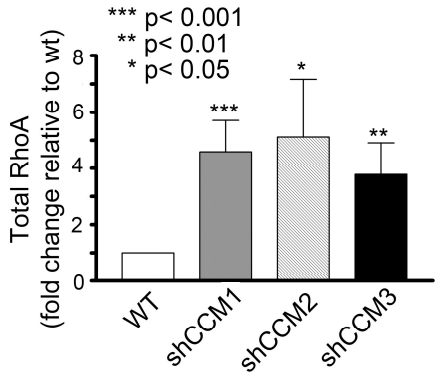

C.

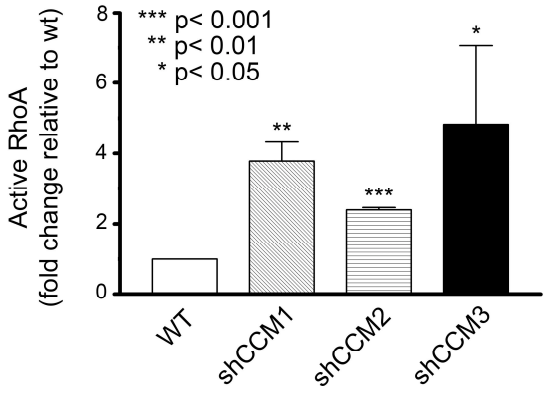

D.

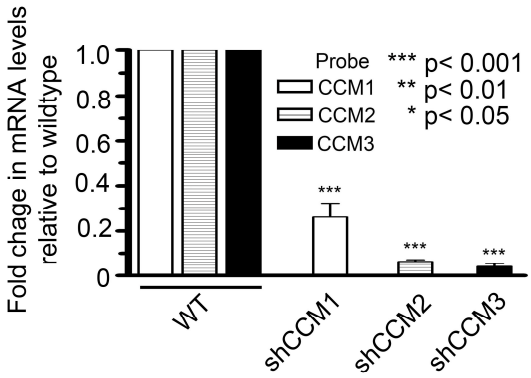

E.

RNA message levels of CCM1, 2 and 3 in shCCM1, 2 and 3 HUVEC assessed by QRT PCR

shCCM1 HUVECs

Cell line	C_T n1	C_T n2	Ave C_T	*Probe:CCM1* Pvalue Ave C_T in WT vs shCCM1 cells	Fold change relative to WT n1	n2	Average
Wildtype	25.85	25.89	25.87	n/a	1.00	1.00	1.00
shCCM1	28.26	27.95	28.10	0.00028 (***)	0.21	0.27	0.24

shCCM2 HUVECs

Cell line	C_T n1	C_T n2	Ave C_T	*Probe:CCM2* Pvalue Ave C_T in WT vs shCCM1 cells	Fold change relative to WT n1	n2	Average
Wildtype	21.33	21.17	21.25	n/a	1.00	1.00	1.00
shCCM2	25.95	25.61	25.78	1.10E-08 (***)	0.06	0.07	0.07

shCCM3 HUVECs

Cell line	C_T n1	C_T n2	Ave C_T	*Probe:CCM2* Pvalue Ave C_T in WT vs shCCM1 cells	Fold change relative to WT n1	n2	Average
Wildtype	24.64	23.91	24.28	n/a	1.00	1.00	1.00
shCCM3	28.97	27.67	28.32	1.82E-07 (***)	0.04	0.07	0.05

F.

RNA message levels of RhoA and CCM1, 2 and 3 in shCCM1, 2 and 3 HUVEC assessed by QRT PCR

shCCM1 HUVECs

Cell line	C_T n1	C_T n2	Ave C_T	*Probe:CCM1* Pvalue Ave C_T in WT vs shCCM1 cells	Fold change relative to WT n1	n2	Average
Wildtype	24.97	24.96	24.96	n/a	1.00	1.00	1.00
shCCM1	27.05	27.59	27.32	0.0129 (*)	0.24	0.20	0.22

Cell line	C_T n1	C_T n2	Ave C_T	*Probe:RhoA* Pvalue Ave C_T in WT vs shCCM1 cells	Fold change relative to WT n1	n2	Average
Wildtype	18.86	18.61	18.74	n/a	1.00	1.00	1.00
shCCM1	18.86	18.69	18.78	0.82 (ns)	1.00	1.18	1.09

shCCM2 HUVECs

Cell line	C_T n1	C_T n2	Ave C_T	*Probe:CCM2* Pvalue Ave C_T in WT vs shCCM1 cells	Fold change relative to WT n1	n2	Average
Wildtype	21.65	21.91	21.78	n/a	1.00	1.00	1.00
shCCM2	26.57	26.97	26.61	0.0060 (**)	0.05	0.05	0.05

Cell line	C_T n1	C_T n2	Ave C_T	*Probe:RhoA* Pvalue Ave C_T in WT vs shCCM1 cells	Fold change relative to WT n1	n2	Average
Wildtype	18.86	18.61	18.74	n/a	1.00	1.00	1.00
shCCM2	18.59	18.96	18.78	0.89 (ns)	1.49	1.26	1.37

shCCM3 HUVECs

Cell line	C_T n1	C_T n2	Ave C_T	*Probe:CCM3* Pvalue Ave C_T in WT vs shCCM1 cells	Fold change relative to WT n1	n2	Average
Wildtype	24.14	23.95	24.05	n/a	1.00	1.00	1.00
shCCM3	27.90	28.14	28.02	0.0015 (**)	0.07	0.06	0.06

Cell line	C_T n1	C_T n2	Ave C_T	*Probe:RhoA* Pvalue Ave C_T in WT vs shCCM1 cells	Fold change relative to WT n1	n2	Average
Wildtype	18.86	18.61	18.74	n/a	1.00	1.00	1.00
shCCM3	18.23	18.57	18.78	0.26 (ns)	1.38	1.03	1.21

Figure 4.1: RhoA abundance and activity are increased in shCCM1, 2 and 3 human endothelial cells. (A) Blots show that the abundance of total and active RhoA are increased with loss of CCM1, 2 and 3 in HUVECs. (B) Bar graph shows that the average fold increase of total RhoA is 4.58 (p value 0.00091), 5.11 (p value 0.013) and 3.78 (p value 0.0018) in shCCM1, 2 and 3 HUVECs respectively based on minimum of five independent western blot experiments. (C) Bar graph shows that the average fold increase in active RhoA is 4.87 (p value 0.0012), 6.72 (p value $2.95x10^{-6}$) and 7.25 (p value 0.048) in shCCM1, 2 and 3 HUVECs respectively based on two independent immunoprecipitation experiments. (D) Bar graph shows mRNA levels of CCM1, 2 and 3 in wildtype HUVECs and in shCCM1, 2 or 3 HUVECs. Knockdown was assayed by RT PCR and the relative mRNA levels for CCM1, CCM2, or CCM3 in shCCM1, 2, or 3 cells were 0.24 (p value 0.00028), 0.07 (p value $1.11x10^{-8}$), and 0.04 (p value $1.82x10^{-7}$) relative to levels in wildtype cells. Bar graph represents average from three independent experiments. (E) Table shows the mRNA detection Ct threshold for each CCM1, 2 or 3 before and after knockdown were within the dynamic range of the RT PCR technology, which is between 16 and 30 Ct. Results from two sets of independently generated cell lines are shown. The p value of the statistical significance in the difference of Cts for wildtype and knockdown cells is also shown. The column 'Fold change relative to WT' shows the decrease in mRNA in knockdown cells relative to wildtype cells. (F) Table displays the Ct mRNA transcript levels of RhoA in wildtype and shCCM1, 2 and 3 HUVECs. The Ct levels of CCM1, 2 or 3 in the same cells are also shown to demonstrate presence of knockdown. Results from two sets of independently generated knockdown cell lines are shown.

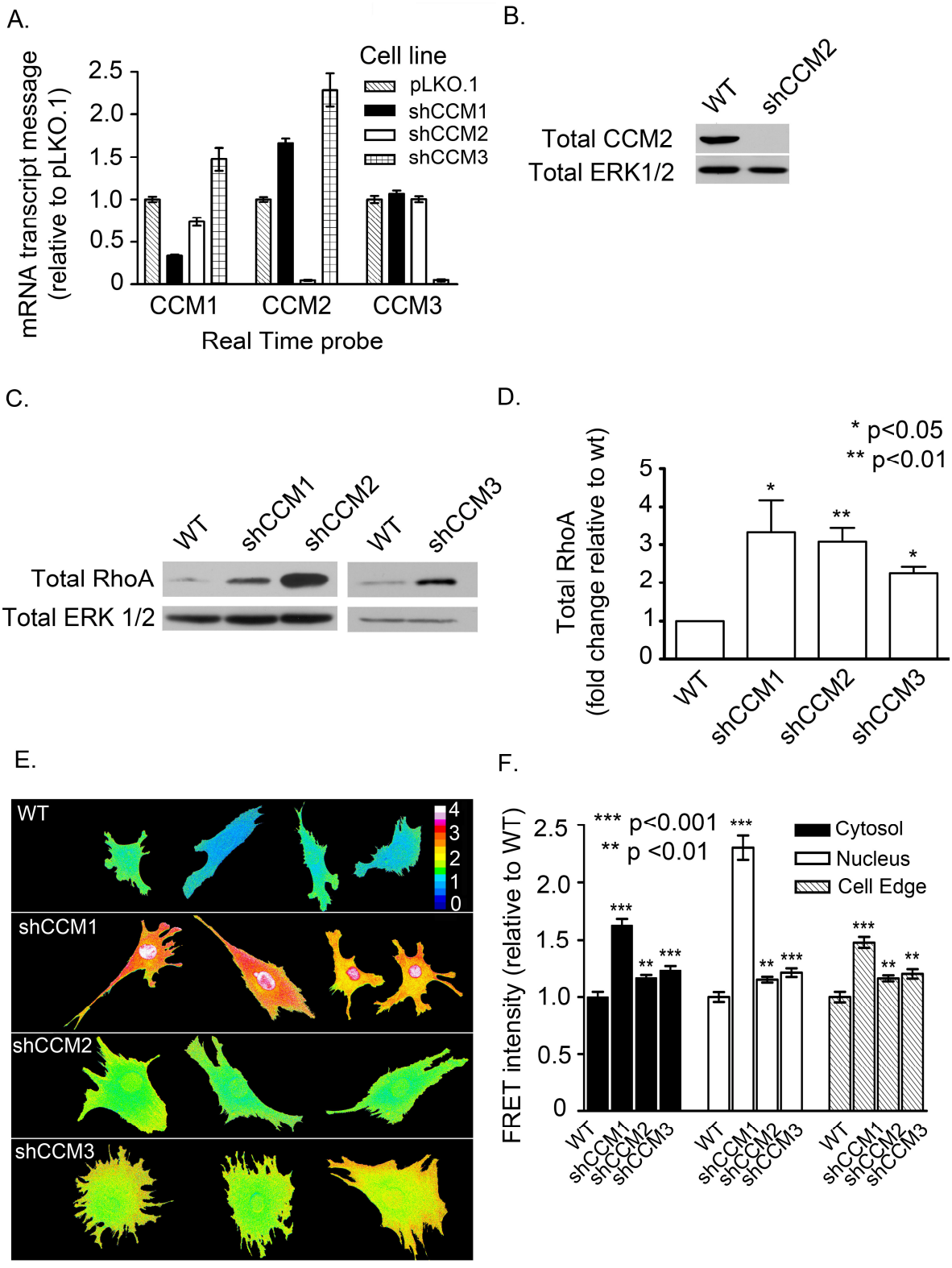
A.
mRNA transcript message (relative to pLKO.1)
2.5
2.0
1.5
1.0
0.5
0
Cell line
pLKO.1
shCCM1
shCCM2
shCCM3
CCM1
CCM2
CCM3
Real Time probe
B.
WT
shCCM2
Total CCM2
Total ERK1/2
C.
WT
shCCM1
shCCM2
WT
shCCM3
Total RhoA
Total ERK 1/2
D.
* p<0.05
** p<0.01
Total RhoA (fold change relative to wt)
5
4
3
2
1
0
WT
shCCM1
shCCM2
shCCM3
E.
WT
shCCM1
shCCM2
shCCM3
4
3
2
1
0
F.
*** p<0.001
** p <0.01
FRET intensity (relative to WT)
2.5
2.0
1.5
1.0
0.5
0
Cytosol
Nucleus
Cell Edge
WT
shCCM1
shCCM2
shCCM3

Figure 4.2: RhoA activity is increased in shCCM1, 2 or 3 mouse endothelial cells. (A) Graph shows RT PCR quantitation of CCM1, 2 or 3 mRNA transcript in wildtype, shCCM1, 2 or 3 MEECs. Expression of CCM1, 2, and 3 mRNA in shCCM1, 2, and 3 cells is knocked down respectively by 70, 96 and 95% relative to pLKO.1 control cells. Graph represents the means ± SEM of three independent experiments performed in triplicate. (B) Western blot of WT and shCCM2 MEECs shows that endogenous CCM2 protein signal is lost in shCCM2 cells. (C) The total RhoA levels in shCCM MEECs is increased. (D) Bar graph is quantitation of total RhoA levels in shCCM MEECs from three independent experiments (E) WT, shCCM1, 2 or 3 MEECs were infected with a FRET-based RhoA biosensor, where activation of RhoA leads to FRET. The measured FRET signal has been pseudocolored, where blue indicates low FRET and low RhoA activity, and red/white indicates high FRET and high RhoA activity. RhoA activity is increased at the cell edge (defined as 1.5 □m width at the edge of the cell), the cytoplasm and nucleus of shCCM1, 2 or 3 endothelial cells. (F) Bar graph shows the fold change in FRET intensity for the cytoplasm, nucleus and cell edge of shCCM1, 2 or 3 relative to WT control cells. Cytoplasm fold FRET increase: shCCM1 cells=1.62 (p value 4e-11), shCCM2 cells=1.16 (p value 0.001), shCCM3=1.23 (p value 0.0003). Nuclear fold FRET increase: shCCM1 cells=2.33 (p value 4.8e-11), shCCM2=1.16 (p value 0.002), shCCM3=1.23 (p value 0.0002). Cell edge fold FRET increase: shCCM1 cells=1.48 (p value 5e-9), shCCM2 cells=1.16 (p value 0.002), shCCM3 cells=1.20 (p value 0.002). Data represents the mean ± SEM for minimum of 25 cells in two independent experiments. Data in Figure 4.2A is courtesy of Christopher F. Dibble, UNC-CH.

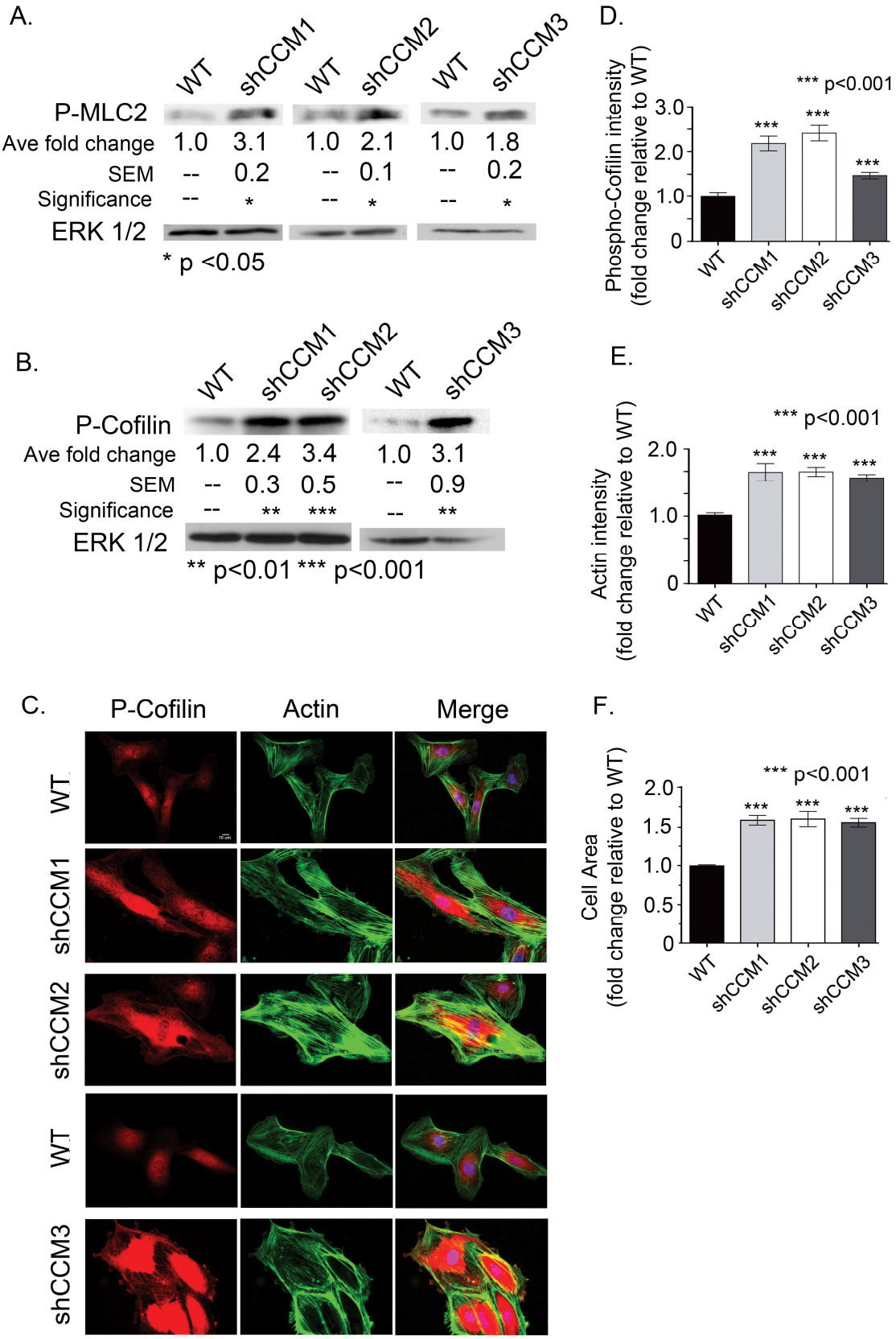
A.
WT
shCCM1
WT
shCCM2
WT
shCCM3
P-MLC2
Ave fold change 1.0 3.1 1.0 2.1 1.0 1.8
SEM -- 0.2 -- 0.1 -- 0.2
Significance -- * -- * -- *
ERK 1/2
* p <0.05
B.
WT
shCCM1
shCCM2
WT
shCCM3
P-Cofilin
Ave fold change 1.0 2.4 3.4 1.0 3.1
SEM -- 0.3 0.5 -- 0.9
Significance -- ** *** -- **
ERK 1/2
** p<0.01 *** p<0.001
C.
P-Cofilin
Actin
Merge
WT
shCCM1
shCCM2
WT
shCCM3
D.
Phospho-Cofilin intensity (fold change relative to WT)
*** p<0.001
3.0
2.0
1.0
0
WT
shCCM1
shCCM2
shCCM3
E.
Actin intensity (fold change relative to WT)
*** p<0.001
2.0
1.0
0
WT
shCCM1
shCCM2
shCCM3
F.
Cell Area (fold change relative to WT)
*** p<0.001
2.0
1.5
1.0
0.5
0
WT
shCCM1
shCCM2
shCCM3

Figure 4.3: Loss of CCM1, 2 and 3 leads to increased P-MLC2, P-Cofilin and actin stress fibers in human endothelial cells. (A and B) Western blots show a statistically significant increase in the levels of P-MLC2 and P-Cofilin in shCCM1, 2 or 3 HUVECS. (C and D) Immunofluorescent staining for P-Cofilin in shCCM1, 2 or 3 HUVECs validates the increase in P-Cofilin. (C and E) Immunofluorescent staining for actin shows the increase in stress fibers in shCCM1, 2 or 3 HUVECs. (F) The cell size of shCCM1, 2 or 3 HUVECs was measured based on the actin staining and is significantly larger relative to control cells.

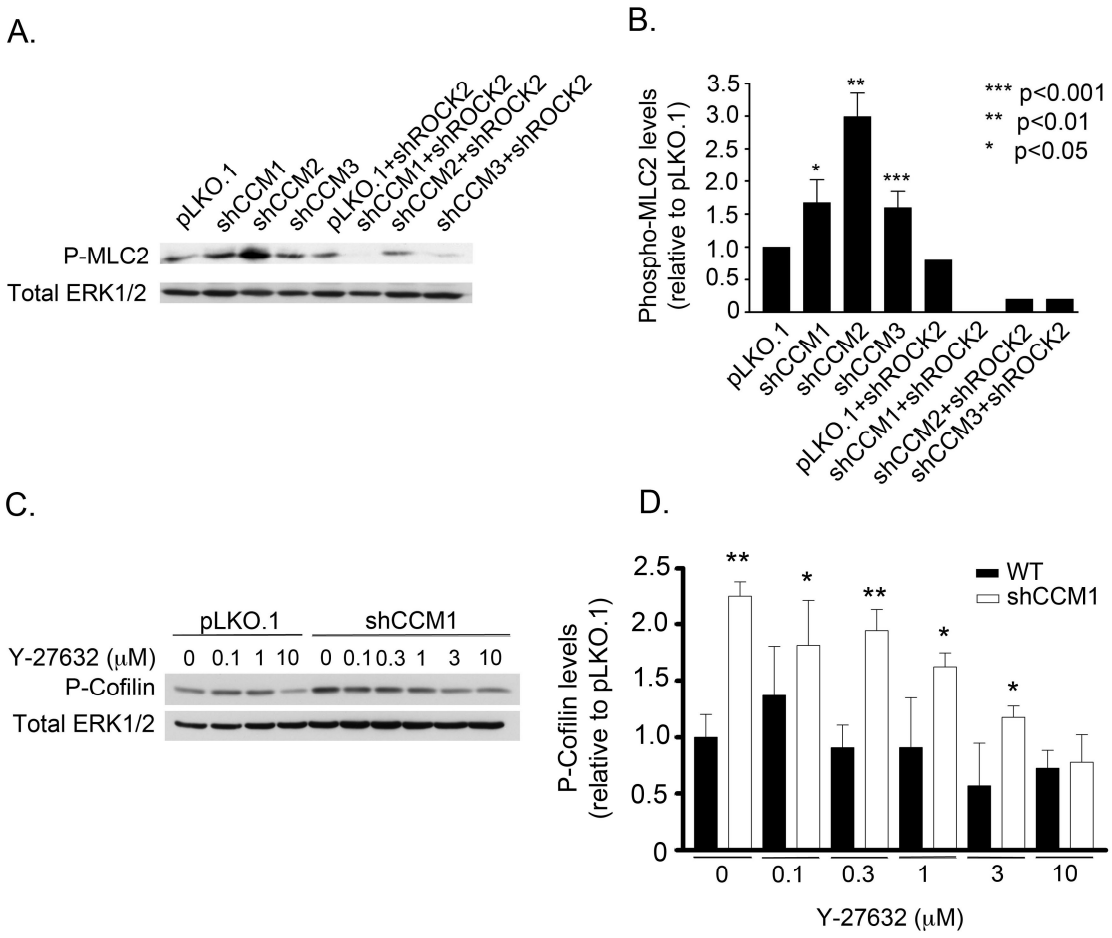

Figure 4.4: Inhibition of ROCK reverses the increased P-MLC2 and P-Cofilin in CCM endothelial cells. (A) Western blots showing an increase in phospho-MLC2 in shCCM1, 2 or 3 mouse endothelial cells, which is lost upon shRNA knockdown of ROCK2. (B) Bar graph shows the abundance of phospho-MLC2 in shCCM1, 2 or 3 cells increases respectively 1.7, 3.0 and 1.6-fold relative to control pLKO.1 cells (graph represents average of three independent experiments). Upon shRNA knockdown of ROCK2, this abundance decreases below detectable levels, 50 and 90% respectively for shCCM1, 2 or 3 relative to control pLKO.1 empty shRNA vector. (C) Dose-dependent decrease in P-Cofilin in pLKO.1 or shCCM1 human endothelial cells treated with increasing concentrations of Y-27632. (D) Bar graph of the dose-dependent decrase in P-Cofilin with Y-27632 treatment of pLKO.1 and shCCM1 human endothelial cells (graph represents average of three independent experiments, where shCCM1 cells were derived three independent times).

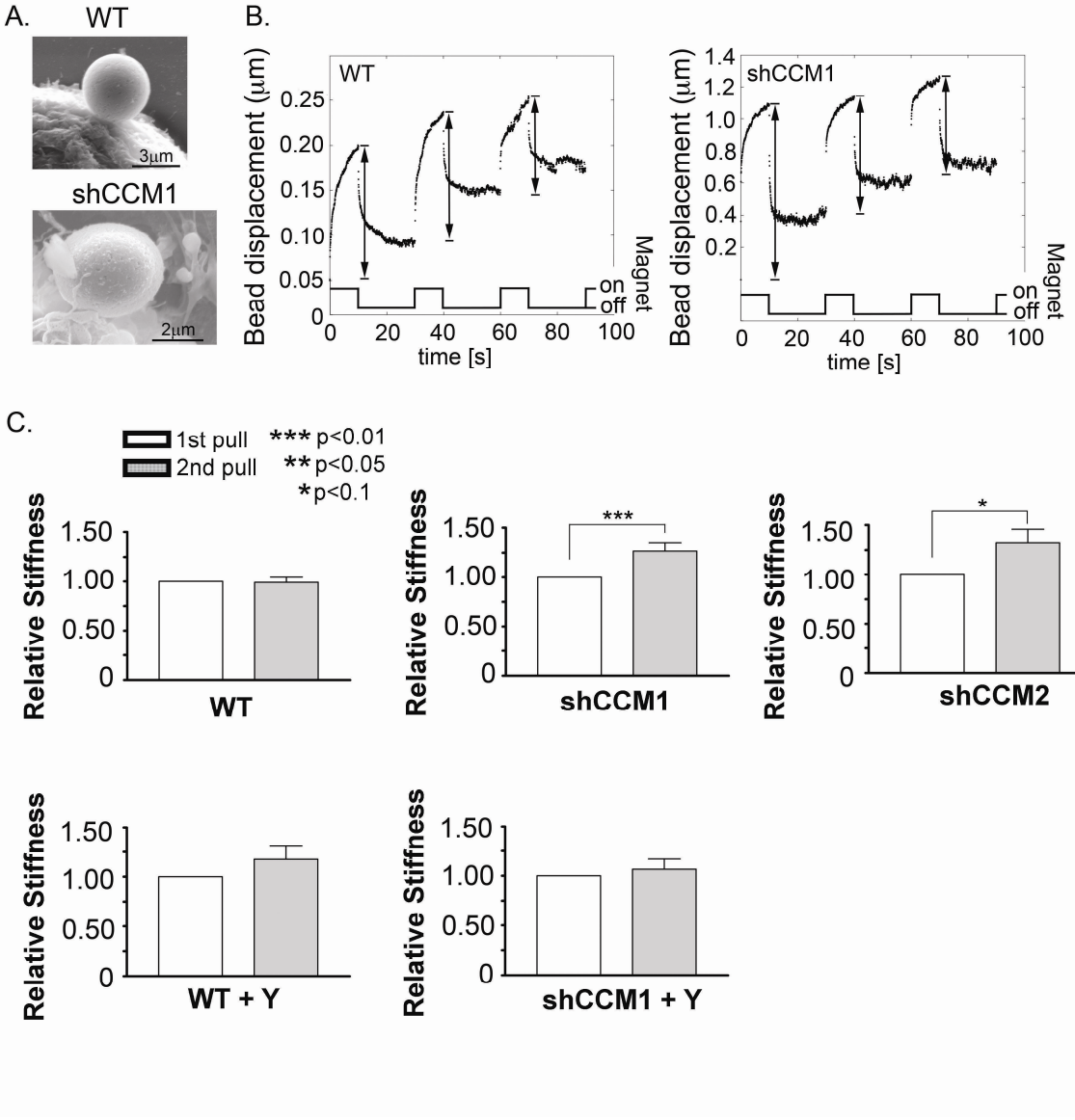
A.
WT
3μm
shCCM1
2μm
B.
WT
Bead displacement (μm)
0.25
0.20
0.15
0.10
0.05
0
0 20 40 60 80 100
time [s]
Magnet
on
off
shCCM1
1.4
1.2
1.0
0.8
0.6
0.4
0.2
C.
1st pull
2nd pull
*** p<0.01
** p<0.05
* p<0.1
Relative Stiffness
1.50
1.00
0.50
0
WT
shCCM1
shCCM2
WT + Y
shCCM1 + Y

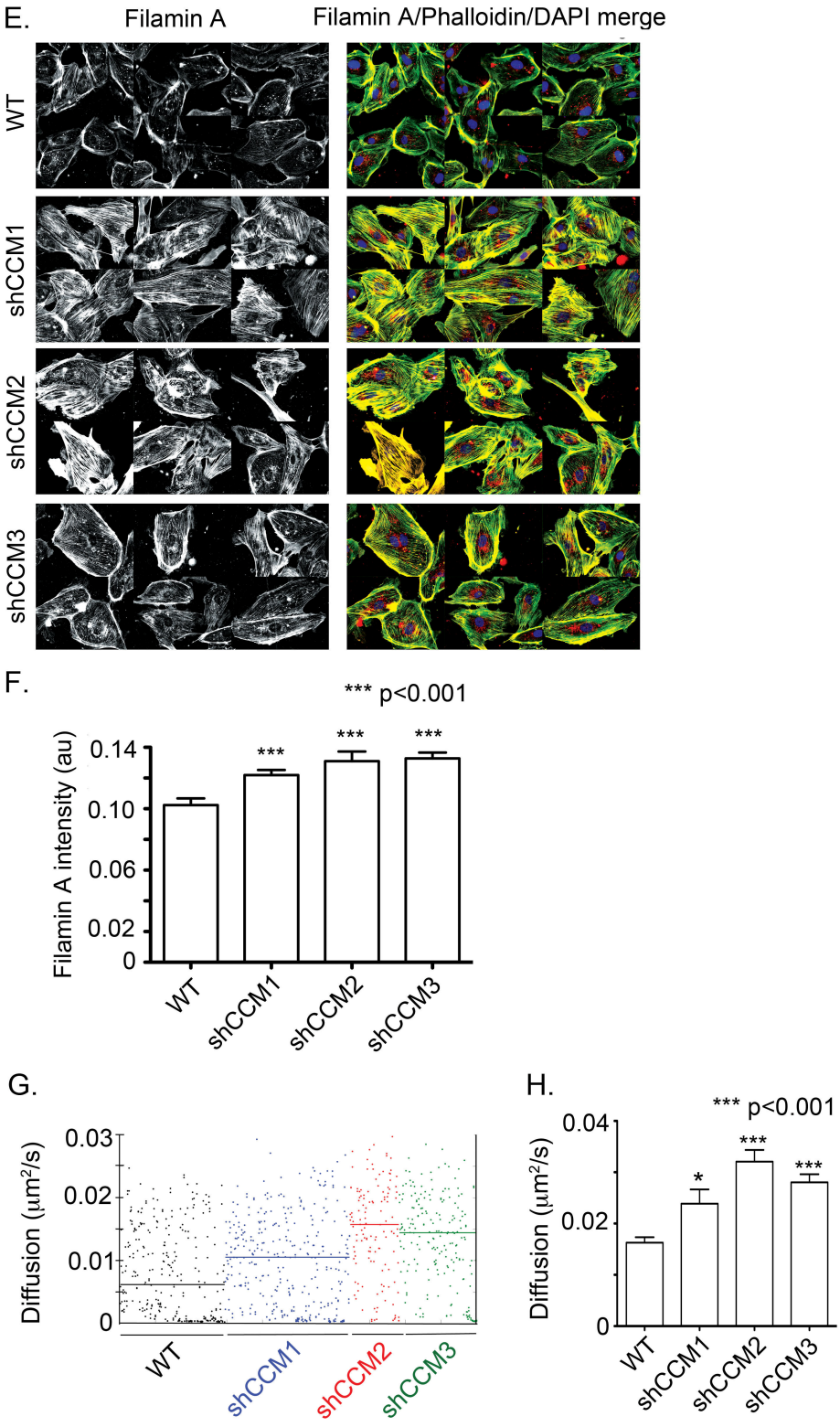
E.
Filamin A
Filamin A/Phalloidin/DAPI merge
WT
shCCM1
shCCM2
shCCM3
F.
*** p<0.001
Filamin A intensity (au)
0.14
0.10
0.06
0.02
0
***
***
***
WT
shCCM1
shCCM2
shCCM3
G.
Diffusion (μm²/s)
0.03
0.02
0.01
0
WT
shCCM1
shCCM2
shCCM3
H.
*** p<0.001
Diffusion (μm²/s)
0.04
0.02
0
*
***
***
WT
shCCM1
shCCM2
shCCM3

Figure 4.5: The biomechanical phenotype of CCM deficient human endothelial cells is increased RhoA/ROCK signaling and increased cytoskeletal stiffening. (A) Atomic Force Microscopy shows the similarly surface-bound beads on top of wildtype and shCCM1 HUVECs. (B) The displacement profile of beads on wildtype or shCCM1 cells in response to three consecutive magnetic pulls with 20second no-force breaks in between pulls. The distance traveled by beads on wildtype cells begins to decrease at the third pull with little decrease between the first and second pulls, whereas the cytoskeleton of shCCM1 cells begins to respond by stiffening by the second pull. (C) Bar graphs quantitate the relative stiffness of the cells during the first and second pulls, where the increase in stiffness at the second pull is statistically significant for shCCM1 and shCCM2 cells. (D) Bar graphs show the decreased response in cytoskeletal stiffening in shCCM1 cells treated with Y-27632 consistent with the established role for RhoA in the regulation of the stiffening response. (E and F) Immunofluorescent staining and quantitation for Filamin A (red), Rhodamine-Phalloidin (green) and DAPI (blue) shows an increase in the signal for Filamin A and Rhodamine Phalloidin with loss of CCM protein expression. Note the increased cell size with loss of CCM proteins. (G and H) A distribution of diffusion coefficients established by passive rheology for individual beads on top of wildtype or CCM knockdown cells. The passive diffusion of shCCM1,2 or 3 cells is respectively 1.51, 2.01 and 1.79 fold higher than for wildtype cells (p values 0.012, $2.94x10^{-11}$, $2.34x10^{-10}$ respectively). For all panels, data representative of minimum of three independent experiments where knockdown cell lines were independently derived for each separate experiment. Scanning Electron Microscopy images are courtesy of Alekhya Yechoor and Alexander Nelson, UNC-CH.

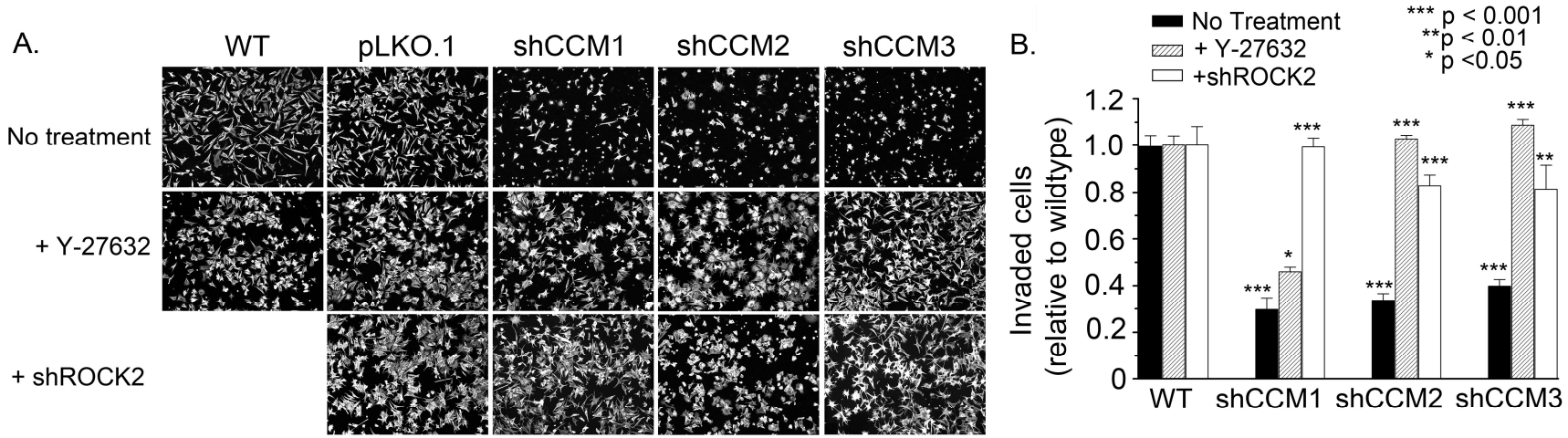

Figure 4.6: ROCK inhibition with Y-27632 or shRNA rescues the invasion defect in shCCM1, 2 or 3 mouse endothelial cells. (A) shCCM1, 2 or 3 MEECs were seeded in the top of a Boyden chamber invasion chamber. Cells invaded to the bottom of the membrane were stained with Rhodamine phalloidin and imaged. Five images per membrane were taken and one image per condition is shown. Invasion of shCCM1, 2 or 3 cells is decreased relative to WT, but rescued upon treatment with 10μM Y-27632 or upon shRNA knockdown of ROCK2. (B) Bar graph showing the fold change in the number of invaded shCCM cells relative to pLKO.1. Invasion in shCCM1, 2 or 3 cells is decreased respectively 70%, 70% and 60% relative to pLKO.1 cells. Data represents mean ± SEM for minimum of three independent experiments.

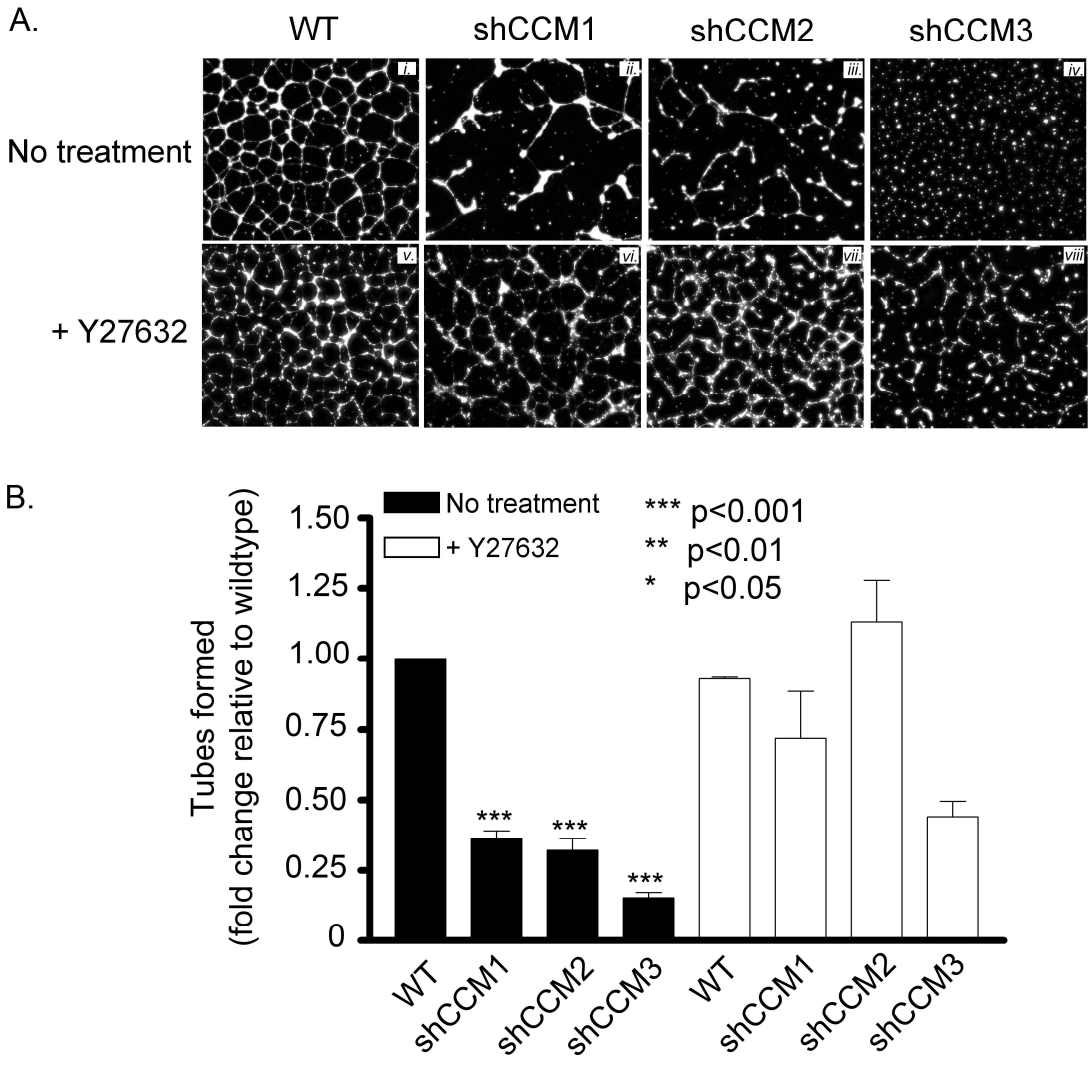

Figure 4.7: The ROCK inhibitor Y-27632 rescues the impaired tube formation of shCCM1, 2 and 3 human endothelial cells. (A*i*) Wildtype HUVECs self-assemble in lumen-like tube structures when plated on matrigel *in vitro*. (A*ii* through *iv*) shCCM1, 2 or 3 HUVECs fail to form tube like structures. (A*v* through *viii*) Treatment with Y-27632 rescues the impaired tube formation in shCCM1, 2 and 3 cells. Bar graph shows the fold change in number of tubes formed relative to wildtype. Tube formation in shCCM1, 2 and 3 cells is respectively 0.36, 0.32 and 0.15 fold relative to wildtype (p values are 0.0005, 0.02, 0.03 respectively). Tube formation in shCCM1, 2 and 3 cell treated with Y-27632 is respectively 0.72, 1.13 and 0.44 fold relative to wildtype (p values are 0.39, 0.35, 0.08 respectively). Bar graph represents minimum of two independent experiments.

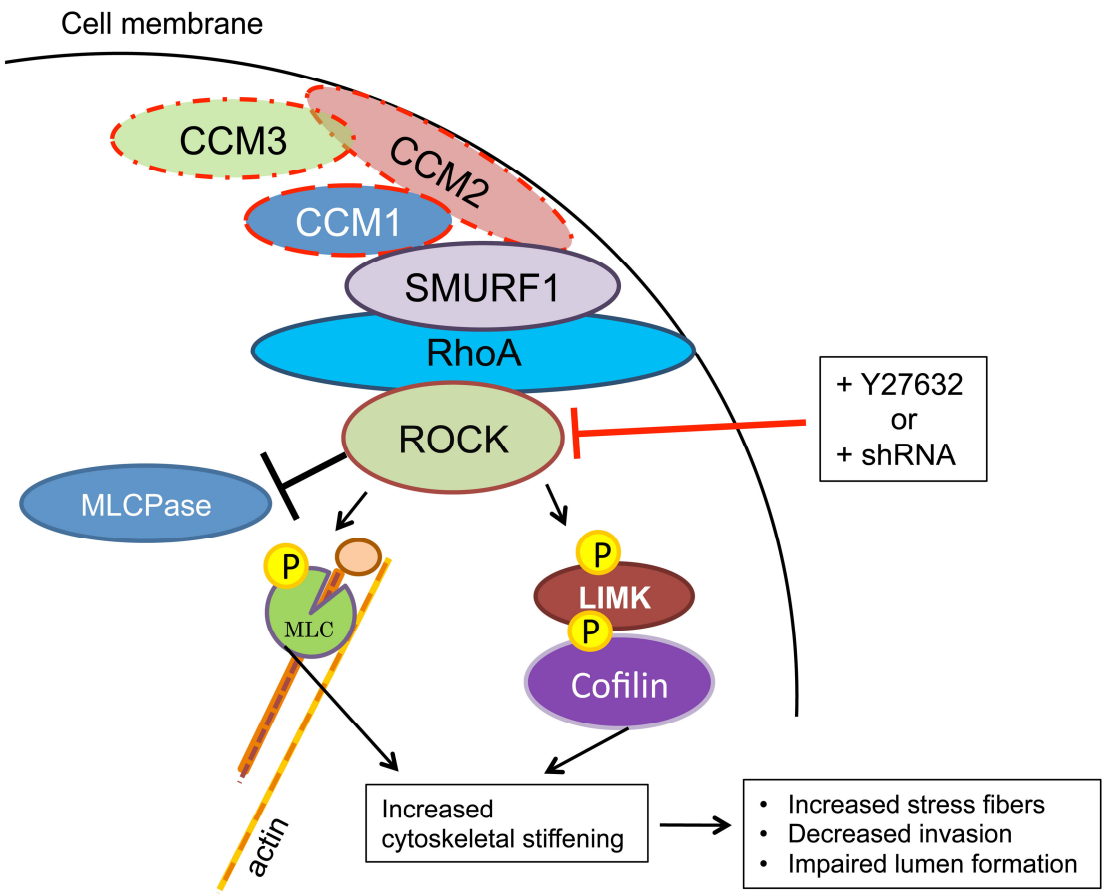

Figure 4.8: Proposed model for CCM as a disease of increased RhoA abundance and activity. CCM1, 2 and 3 coordinately regulate Smurf1-dependent degradation of RhoA. Loss of CCM1, 2 or 3 increases RhoA abundance and activity and leads to increased ROCK activity, increased phosphorylation of myosin light chain (MLC) and Cofilin which co-regulate cytoskeletal turnover. This leads to functional defects including increased cytoskeletal stiffening in response to mechanical force, increased stress fiber formation, decreased invasion and impaired tube-like lumen formation. These functional defects are rescued by ROCK inhibition through Y-27632 or shRNA knockdown.

CHAPTER V

CEREBRAL CAVERNOUS MALFORMATIONS PROTEINS CONTROL SMURF2-MEDIATED DEGRADATION OF RAP1 IN ENDOTHELIAL CELLS

Introduction

The only known common molecular pathway for CCM1, 2 and 3 in endothelial cells is based on the finding of Crose *et al.* that CCM2 is a binding partner for the E3 ubiquitin ligase Smurf1, where CCM2 regulates the Smurf1-mediated degradation of RhoA. The functional significance of the CCM2-Smurf1 interaction is that CCM2 targets Smurf1 to sites of active RhoA at the plasma membrane, where loss of CCM2 expression led to the increased abundance and activity of RhoA (Crose et al., 2009). Furthermore, CCM2 deficient cells displayed increased stress fiber formation and decreased migration consistent with an increase in RhoA activity (Crose et al., 2009). Subsequently we showed that consistent with a common molecular function as a ternary complex, knockdown of CCM1, 2 and 3 by shRNA leads to the increased protein abundance and activity of RhoA (Borikova et al., 2010b). The functional consequence of this increase in RhoA activity was increased phosphorylated myosin light chain 2 (P-MLC2), decreased invasion and impaired self-assembly in lumen-like tubes *in vitro* for shCCM1, 2 or 3 endothelial cell where inhibition of Rho Kinase (ROCK), a downstream effector of RhoA, reverses these

defects(Borikova et al., 2010b). The vascular leak of CCM mice was rescued upon treatment with the small molecule inhibitor for RhoA Fasudil (McDonald et al., 2012; Stockton et al., 2010). These studies have strongly established that Smurf1-dependent dysregulation of RhoA protein levels is an underlying molecular cause for CCM.

To date regulation of the RhoA-ROCK pathway remains the only identified common molecular pathway for CCM1, 2 and 3. Rap1 is a small GTPase of the Ras family that regulates multiple endothelial cell functions including actin remodeling, endothelial tube formation, establishment of polarity and vascular leak (Kooistra et al., 2006; Kooistra et al., 2005). Several groups have independently defined Rap1 as a binding partner for CCM1 (Glading et al., 2007) however little remains known about the functional significance of the interaction of CCM1 and Rap1. Morpholino-mediated knockout of the *Rap1b* isoform of Rap1 in zebrafish embryos causes intracranial hemorrhage in 70% of the fish. The combined morpholino knockout of *Rap1b* and *CCM1* at morpholino concentrations that alone produce a defect in less than 10% of embryos leads to intracranial hemorrhage in 30% of the injected embryos and cardiac blockage in 70% of the injected fish (Gore et al., 2008), establishing that Rap1b and CCM1 participate in a common molecular pathway. CCM1 binds both Rap1a and Rap1b isoforms of Rap1, suggesting a general Rap1 regulation by CCM1. We set out to define the functional significance of Rap1 in CCM biology. We show that similarly to the coordinate regulation of the RhoA through Smurf1, CCM1, 2 and 3 coordinately regulate the abundance and activity of Rap1 through a novel CCM2-Smurf2 interaction, where Smurf2 has previously been

defined as an E3 ligase for Rap1 (Schwamborn et al., 2007). Rap1 is a negative regulator of RhoA through the activation of the RhoGAP Arap3. *Arap3*$^{-/-}$ mice die at E11 due to endothelial cell autonomous defect that leads to clusters of cavernous vessels with little branching that are most prominently observed in the cerebral vasculature (Gambardella et al., 2010). We show that cAMP-mediated activation of Rap1 leads to Arap3 RhoGAP-dependent inactivation of RhoA in CCM1, 2 and 3 cells. However, Arap3 RhoGAP-mediated decrease in RhoA activity is sufficient to rescue the tube formation defect in shCCM1 cells but not shCCM2 or shCCM3 cells suggesting that Smurf1-mediated inactivation of RhoA is required for the regulation of RhoA in CCM.

Much emphasis has been placed on understanding the regulation of small GTPases through Guanine Exchange Factors (GEF) and GTPase activating proteins (GAP), however an equally necessary role for regulation through E3 ubiquitin ligases has began to emerge. The stepwise process of protein ubiquitination through E1-E2-E3 ligases targets proteins for degradation through the ubiquitin proteasome system or targets the protein for a specific subcellular location. To date only 2 E1 and 30 E2 ligases have been identified, whereas the number of known E3 ligases exceeds 600 (Rotin and Kumar, 2009; Bernassola et al., 2008). This has indicated that E1s and E2s show little target specificity, whereas E3s regulate the degradation or localization of a specific set of proteins. Several studies have shown that E3-mediated degradation of small GTPases is a regulatory mechanism for GTPase signaling. siRNA-mediated knockdown of Smurf1 in epithelial cells has been shown to not only increase RhoA abundance but to increase the levels of GTP-RhoA, P-

MLC2 and stress fiber formation, with a decrease in cell migration (Sahai et al., 2007; Rotin and Kumar, 2009; Bernassola et al., 2008). Synaptopodin is an adaptor protein which competes with Smurf1 for RhoA binding. Knockdown of synaptopodin leads to decreased RhoA abundance - due to increased Smurf1-mediatd RhoA degradation - and decreased stress fiber formation and increased migration. Reversely, overexpression of synaptopodin leads to increase in total and GTP-RhoA(Asanuma et al., 2006). These studies provide evidence that aberrant degradation of RhoA leads not only to aberrant overall abundance of RhoA but also to a parallel change in the levels of the active GTPase, suggesting that E3 ligases are an independent mechanism for the regulation of small GTPase activity. An additional level of regulation of signaling downstream of effector targets for E3 ligases is through the E3-exerted fine control of the special distribution of targets. During neuronal maturation axon specification requires the localized activity of Rap1 in a single neurite, which eventually becomes the axon. Smurf2 mediates the degradation of Rap1 in all but one of the neurites, which subsequently matures as an axon. In combination with our previously published findings, the work presented here delineates CCM is a disease of disrupted E3 ligase activity and subsequent disrupted RhoA and Rap1 regulation of endothelial cell functions.

Results

Loss of CCM1, 2 or 3 leads to increased total Rap1 protein

shRNA mediated knockdown of CCM1, 2 and 3 in HUVECs was established as previously described (Figure 4.1E). Knockdown of CCM1, 2 or 3 in HUVECs led respectively to the 3.83, 3.98 and 3.41 fold increased in Rap1 protein levels in a

miminum of five independent experiments (p values respectively 0.0001, 0.0013, and 0.0016 Figure 5.1A and B). Rap1 protein levels were increased respectively 7.43, 8.87 and 7.58 fold in CCM1, 2 and 3 MEECs (Figure 5.1C and D) and 3.95, 5.05 and 3.62 fold in human endothelial progenitor cells (EPC; p values respectively 0.0001, 0.03, 0.02; Figure 5.1E and F) in two independent experiments. Although two isoforms of Rap1 are known, Rap1a and Rap1b, currently available antibodies do not distinguish the two and the data herein report an increase in the combined population of Rap1a and Rap1b. New knockdown cell lines were created for each independent experiment in HUVECs, and CCM knockdown EPCs were created from two different human donors. Loss of CCM1, 2 or 3 expression in three independent endothelial cell lines consistently caused the increased abundance of Rap1 indicating that CCM protein regulation of Rap1 abundance is a general endothelial event and a common function for CCM1, 2 and 3. To date RhoA is the only identified common effector for CCM1, 2 and 3. While each of the CCM proteins has been individually linked with several different signaling factors the fact that loss of function in any one of the CCM genes leads to pathogenesis and that CCM1, 2 and 3 form a ternary complex suggests that pathogenesis results from the loss of a common molecular function for CCM1, 2 and 3. Defining regulation of Rap1 abundance as a common molecular role of CCM1,2 and 3 establishes a new signaling paradigm in CCM pathogenesis.

To establish the mechanism for this increase in Rap1 abundance with loss of CCM proteins, the mRNA transcript levels of Rap1a and Rap1b were measured in CCM protein knockdown HUVECs. In all three CCM knockdown cell lines the

message levels of both Rap1a and Rap1b relative to wildtype cells remained unchanged (Figure 5.1G and H). Based on two independently generated sets of CCM1, 2 or 3 knockdown cell lines, the Ct detection threshold cycles for Rap1a mRNA in shCCM1, 2 and 3 were respectively 0.98, 1.06 and 0.96 fold different from the Ct detection cycle in wildtype cells (p values 0.59, 0.54 and 0.69 respectively). Similarly, the Ct threshold cycles for Rap1b in shCCM1, 2 and 3 cells were respectively 0.91, 1.72 and 1.08 fold different from the Ct detection cycle in wildtype cells (p values 0.65, 0.64 and 0.73). The slight increase in Rap1b transcript in shCCM2 cells consistently occurred in both independently generated shCCM2 cell lines assayed, however this elevation in transcript was not statistically significant with a p value of 0.64. These findings indicated that the increased Rap1 protein levels are not due to an increase in Rap1 translation but possibly due to a dysregulation of Rap1 degradation or post-transcriptional regulation of Rap1 mRNAs.

CCM2 binds the E3 ubiquitin ligase Smurf2

The interaction between CCM2 and the RhoA ubiquitin ligase Smurf1 is mediated through the Phosphotyrosine Binding Domain (PTB) of CCM2 and the HECT domain of Smurf1 (Crose et al., 2009). The degradation of Rap1 in neurons is mediated by the HECT family E3 ubiquitin ligase Smurf2. We hypothesized that similarly to the interaction of CCM2 with Smurf1, CCM2 binds Smurf2 through their respective PTB and HECT domains. When CCM2 and Smurf2 were co-expessed, CCM2 was isolated with Smurf2 in immunoprecipitation assays (Figure 5.2). This is the first report of a CCM2-Smurf2 interaction. In combination with Crose *et al*.'s

original report of a CCM2-Smurf1 interaction, the formation of a CCM2-Smurf2 complex suggests that the molecular function of CCM2 may be in the localized delivery of the Smurf1 and Smurf2 E3 ubiquitin ligases to RhoA and Rap1 for the regulation of RhoA and Rap1-dependent endothelial cell functions. However, not just loss of CCM2 but also loss of CCM1 and CCM3 expression leads to an increase in the total levels of Rap1 suggesting that the CCM1, 2 and 3 complex coordinately regulates Smurf2-dependent Rap1 degradation.

Loss of CCM1, 2 or 3 leads to increased activated Rap1

To define the effect of the increase in total Rap1 on Rap1 activity, the levels of active Rap1 were measured in shCCM1, 2 or 3 HUVECs. The loss of CCM1, 2 or 3 expression caused respectively a 4.87, 5.85 and 5.90 fold increase in the levels of active Rap1 (p values 0.014, 0.035 and 0.029 respectively; Figure 5.3). The increased levels of active Rap1 correlate precisely with the observed increase in Rap1 abundance. These findings are consistent with published reports of the signaling effect with loss of E3 expression such as the increase in total and active RhoA with siRNA mediated knockdown of Smurf1 (Sahai et al., 2007) and suggest that CCM1, 2 and 3 are required for Smurf2 degradation of Rap1.

Rap1 in CCM knockdown cells can be activated by Forskolin leading to decrease in active RhoA

Stimulus-induced activation of Rap1, such as by neurite growth factor(Jeon et al., 2010a)', (Jeon et al., 2010b), or pharmacological agents for the activation of RapGEFs, leads to the inactivation of RhoA through the Rap1-activated RhoGAP Arap3 (Adamson et al. 2006; Zieba et al., 2011). The increased activity of both Rap1

and RhoA in CCM deficient endothelial cells suggests that either Rap1-Arap3-RhoA signaling is disrupted or is insufficient under quiescent conditions to normalize the elevated RhoA activity if RhoA inactivation in CCM requires the activation of more than one GAP or the presence of Smurf1.

To define whether Rap1-RhoA signaling is functional in the absence of CCM protein expression, the levels of active RhoA were measured in shCCM1, 2 and 3 HUVECs treated with the small molecule Forskolin. Stimulation of endothelial cells with the Adenylyl Cyclase agonist Forskolin leads to the Rap1-mediated inhibition of RhoA. Adenylyl Cyclase stimulates the production of cAMP, which in turn activates the Rap1GEF EPAC leading to Rap1 activation (Breckler et al., 2011; Zieba et al., 2011; Adamson et al. 2006). Despite the increased basal activity of Rap1 in shCCM1, 2 or 3 HUVECs, treatment with Forskolin further increased the levels of active Rap1 in shCCM1 and 2 HUVECs (Figure 5.4A) and concomitantly decreased the levels of active RhoA in shCCM1, 2 and 3 HUVECs (Figure 5.4B). Further activation of the elevated levels of Rap1 suggests that only a portion of the total available Rap1 proteins is basally activated with loss of CCM proteins as a sufficient population of GDP-Rap1 is available for activation by EPAC. The decrease in RhoA activity in all three CCM knockdown cell lines indicates that Rap1-mediated signaling for the inactivation of RhoA is an intact signaling system in CCM deficient cells, however is insufficient in normalizing the active RhoA to levels similar to RhoA levels in wildtype cells.

These findings bear a broader significance for the molecular cause of CCM in the mechanistic inactivation of the dysregulated RhoA. An additional target activated

by cAMP is Protein Kinase A (PKA) which phosphorylates RhoA at Ser188 which induces the binding of Rho Guanine Dissociation Inhibitor alpha (RhoGDIα) and internalization and inactivation of RhoA(Wang et al., 2006). The findings that stimulation of two RhoA inactivating pathways, through the RhoGAP Arap3 and through RhoGDIα only partially decreases the overactivated RhoA in CCM deficient cells suggests that RhoA inhibition through Smurf1 is a dominant defect in dysregulation of RhoA in CCM.

Activation of Rap1 rescues the tube formation defect in CCM1 but not CCM2 or CCM3 HUVECs

One *in vitro* phenotypic defect of CCM knockdown endothelial cells is the loss of self-assembly into tube like structures when cells are seeded in a three dimensional collagen substrate(Borikova et al., 2010a), (Crose et al., 2009). To define whether the Forskolin-mediated decrease in active in RhoA is sufficient to rescue the tube formation defect of CCM deficient endothelial cells, shCCM1, 2 and 3 HUVECs were treated with Forskolin and assayed for tube formation. Forskolin was sufficient to rescue the tube formation defect in shCCM1, but not shCCM2 or shCCM3 HUVECs (Figure 5.5). Similar results were obtained when cells were treated with 8-CPT-cAMP, a cAMP analog that activates EPAC and PKA (Figure 5.5). However, the tube formation defect of shCCM1 cells was not rescued upon treatment with 6-Bnz-cAMP which is a cAMP analogue that specifically activates PKA but not EPAC (Figure 5.5). These data delineate a Rap1-specific pathway for the rescue of tube formation in shCCM1 cells. Despite the Forskolin-stimulated decrease in active RhoA in all three CCM knockdown cell lines, this decrease was

sufficient to induce functionally-significant changes only in shCCM1 cells. A previous study had defined CCM1 as a downstream effector of Rap1 based on the evidence that Forskolin failed to rescue the permeability defect of shCCM1 HUVECs, where Forskolin-mediated activation of Rap1 reduces monolayer permeability in wildtype cells (Glading et al., 2007). The spatial distribution of active RhoA in shCCM1 cells is also prominently different that the distribution in shCCM2 and shCCM3 cells (Figure 4.2E). Thus in addition to the common function of regulating Rap1 and RhoA abundance and activity, each of the CCM proteins appears to play an additional, differential role in Rap1, RhoA and Rap1-RhoA signaling.

The Rap1-activated RhoGAP Arap3 is required for Rap1-mediated inactivation of RhoA

To better define the mechanism through which Forskolin rescues the tube formation defect in shCCM1 cells, these cells were treated with siRNA for Arap3 and Forskolin. An average of 61% knockdown in Arap3 mRNA was confirmed by QRT PCR (Figure 5.6A). In the absence of Arap3, Forskolin failed to rescue tube formation in shCCM1 cells (Figure 5.6B). In combination with our findings that Forskolin activates Rap1 in shCCM1 cells and decreases the levels of active RhoA, these data provide evidence that Rap1-Arap3-RhoA signaling is functionally significant in shCCM1 cells and pharmacological activation of this pathway is sufficient to rescue the tube formation defect in shCCM1 cells.

Discussion

To date disruption of Smurf1-mediated RhoA degradation and resultant increase in RhoA abundance, activity and signaling through ROCK for regulation of

actin cytoskeleton remains the only identified common pathway for CCM1, 2 and 3 functions. The disease relevance of the elevated RhoA-ROCK signaling is demonstrated by mouse studies in which the lesion burden (number, progression to bleeding and hemorrhage incidence) was significantly decreased with the addition of the ROCK inhibitor Fasudil(Stockton et al., 2010; McDonald et al., 2011; 2012).

Here we identify a second molecular pathway commonly regulated by all three CCM proteins – the regulation of Rap1 degradation through a novel CCM2-Smurf2 interaction. Smurf2 is an E3 ligase that was originally shown to regulate the degradation of Rap1 during neuronal axonal specification(Schwamborn et al., 2007). The functional outcome of the Smurf2-CCM2 interaction appears to be identical to the functional outcome of the Smurf1-CCM2 interaction - an increase in the abundance and activity of the small GTPases Rap1 and RhoA, respectively, with loss of CCM2. Furthermore, loss of CCM1 or CCM3 expression similarly leads to an increase in Rap1 abundance, without an increase in the expression of either the Rap1a or Rap1b isoforms (Figure 5.1), and an increase in activity (Figure 5.2). Consistent with the previously identified ternary complex between CCM1, 2 and 3 and the common disease pathology with loss of function in any one of the three CCM genes, these findings delineate a novel common pathway for CCM1,2 and 3 proteins in the regulation of Smurf2-mediated control of the abundance and activity of Rap1. The broader significance of these findings is that they define CCM as a disease of aberrant Smurf1 and Smurf2 E3 ligase activity for the regulation of RhoA and Rap1.

Currently available antibodies do not distinguish between the Rap1a and Rap1b isoform due to their high sequence homology (95% sequence coverage). Due to this limitation, the original report demonstrating that Smurf2 mediates the degradation of Rap1b used QRT PCR to show that Rap1b is the dominant isoform expressed in neurons to make the distinction in the degraded Rap1 isoform (Schwamborn et al., 2007). However, a specific preferential interaction of Smurf2 with Rap1b over Rap1a was not demonstrated and Rap1a is expressed in neuronal cells albeit at mRNA transcript levels lower than Rap1b (Schwamborn et al., 2007). Our QRT PCR analysis shows that the C_T mRNA message level threshold at which Rap1a and Rap1b are detected in wildtype HUVECs are 22.39 and 27.40, respectively where a C_T threshold lower than 30 is commonly accepted to indicate proteins expressed at biologically significant levels. Furthermore, CCM1 interacts with both Rap1a and Rap1b (Béraud-Dufour et al., 2007a). Thus our findings of the increase of total Rap1 in CCM1, 2 or 3 knockdown cells in a manner dependent on CCM2-Smurf2-mediated Rap1 degradation is consistent with the current understanding of Smurf2-Rap1 degradation.

In agreement with the classically established role of Rap1 as a negative regulator of cell permeability, RhoA activity and actin stress fiber formation, the increase in Rap1 activity observed with loss of CCM can be expected to result in decreased permeability, decreased RhoA activity and decreased RhoA-mediated stress fiber formation. However, CCM endothelial cells are characterized by an increase in permeability when in a monolayer, increase in RhoA activity and increase in stress fiber formation (Crose et al., 2009). This discrepancy suggests

that that either the active Rap1 observed with loss of CCM is not properly localized, or that CCM proteins function downstream of Rap to additionally regulate permeability and RhoA activity. Consistent with this prediction, CCM proteins regulate the degradation and activity of RhoA through Smurf1. Glading *et al.* showed that activation of Rap1 failed to rescue the increase permeability in CCM1 deficient endothelial cells and placed CCM1 downstream of Rap1 (Glading et al., 2007). The loss of Smurf1-mediated degradation of RhoA is further consistent with an additional role for CCM proteins downstream of Rap1. Additional studies are needed to delineate the spatiotemporal localization of active and total Rap1 with loss of CCM protein expression.

Rap1 mediated inactivation of RhoA occurs through the activation of the Rap1-dependent RhoGAP Arap3 in response to an increase in the intracellular levels of cAMP (Gambardella et al., 2010; Jeon et al., 2010a). To define whether the Rap1-Arap3-RhoA signaling pathway can be activated in CCM knockdown cells, RhoA activity and tube formation were assayed following Rap1 stimulation with the AC agonist Forskolin or cAMP analogues. The tube formation defect can be rescued in CCM1 knockdown cells but not in CCM2 or CCM3 cells, despite the decrease in active RhoA following treatment with Forskolin in all three CCM knockdown cell lines. Importantly, upon loss of siRNA-mediated Arap3 expression Forskolin fails to rescue tube formation in shCCM1 HUVECs, demonstrating that the effect of Forskolin is mediated by Rap1-Arap3 signaling specifically. Furthermore, these data indicate that GAP-mediated decrease in the activation of RhoA is insufficient to overcome the Smurf1-dependent regulation of RhoA in shCCM2 and shCCM3

endothelial cells. Further studies of the localization of activated Rap1 and RhoA in CCM1 versus CCM2 and CCM3 cells is needed to delineate the differences in signal transduction in these cell lines.

The significance of our findings is threefold. First we define a second molecular pathway in which CCM1, 2 and 3 coordinately regulate the abundance and activity of a small GTPase, Rap1, where CCM2 interacts with the E3 ligase required for the degradation of that GTPase, Smurf2. Second, we delineate that cAMP-Rap1-Arap3RhoGAP-RhoA signaling is a mechanism for the pharmacological regulation of the formation defects with loss of CCM1 expression. Finally, we provide evidence that while GAP-mediated inactivation of RhoA through Rap1-Arap3RhoGAP-RhoA signaling is sufficient to reverse the increased RhoA activity in shCCM1,2 and 3 cell this is insufficient to rescue the tube formation defect of shCCM2 and 3 cells, arguing that Smurf-mediated inactivation of RhoA is required for the regulation of RhoA activity in CCM. These studies delineate the functional significance of Rap1 in CCM pathology and redefine CCM as a disease of loss of Smurf1 and Smurf2 E3 ubiquitin ligase regulation of RhoA and Rap1 activity.

A.

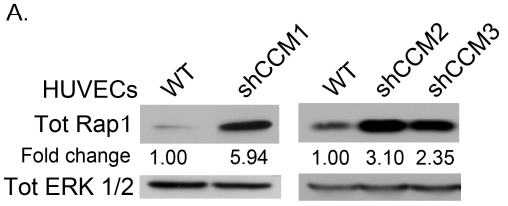

B.

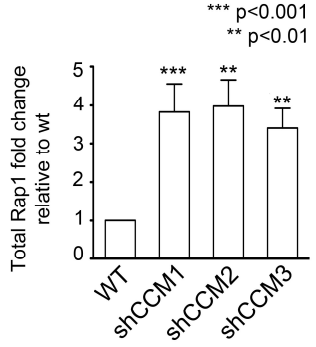

C.

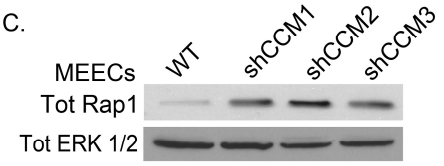

D.

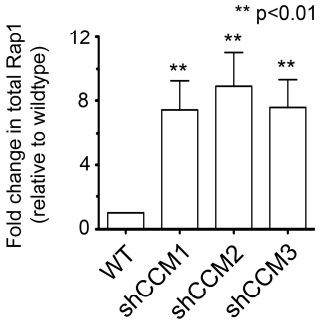

E.

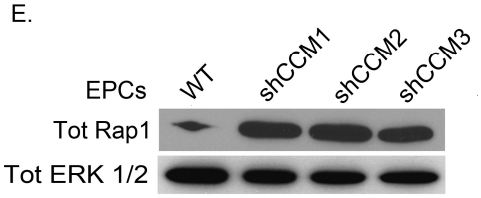

F.

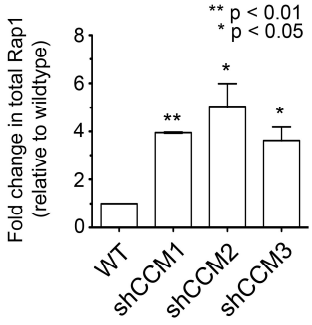

G.

RNA message levels of Rap1a and Rap1b in shCCM1, 2 and 3 HUVEC assessed by QRT PCR

Cell line	Rap1a				
	C_T n1	C_T n2	Ave C_T	Pvalue Ave C_T in WT vs shCCM1,2,3 cells	Fold change relative to WT
Wildtype	22.56	22.22	22.39	n/a	1.00
shCCM1	22.74	22.37	22.55	0.59	0.98
shCCM2	22.61	22.45	22.53	0.54	1.06
shCCM3	22.51	21.99	22.25	0.69	0.96

Cell line	Rap1b				
	C_T n1	C_T n2	Ave C_T	Pvalue Ave C_T in WT vs shCCM1,2,3 cells	Fold change relative to WT
Wildtype	26.96	27.83	27.40	n/a	1.00
shCCM1	27.37	27.97	27.67	0.65	0.91
shCCM2	26.66	27.47	27.07	0.64	1.72
shCCM3	26.68	27.61	27.14	0.73	1.08

H.

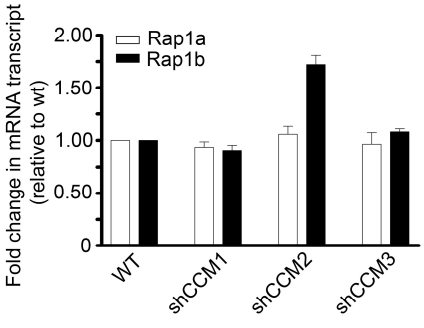

Figure 5.1: Rap1 abundance is increased in shCCM1, 2 or 3 endothelial cells. (A, C, E) Western blots for total Rap1a/b protein from HUVEC, MEEC and EPS cells show increase in Rap1a/b abundance. (B, D, F) Bar graph quantitations of total Rap1a/b from western blots in A, C and E. (B) Bar graph quantitation of average 3.83, 3.98 and 3.41 fold increase in total Rap1a/b in shCCM1, 2 or 3 HUVECs (p values 0.0001, 0.0013, and 0.0016 respectively). Graph represents minimum of five independent experiments using independently generated shRNA knockdown cell lines. (D) Bar graph quantitation of average 7.43, 8.87 and 7.58 fold increase in total Rap1a/b in shCCM1, 2 or 3 MEECs. Graph represents two independent experiments. (E) Bar graph quantitation of average 3.95, 5.05 and 3.62 fold increase in total Rap1a/b levels in shCCM1, 2 or 3 EPCs (p values 0.0001, 0.03, 0.02 respectively). Graph represents two independent experiments using cells isolated from two different human donors. (G) Quantitative Real Time PCR analysis of the mRNA abundance of Rap1a and Rap1b in two independently generated sets of shCCM1, 2 and 3 HUVECs. (H) Graphical quantitation of the fold change in Rap1a and Rap1b mRNA levels in shCCM1, 2 and 3 HUVECs. Figures 5.1C-F are courtesy of Christopher F Dibble, UNC-CH.

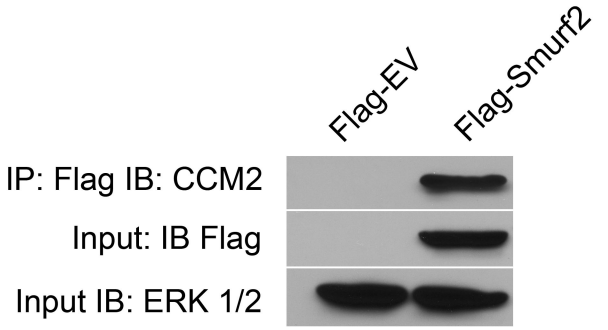

Figure 5.2: CCM2 interacts with the Rap1 E3 ligase Smurf2. Western blot shows that CCM2 is pulled down with Flag-Smurf2 when the two are expressed in HEK293 cells and cell lysates are separated with anti-Flag antibody, then probed for CCM2. The isolated CCM2 is specifically bound to Smurf2 rather than non-specifically pulled down as no CCM2 signal is detected when CCM2 is expressed with the Flag-EV. Figure courtesy of Bryan Richardson, UNC-CH.

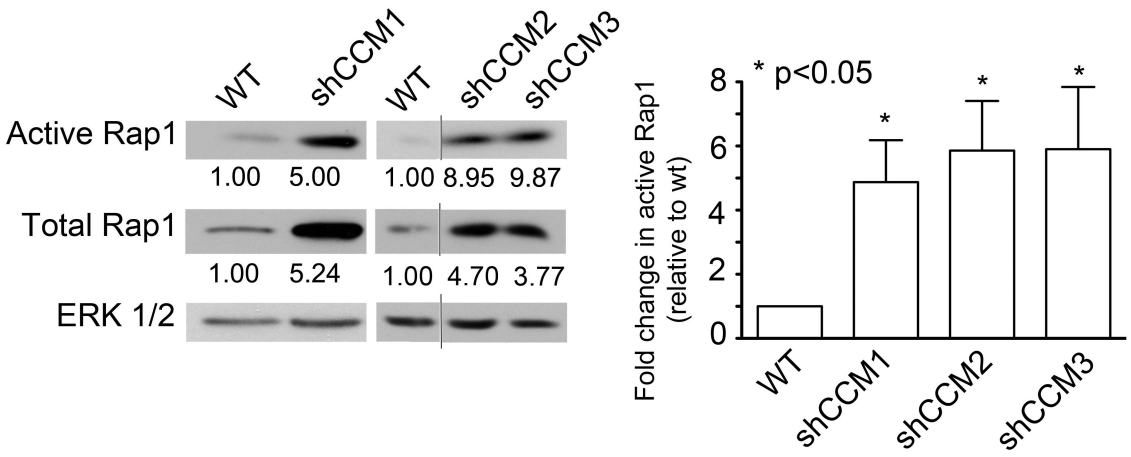

Figure 5.3: Active Rap1 is increased in shCCM1, 2 or 3 HUVECs. The levels of active Rap1 were on average 4.87, 5.85 and 5.90 fold higher in shCCM1, 2 or 3 HUVECs, respectively (p values 0.014, 0.035, and 0.029). Data represents minimum of five independent experiments with independently derived knockdown cell lines.

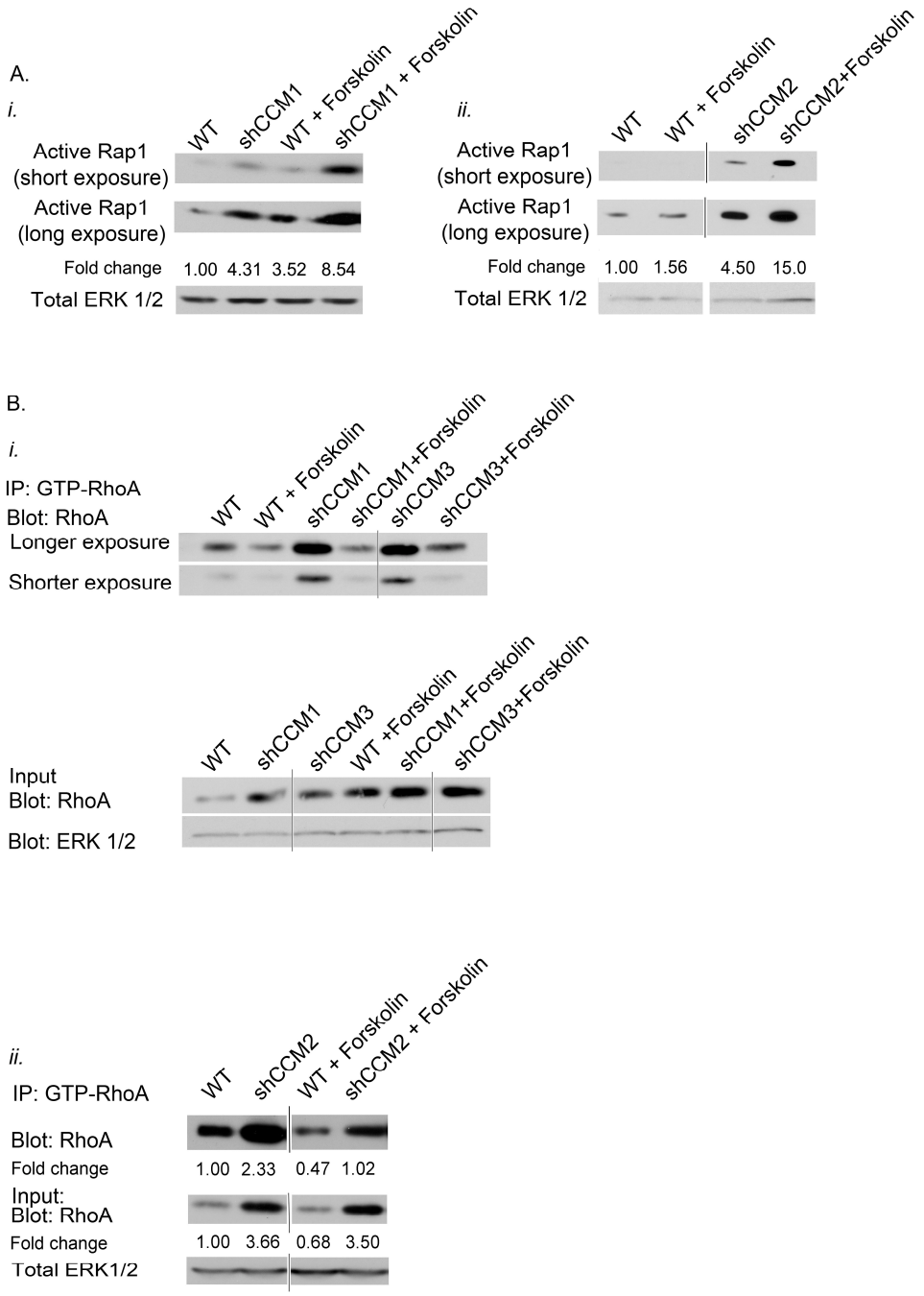

Figure 5.4: Forskolin increases active Rap1 levels and decreases active RhoA levels in shCCM1, 2 or 3 HUVECs. (A) Pulldown assays showing activation of Rap1 in shCCM1 (*i*) and 2 (*ii*) HUVECs following stimulation with Forskolin. (B) Immunoprecipitation showing that levels of active RhoA are decreased with Forskolin treatment in shCCM1, 2 (*i*) *and* 3 (*ii*) HUVECs

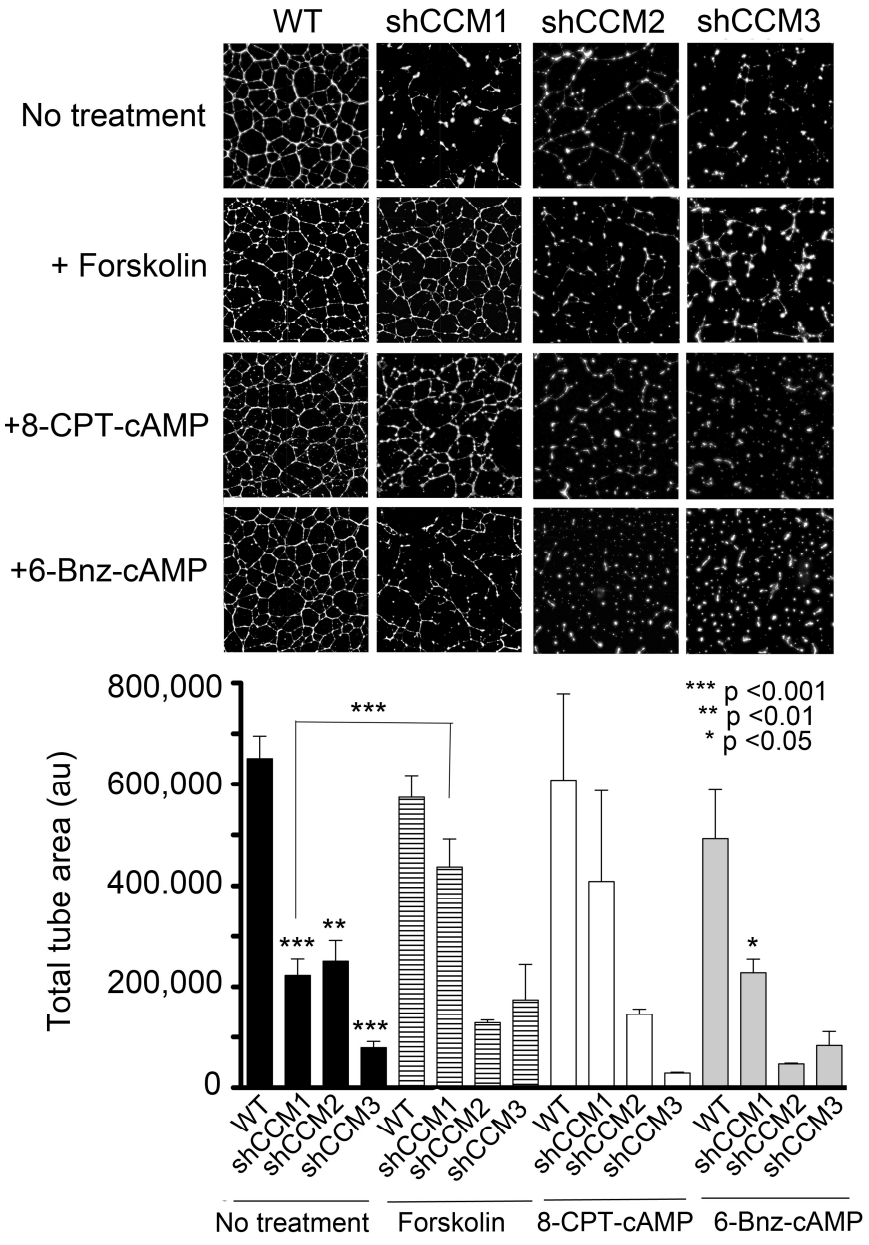

Figure 5.5: Forskolin rescues the tube formation defect in shCCM1 but not shCCM2 or shCCM3 HUVECs. shCCM1, 2 and 3 HUVECs fail to self assemble in tube-like structures (top panels horizontal across). Treatment with Forskolin and the EPAC and PKA agonist 8-CPT-cAMP rescues the tube formation defect in shCCM1 cells but not in shCCM2 or shCCM3 cells. Treatment with the PKA specific agonist 6-Bnz-cAMP fails to rescue the tube formation defect in shCCM1 cells. Bar graph represents minimum of two independent experiments.

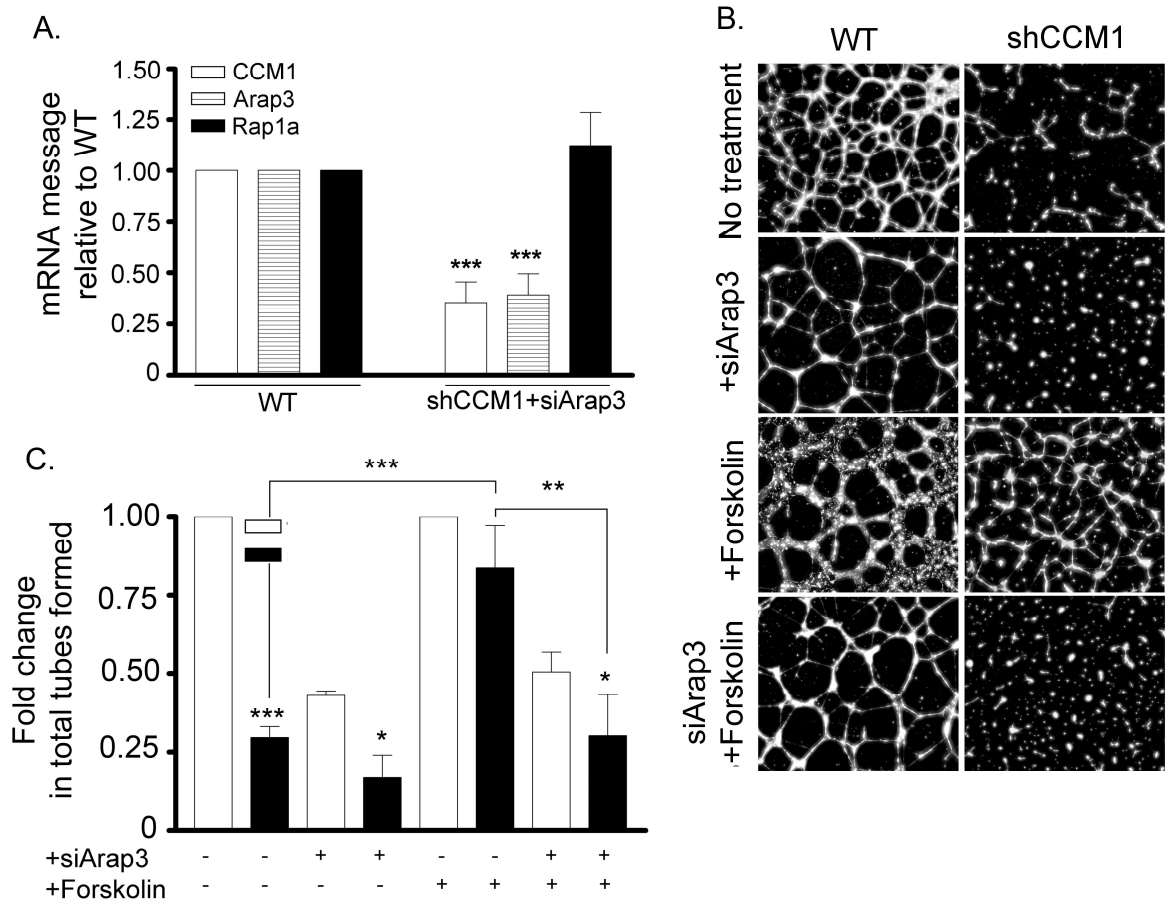

Figure 5.6: Knockdown of Arap3 abrogates the Forskolin-mediated rescue of the tube formation defect in shCCM1 endothelial cells. (A) Bar graph represents the average of three independent experiments of the mRNA transcript level of CCM1, Arap3 and Rap1 in shCCM1+siArap3 relative to wildtype cells as assessed by Quantitative Real Time PCR. Average knockdown of CCM1 and Arap3 were respectively 65% and 61% (p values 0.0096 and 0.0091 respectively). The levels of Rap1 in shCCM1+siArap3 cells were 1.12 fold relative to levels in wildtype cells (p value 0.29). (B) Forskolin rescues the disrupted tube formation of shCCM1 cells, however fails to rescue the tube formation of shCCM1 cells when they are additionally treated with siRNA for Arap3 (bottom across). (C) Bar graph represent quantitation of the fold change in number of tubes formed with the conditions described in B. Graph represents average of three independent experiments.

CHAPTER VI

CONCLUSIONS AND FUTURE DIRECTIONS

The CCM field has dramatically expanded within the last four years. At the beginning of this project the biological functions of the CCM proteins were yet to be identified. However the finding that CCM1,2 and 3 (Hilder et al., 2007) form a ternary complex was a paradigm shift in CCM as it gave rise to the hypothesis that CCM1, 2 and 3 participate in a common molecular pathway. Within the next several years several additional key discoveries were made. The most important of these was the identification that the CCM2 interacts with the E3 ubiquitin ligase Smurf1 for the regulation of the cytoskeletal regulator RhoA. Loss of CCM2 expression gave rise to upregulation of the abundance and activity of RhoA suggesting that CCM is a disease of disrupted cytoskeletal remodeling. The dysregulation of RhoA with loss of CCM2 expression was defined by two independent groups within several weeks of each other (Crose et al., 2009; Whitehead et al., 2009).

Our findings demonstrated that aberrant cytoskeletal stability resultant from increased RhoA abundance and activity resulted from the loss of each CCM1 or CCM3, providing the first biochemical evidence that the CCM proteins regulate a common pathway (Figure 6.1). Furthermore, the functional defects arising from deregulation of the RhoA and resulting ROCK activation were reversed with

inhibition of ROCK suggesting that ROCK is a potential therapeutic target for CCM. ROCK is a particularly promising target as the ROCK inhibitor Fasudil has been used for the treatment of cerebral vasospasms for over ten years in Japan and is well tolerated in humans (İnan and Büyükafşar, 2008). Consistent with the requirement for the CCM complex at the cell membrane for the regulation of Smurf1-mediated RhoA degradation, impairing the nucleocytoplasmic translocation of CCM2 by mutating the nuclear export sequence in CCM2 led to loss of endothelial cell tube formation.

The next key advancement in CCM comes from our discovery of the CCM1, 2 and 3 common regulation of the abundance and activity of the small GTPase Rap1 (Figure 6.1). The finding that CCM2 interacts with the E3 ligase Smurf2 has provided the preliminary basis for the next paradigm shift in molecular functions of the CCM proteins – the regulation of HECT family E3 ligases Smurf1 and Smurf2 for the regulation of RhoA and Rap1 signaling. The interaction between CCM2 and Smurf1 and Smurf2 occurs between the PTB domain of CCM2 and the HECT domain of Smurf1 and Smurf2. The HECT family of E3 ligases encompasses twenty eight E3s (Rotin and Kumar, 2009; Bernassola et al., 2008). Whether CCM proteins regulate the activity of additional HECT E3 members remains unknown and a screen for additional HECT E3 interaction partners for CCM2 can provide the first comprehensive understanding of the molecular role of CCM proteins in cell physiology.

Immunofluorescent staining for the phosphorylated form of the downstream effector for ROCK LIM Kinase in lesions extracted from CCM1, 2 and 3 patients has

shown an increase in phospho-cofilin in the endothelial monolayer of the lesions (unpublished data from Christopher F. Dibble, UNC-CH). This provided *in vivo* validation for the disease-relevance of our *in vitro* findings and defined CCM as a disease of aberrant cytoskeletal dynamics. Multiple signaling pathways converge on the regulation of the cytoskeleton, including signaling from RhoA and Rap1. Future studies will need to elucidate the relative contribution of RhoA, Rap1 and other small GTPases such as Rac1 and cdc42 which frequently function in conjunction with RhoA and Rap1 for the regulation of the cytoskeletal defect in CCM deficient endothelial cells. While we currently present preliminary evidence for the Smurf1 and Smurf2-dependent dysregulation of RhoA and Rap1 activity with loss of CCM proteins, additional experiments will need to validate the importance of Smurf1 and Smurf2 for the regulation RhoA and Rap1 relative to regulation by RhoGAPs and RhoGEFs. Specifically, the MTC and passive diffusion biophysical approaches presented here will be used to define the biomechanical profile in CCM deficient cells with agonist-induced activation of Rap1, inhibition of RhoA, or in wildtype cells with knockdown of Smurf1 or Smurf2. These studies will provide comprehensive understanding of the relative contribution of the two GTPases currently known to be dysregulated in CCM in the regulation of the cytoskeleton of CCM deficient cells, and will test for the involvement of additional GTPases in the cytoskeletal defect in CCM.

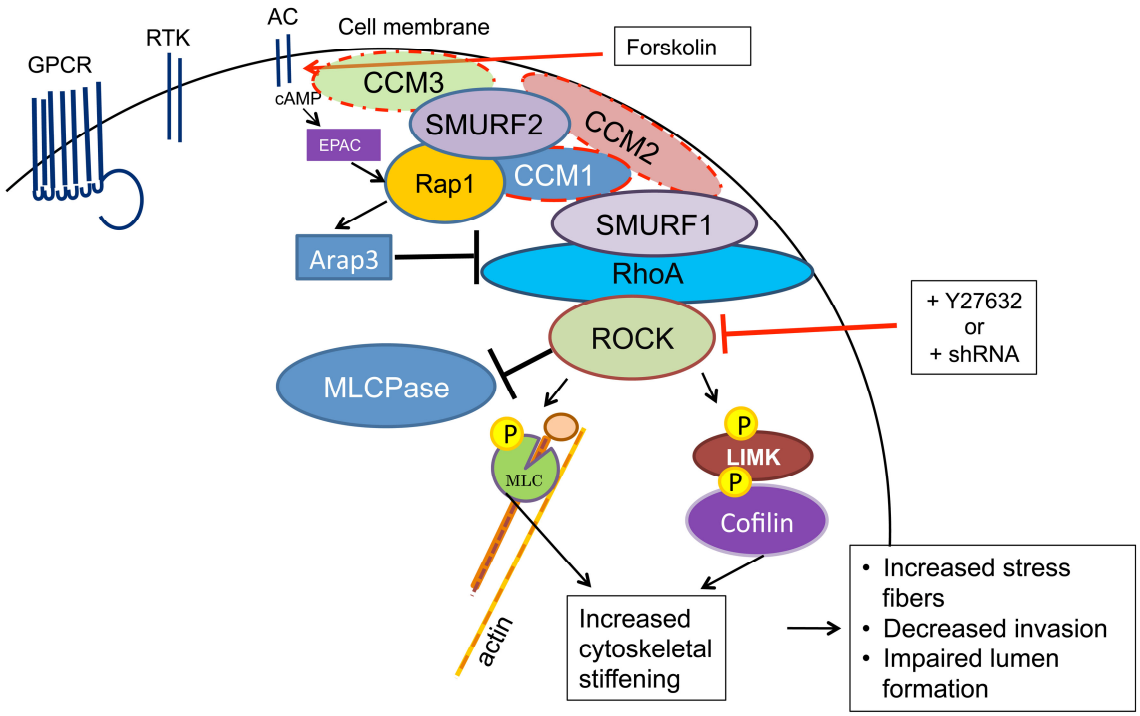

Figure 6.1: Proposed model for the molecular basis of CCM. We propose that through the interaction of CCM2 with Smurf1 and Smurf2, CCM1, 2 and 3 coordinately regulate the degradation of RhoA and Rap1, leading to the increased RhoA and Rap1 activity. The increase in RhoA activity causes upregulation of phospho-MLC and phospho-Cofilin with a functional outcome of increased cytoskeletal stiffening and impaired lumen formation. Inhibition of ROCK with Y29632 or shRNA knockdown reverses the cytoskeletal stiffening defect and the impaired lumen-like tube formation in each of the CCM knockdown cell lines and marks ROCK as a potential therapuetic target for CCM. We propose that activation of Rap1 with Forskolin leads to activation of the the RhoGAP Arap3 and decrease in RhoA activity in each CCM1, 2 and 3 knockdown HUVECs. Rap1 activation rescues tube formation only in shCCM1 cells suggesting that while Arap3 GAP-mediated inactivation of RhoA is possible, the inactivation is not sufficent to reverse the phenotype in shCCM2 and shCCM3 cells presumably due to the requirement for Smurf1-dependent inactivation of RhoA.

References

Abbott, N.J., Rönnbäck, L., and Hansson, E. (2006). Astrocyte–endothelial interactions at the blood–brain barrier. Nat Rev Neurosci *7*, 41–53.

Adamson, R.H., Ly, J.C., Sarai, R.K., Lenz, J.F., Altangerel, A., Drenckhahn, D., and Curry, F.E. Epac/Rap1 pathway regulates microvascular hyperpermeability induced by PAF in rat mesentery.

Akers, A.L., Johnson, E., Steinberg, G.K., Zabramski, J.M., and Marchuk, D.A. (2008). Biallelic Somatic and Germline Mutations in Cerebral Cavernous Malformations (CCM): Evidence for a Two-Hit Mechanism of CCM Pathogenesis. Human Molecular Genetics.

Armulik, A., Genové, G., Mäe, M., Nisancioglu, M.H., Wallgard, E., Niaudet, C., He, L., Norlin, J., Lindblom, P., Strittmatter, K., et al. (2010). Pericytes regulate the blood-brain barrier. Nature *468*, 557–561.

Arthur, W.T., Quilliam, L.A., and Cooper, J.A. (2004). Rap1 promotes cell spreading by localizing Rac guanine nucleotide exchange factors. The Journal of Cell Biology *167*, 111–122.

Asanuma, K., Yanagida-Asanuma, E., Faul, C., Tomino, Y., Kim, K., and Mundel, P. (2006). Synaptopodin orchestrates actin organization and cell motility via regulation of RhoA signalling. Nature Publishing Group *8*, 485–491.

Awad, I., and Jabbour, P. (2006). Cerebral cavernous malformations and epilepsy. Neurosurg Focus *21*, e7.

Awad, I.A. (2005). Unfolding knowledge on cerebral cavernous malformations. Surgical Neurology *63*, 317–318.

Batra, S., Lin, D., Recinos, P.F., Zhang, J., and Rigamonti, D. (2009). Cavernous malformations: natural history, diagnosis and treatment. Nat Rev Neurol *5*, 659–670.

Bernassola, F., Karin, M., Ciechanover, A., and Melino, G. (2008). The HECT Family of E3 Ubiquitin Ligases: Multiple Players in Cancer Development. Cancer Cell *14*, 10–21.

Béraud-Dufour, S., Gautier, R., Albiges-Rizo, C., Chardin, P., and Faurobert, E.

(2007a). Krit 1 interactions with microtubules and membranes are regulated by Rap1 and integrin cytoplasmic domain associated protein-1. FEBS Journal *274*, 5518–5532.

Béraud-Dufour, S., Gautier, R., Albiges-Rizo, C., Chardin, P., and Faurobert, E. (2007b). Krit 1 interactions with microtubules and membranes are regulated by Rap1 and integrin cytoplasmic domain associated protein-1. FEBS Journal *274*, 5518–5532.

Bhattacharya, S. (2003). Regulation of Stat3 nuclear export. J. Clin. Invest. *111*, 553–559.

Bishop, A.L., and Hall, A. (2000). Rho GTPases and their effector proteins. Biochem. J. *348 Pt 2*, 241–255.

Bivona, T.G. (2004). Rap1 up-regulation and activation on plasma membrane regulates T cell adhesion. The Journal of Cell Biology *164*, 461–470.

Boon, L.M., Ballieux, F., and Vikkula, M. (2011). Pathogenesis of vascular anomalies. Clin Plast Surg *38*, 7–19.

Borikova, A.L., Dibble, C.F., Sciaky, N., Welch, C.M., Abell, A.N., Bencharit, S., and Johnson, G.L. (2010a). Rho kinase inhibition rescues the endothelial cell cerebral cavernous malformation phenotype. J. Biol. Chem. *285*, 11760–11764.

Borikova, A.L., Dibble, C.F., Sciaky, N., Welch, C.M., Abell, A.N., Bencharit, S., and Johnson, G.L. (2010b). Rho Kinase Inhibition Rescues the Endothelial Cell Cerebral Cavernous Malformation Phenotype. J. Biol. Chem. *285*, 11760–11764.

Bouvard, D., Millonfremillon, A., Dupemanet, S., Block, M., and Albigesrizo, C. (2006). Unraveling ICAP-1 function: Toward a new direction? European Journal of Cell Biology *85*, 275–282.

Brameier, M., Krings, A., and MacCallum, R.M. (2007). NucPred--predicting nuclear localization of proteins. Bioinformatics *23*, 1159–1160.

Breckler, M., Berthouze, M., Laurent, A.-C., Crozatier, B., Morel, E., and Lezoualc'h, F. (2011). Rap-linked cAMP signaling Epac proteins: Compartmentation, functioning and disease implications. Cellular Signalling *23*, 1257–1266.

Brunton, V.G., MacPherson, I.R.J., and Frame, M.C. (2004). Cell adhesion receptors, tyrosine kinases and actin modulators: a complex three-way circuitry. Biochim. Biophys. Acta *1692*, 121–144.

Casar, B., Sanz-Moreno, V., Yazicioglu, M.N., Rodríguez, J., Berciano, M.T., Lafarga, M., Cobb, M.H., and Crespo, P. (2007). Mxi2 promotes stimulus-independent ERK nuclear translocation. Embo J *26*, 635–646.

Cavalcanti, D.D., Kalani, M.Y.S., Martirosyan, N.L., Eales, J., Spetzler, R.F., and Preul, M.C. (2012). Cerebral cavernous malformations: from genes to proteins to disease. J. Neurosurg. *116*, 122–132.

Chan, A.C., Drakos, S.G., Ruiz, O.E., Smith, A.C.H., Gibson, C.C., Ling, J., Passi, S.F., Stratman, A.N., Sacharidou, A., Revelo, M.P., et al. (2011). Mutations in 2 distinct genetic pathways result in cerebral cavernous malformations in mice. J. Clin. Invest. *121*, 1871–1881.

Cheng, P.-L., Lu, H., Shelly, M., Gao, H., and Poo, M.-M. (2011). Phosphorylation of E3 Ligase Smurf1 Switches Its Substrate Preference in Support of Axon Development. Neuron *69*, 231–243.

Chrissobolis, S., and Sobey, C.G. (2006). Recent evidence for an involvement of rho-kinase in cerebral vascular disease. Stroke *37*, 2174–2180.

Chuderland, D., Konson, A., and Seger, R. (2008). Identification and Characterization of a General Nuclear Translocation Signal in Signaling Proteins. Molecular Cell *31*, 850–861.

Clatterbuck, R.E., and Rigamonti, D. (2002). Cherry angiomas associated with familial cerebral cavernous malformations. Case illustration. J. Neurosurg. *96*, 964.

Clatterbuck, R.E., Eberhart, C.G., Crain, B.J., and Rigamonti, D. (2001). Ultrastructural and immunocytochemical evidence that an incompetent blood-brain barrier is related to the pathophysiology of cavernous malformations. J. Neurol. Neurosurg. Psychiatr. *71*, 188–192.

Costa, M., Marchi, M., Cardarelli, F., Roy, A., Beltram, F., Maffei, L., and Ratto, G.M. (2006). Dynamic regulation of ERK2 nuclear translocation and mobility in living cells. Journal of Cell Science *119*, 4952–4963.

Coughlin, M.F., Puig-de-Morales, M., Bursac, P., Mellema, M., Millet, E., and Fredberg, J.J. (2006). Filamin-A and Rheological Properties of Cultured Melanoma Cells. Biophysical Journal *90*, 2199–2205.

Couteulx, S.L.-L., Brézin, A.P., Fontaine, B., Tournier-Lasserve, E., and Labauge, P. (2002). A novel KRIT1/CCM1 truncating mutation in a patient with cerebral and retinal cavernous angiomas. Arch. Ophthalmol. *120*, 217–218.

Craig, H.D., Gunel, M., Cepeda, O., Johnson, E.W., Ptacek, L., Steinberg, G.K., Ogilvy, C.S., Berg, M.J., Crawford, S.C., Scott, R.M., et al. (1998). Multilocus linkage identifies two new loci for a mendelian form of stroke, cerebral cavernous malformation, at 7p15-13 and 3q25.2-27. Human Molecular Genetics *7*, 1851–1858.

Crose, L.E.S., Hilder, T.L., Sciaky, N., and Johnson, G.L. (2009). Cerebral Cavernous Malformation 2 Protein Promotes Smad Ubiquitin Regulatory Factor 1-mediated RhoA Degradation in Endothelial Cells. J. Biol. Chem. *284*, 13301–13305.

Cunningham, K., Uchida, Y., O'Donnell, E., Claudio, E., Li, W., Soneji, K., Wang, H., Mukouyama, Y.S., and Siebenlist, U. (2011). Conditional deletion of Ccm2 causes hemorrhage in the adult brain: a mouse model of human cerebral cavernous malformations. Human Molecular Genetics *20*, 3198–3206.

Davenport, W.J., Siegel, A.M., Dichgans, J., Drigo, P., Mammi, I., Pereda, P., Wood, N.W., and Rouleau, G.A. (2001). CCM1 gene mutations in families segregating cerebral cavernous malformations. Neurology *56*, 540–543.

Davis, M.A., Ireton, R.C., and Reynolds, A.B. (2003). A core function for p120-catenin in cadherin turnover. The Journal of Cell Biology *163*, 525–534.

Dejana, E. (2004). Endothelial cell–cell junctions: happy together. Nat Rev Mol Cell Biol *5*, 261–270.

Denier, C., Goutagny, S., Labauge, P., Krivosic, V., Arnoult, M., Cousin, A., Benabid, A.L., Comoy, J., Frerebeau, P., Gilbert, B., et al. (2004). Mutations within the MGC4607 gene cause cerebral cavernous malformations. Am. J. Hum. Genet. *74*, 326–337.

Donaldson, J.G., and Jackson, C.L. (2011). ARF family G proteins and their regulators: roles in membrane transport, development and disease. Nat Rev Mol Cell Biol *12*, 362–375.

Eerola, I., Plate, K.H., Spiegel, R., Boon, L.M., Mulliken, J.B., and Vikkula, M. (2000). KRIT1 is mutated in hyperkeratotic cutaneous capillary-venous malformation associated with cerebral capillary malformation. Human Molecular Genetics *9*, 1351–1355.

Faurobert, E., and Albiges-Rizo, C. (2010). Recent insights into cerebral cavernous malformations: a complex jigsaw puzzle under construction. Febs J. *277*, 1084–1096.

Francalanci, F., Avolio, M., De Luca, E., Longo, D., Menchise, V., Guazzi, P., Sgrò, F., Marino, M., Goitre, L., Balzac, F., et al. (2009). Structural and functional differences between KRIT1A and KRIT1B isoforms: A framework for understanding CCM pathogenesis. Experimental Cell Research *315*, 285–303.

Gambardella, L., Hemberger, M., Hughes, B., Zudaire, E., Andrews, S., and Vermeren, S. (2010). PI3K Signaling Through the Dual GTPase-Activating Protein ARAP3 Is Essential for Developmental Angiogenesis. Science Signaling *3*, ra76–ra76.

Glading, A., Han, J., Stockton, R.A., and Ginsberg, M.H. (2007). KRIT-1/CCM1 is a Rap1 effector that regulates endothelial cell cell junctions. The Journal of Cell Biology *179*, 247–254.

Gore, A.V., Lampugnani, M.G., Dye, L., Dejana, E., and Weinstein, B.M. (2008).

Combinatorial interaction between CCM pathway genes precipitates hemorrhagic stroke. Disease Models and Mechanisms *1*, 275–281.

Guilluy, C., Swaminathan, V., Garcia-Mata, R., O'Brien, E.T., Superfine, R., and Burridge, K. (2011). The Rho GEFs LARG and GEF-H1 regulate the mechanical response to force on integrins. Nature Publishing Group *13*, 722–727.

Haasdijk, R.A., Cheng, C., Maat-Kievit, A.J., and Duckers, H.J. (2012). Cerebral cavernous malformations: from molecular pathogenesis to genetic counselling and clinical management. Eur. J. Hum. Genet. *20*, 134–140.

He, Y., Zhang, H., Yu, L., Gunel, M., Boggon, T.J., Chen, H., and Min, W. (2010). Stabilization of VEGFR2 Signaling by Cerebral Cavernous Malformation 3 Is Critical for Vascular Development. Science Signaling *3*, ra26–ra26.

Henderson, B. (2000). A Comparison of the Activity, Sequence Specificity, and CRM1-Dependence of Different Nuclear Export Signals. Experimental Cell Research *256*, 213–224.

Henderson, B.R., and Percipalle, P. (1997). Interactions between HIV Rev and nuclear import and export factors: the Rev nuclear localisation signal mediates specific binding to human importin-beta. Journal of Molecular Biology *274*, 693–707.

Hilder, T.L., Malone, M.H., Bencharit, S., Colicelli, J., Haystead, T.A., Johnson, G.L., and Wu, C.C. (2007). Proteomic Identification of the Cerebral Cavernous Malformation Signaling Complex. J. Proteome Res. *6*, 4343–4355.

Hoffman, B.D., and Crocker, J.C. (2009). Cell Mechanics: Dissecting the Physical Responses of Cells to Force. Annu. Rev. Biomed. Eng. *11*, 259–288.

Hogan, C., Serpente, N., Cogram, P., Hosking, C.R., Bialucha, C.U., Feller, S.M., Braga, V.M.M., Birchmeier, W., and Fujita, Y. (2004). Rap1 regulates the formation of E-cadherin-based cell-cell contacts. Molecular and Cellular Biology *24*, 6690–6700.

İnan, S.Y., and Büyükafşar, K. (2008). Antiepileptic effects of two Rho-kinase inhibitors, Y-27632 and fasudil, in mice. British Journal of Pharmacology *155*, 44–51.

Jaffe, A.B., and Hall, A. (2005). Rho GTPases: biochemistry and biology. Annu. Rev. Cell Dev. Biol. *21*, 247–269.

Jeon, C.Y., Kim, H.J., Lee, J.Y., Kim, J.B., Kim, S.C., and Park, J.B. (2010a). p190RhoGAP and Rap-dependent RhoGAP (ARAP3) inactivate RhoA in response to nerve growth factor leading to neurite outgrowth from PC12 cells. Exp. Mol. Med. *42*, 335–344.

Jeon, C.Y., Kim, H.J., Morii, H., Mori, N., Settleman, J., Lee, J.Y., Kim, J., Kim, S.C., and Park, J.B. (2010b). Neurite outgrowth from PC12 cells by basic fibroblast growth

factor (bFGF) is mediated by RhoA inactivation through p190RhoGAP and ARAP3. J. Cell. Physiol. *224*, 786–794.

Jiang, X.-S., Wassif, C.A., Backlund, P.S., Song, L., Holtzclaw, L.A., Li, Z., Yergey, A.L., and Porter, F.D. (2010). Activation of Rho GTPases in Smith-Lemli-Opitz syndrome: pathophysiological and clinical implications. Human Molecular Genetics *19*, 1347–1357.

Kasza, K.E., Nakamura, F., Hu, S., Kollmannsberger, P., Bonakdar, N., Fabry, B., Stossel, T.P., Wang, N., and Weitz, D.A. (2009). Filamin A Is Essential for Active Cell Stiffening but not Passive Stiffening under External Force. Biophysical Journal *96*, 4326–4335.

Kleaveland, B., Zheng, X., Liu, J.J., Blum, Y., Tung, J.J., Zou, Z., Chen, M., Guo, L., Lu, M.-M., Zhou, D., et al. (2009a). Regulation of cardiovascular development and integrity by the heart of glass–cerebral cavernous malformation protein pathway. Nature Medicine *15*, 169–176.

Kleaveland, B., Zheng, X., Liu, J.J., Blum, Y., Tung, J.J., Zou, Z., Chen, M., Guo, L., Lu, M.-M., Zhou, D., et al. (2009b). Regulation of cardiovascular development and integrity by the heart of glass–cerebral cavernous malformation protein pathway. Nature Medicine *15*, 169–176.

Koenderink, G.H., Dogic, Z., Nakamura, F., Bendix, P.M., Mackintosh, F.C., Hartwig, J.H., Stossel, T.P., and Weitz, D.A. (2009). An active biopolymer network controlled by molecular motors. Proc. Natl. Acad. Sci. U.S.a. *106*, 15192–15197.

Kooistra, M.R.H., Corada, M., Dejana, E., and Bos, J.L. (2005). Epac1 regulates integrity of endothelial cell junctions through VE-cadherin. FEBS Letters *579*, 4966–4972.

Kooistra, M.R.H., Dube, N., and Bos, J.L. (2006). Rap1: a key regulator in cell-cell junction formation. Journal of Cell Science *120*, 17–22.

Laberge, S., Labauge, P., Marechal, E., Maciazek, J., and Tournier-Lasserve, E. (1999). Genetic heterogeneity and absence of founder effect in a series of 36 French cerebral cavernous angiomas families. Eur. J. Hum. Genet. *7*, 499–504.

Lakshmikanthan, S., Sobczak, M., Chun, C., Henschel, A., Dargatz, J., Ramchandran, R., and Chrzanowska-Wodnicka, M. (2011). Rap1 promotes VEGFR2 activation and angiogenesis by a mechanism involving integrin v 3. Blood *118*, 2015–2026.

Lange, A., Mills, R.E., Lange, C.J., Stewart, M., Devine, S.E., and Corbett, A.H. (2006). Classical Nuclear Localization Signals: Definition, Function, and Interaction with Importin. J. Biol. Chem. *282*, 5101–5105.

Lee, H.-S., Lim, C.J., Puzon-McLaughlin, W., Shattil, S.J., and Ginsberg, M.H.

(2009). RIAM activates integrins by linking talin to ras GTPase membrane-targeting sequences. J. Biol. Chem. *284*, 5119–5127.

Leung, S.W. (2003). Dissection of the Karyopherin Nuclear Localization Signal (NLS)-binding Groove: FUNCTIONAL REQUIREMENTS FOR NLS BINDING. J. Biol. Chem. *278*, 41947–41953.

Li, J., Mahajan, A., and Tsai, M.-D. (2006). Ankyrin repeat: a unique motif mediating protein-protein interactions. Biochemistry *45*, 15168–15178.

Li, S.Y. (2006). Transport of galectin-3 between the nucleus and cytoplasm. II. Identification of the signal for nuclear export. Glycobiology *16*, 612–622.

Li, X., Zhang, R., Draheim, K.M., Liu, W., Calderwood, D.A., and Boggon, T.J. (2012). Structural basis for the small G-protein-effector interaction of Ras-related protein 1 (Rap1) and the adaptor protein Krev interaction trapped 1 (KRIT1). J. Biol. Chem.

Li, X., Zhang, R., Zhang, H., He, Y., Ji, W., Min, W., and Boggon, T.J. (2010). Crystal Structure of CCM3, a Cerebral Cavernous Malformation Protein Critical for Vascular Integrity. J. Biol. Chem. *285*, 24099–24107.

Liquori, C.L., Berg, M.J., Siegel, A.M., Huang, E., Zawistowski, J.S., Stoffer, T., Verlaan, D., Balogun, F., Hughes, L., Leedom, T.P., et al. (2003). Mutations in a gene encoding a novel protein containing a phosphotyrosine-binding domain cause type 2 cerebral cavernous malformations. Am. J. Hum. Genet. *73*, 1459–1464.

Liu, J.J., Stockton, R.A., Gingras, A.R., Ablooglu, A.J., Han, J., Bobkov, A.A., and Ginsberg, M.H. (2011). A mechanism of Rap1-induced stabilization of endothelial cell--cell junctions. Mol. Biol. Cell *22*, 2509–2519.

Louvi, A., Chen, L., Two, A.M., Zhang, H., Min, W., and Günel, M. (2011). Loss of cerebral cavernous malformation 3 (Ccm3) in neuroglia leads to CCM and vascular pathology. Proc. Natl. Acad. Sci. U.S.a. *108*, 3737–3742.

Lunsford, L.D., Khan, A.A., Niranjan, A., Kano, H., Flickinger, J.C., and Kondziolka, D. (2010). Stereotactic radiosurgery for symptomatic solitary cerebral cavernous malformations considered high risk for resection. J. Neurosurg. *113*, 23–29.

Mably, J.D. (2006). santa and valentine pattern concentric growth of cardiac myocardium in the zebrafish. Development *133*, 3139–3146.

Machacek, M., Hodgson, L., Welch, C., Elliott, H., Pertz, O., Nalbant, P., Abell, A., Johnson, G.L., Hahn, K.M., and Danuser, G. (2009). Coordination of Rho GTPase activities during cell protrusion. Nature *461*, 99–103.

Marchuk, D.A. (2003). Vascular morphogenesis: tales of two syndromes. Human Molecular Genetics *12*, 97R–112.

McDonald, D.A., Shenkar, R., Shi, C., Stockton, R.A., Akers, A.L., Kucherlapati, M.H., Kucherlapati, R., Brainer, J., Ginsberg, M.H., Awad, I.A., et al. (2011). A novel mouse model of cerebral cavernous malformations based on the two-hit mutation hypothesis recapitulates the human disease. Human Molecular Genetics *20*, 211–222.

McDonald, D.A., Shi, C., Shenkar, R., Stockton, R.A., Liu, F., Ginsberg, M.H., Marchuk, D.A., and Awad, I.A. (2012). Fasudil decreases lesion burden in a murine model of cerebral cavernous malformation disease. Stroke *43*, 571–574.

Mekhail, K., Rivero-Lopez, L., Al-Masri, A., Brandon, C., Khacho, M., and Lee, S. (2007). Identification of a common subnuclear localization signal. Mol. Biol. Cell *18*, 3966–3977.

Moon, S.Y., and Zheng, Y. (2003). Rho GTPase-activating proteins in cell regulation. Trends in Cell Biology *13*, 13–22.

Murphy, M.M., Zayed, M.A., Evans, A., Parker, C.E., Ataga, K.I., Telen, M.J., and Parise, L.V. (2005). Role of Rap1 in promoting sickle red blood cell adhesion to laminin via BCAM/LU. Blood *105*, 3322–3329.

Otten, P., Pizzolato, G.P., Rilliet, B., and Berney, J. (1989). [131 cases of cavernous angioma (cavernomas) of the CNS, discovered by retrospective analysis of 24,535 autopsies]. Neurochirurgie *35*, 82–3–128–31.

Pertz, O., Hodgson, L., Klemke, R.L., and Hahn, K.M. (2006). Spatiotemporal dynamics of RhoA activity in migrating cells. Nature *440*, 1069–1072.

Plummer, N.W., Gallione, C.J., Srinivasan, S., Zawistowski, J.S., Louis, D.N., and Marchuk, D.A. (2004). Loss of p53 sensitizes mice with a mutation in Ccm1 (KRIT1) to development of cerebral vascular malformations. Am. J. Pathol. *165*, 1509–1518.

Porter, R.W., Detwiler, P.W., Spetzler, R.F., Lawton, M.T., Baskin, J.J., Derksen, P.T., and Zabramski, J.M. (1999). Cavernous malformations of the brainstem: experience with 100 patients. J. Neurosurg. *90*, 50–58.

Revencu, N., and Vikkula, M. (2006). Cerebral cavernous malformation: new molecular and clinical insights. J. Med. Genet. *43*, 716–721.

Rigamonti, D., Drayer, B.P., Johnson, P.C., Hadley, M.N., Zabramski, J., and Spetzler, R.F. (1987). The MRI appearance of cavernous malformations (angiomas). J. Neurosurg. *67*, 518–524.

Rigamonti, D., Hadley, M.N., Drayer, B.P., Johnson, P.C., Hoenig-Rigamonti, K., Knight, J.T., and Spetzler, R.F. (1988). Cerebral cavernous malformations. Incidence and familial occurrence. N. Engl. J. Med. *319*, 343–347.

Rodriguez, J.J., Cruz, C.D., and Horvath, C.M. (2004). Identification of the nuclear

export signal and STAT-binding domains of the Nipah virus V protein reveals mechanisms underlying interferon evasion. J. Virol. *78*, 5358–5367.

Rossman, K.L., Der, C.J., and Sondek, J. (2005). GEF means go: turning on RHO GTPases with guanine nucleotide-exchange factors. Nat Rev Mol Cell Biol *6*, 167–180.

Rotin, D., and Kumar, S. (2009). Physiological functions of the HECT family of ubiquitin ligases. Nat Rev Mol Cell Biol *10*, 398–409.

Sahai, E., Garcia-Medina, R., Pouyssegur, J., and Vial, E. (2007). Smurf1 regulates tumor cell plasticity and motility through degradation of RhoA leading to localized inhibition of contractility. The Journal of Cell Biology *176*, 35–42.

Sahoo, T., Johnson, E.W., Thomas, J.W., Kuehl, P.M., Jones, T.L., Dokken, C.G., Touchman, J.W., Gallione, C.J., Lee-Lin, S.Q., Kosofsky, B., et al. (1999a). Mutations in the gene encoding KRIT1, a Krev-1/rap1a binding protein, cause cerebral cavernous malformations (CCM1). Human Molecular Genetics *8*, 2325–2333.

Sahoo, T., Johnson, E.W., Thomas, J.W., Kuehl, P.M., Jones, T.L., Dokken, C.G., Touchman, J.W., Gallione, C.J., Lee-Lin, S.Q., Kosofsky, B., et al. (1999b). Mutations in the gene encoding KRIT1, a Krev-1/rap1a binding protein, cause cerebral cavernous malformations (CCM1). Human Molecular Genetics *8*, 2325–2333.

Schwamborn, J.C., Müller, M., Becker, A.H., and Püschel, A.W. (2007). Ubiquitination of the GTPase Rap1B by the ubiquitin ligase Smurf2 is required for the establishment of neuronal polarity. Embo J *26*, 1410–1422.

Serebriiskii, I., Estojak, J., Sonoda, G., Testa, J.R., and Golemis, E.A. (1997). Association of Krev-1/rap1a with Krit1, a novel ankyrin repeat-containing protein encoded by a gene mapping to 7q21-22. Oncogene *15*, 1043–1049.

Shen, Q., Rigor, R.R., Pivetti, C.D., Wu, M.H., and Yuan, S.Y. (2010). Myosin light chain kinase in microvascular endothelial barrier function. Cardiovascular Research *87*, 272–280.

Shenkar, R., Venkatasubramanian, P.N., Wyrwicz, A.M., Zhao, J.-C., Shi, C., Akers, A., Marchuk, D.A., and Awad, I.A. (2008). ADVANCED MAGNETIC RESONANCE IMAGING OF CEREBRAL CAVERNOUS MALFORMATIONS. Neurosurgery *63*, 790–798.

Shi, C., Shenkar, R., Batjer, H.H., Check, I.J., and Awad, I.A. (2007). Oligoclonal immune response in cerebral cavernous malformations. Laboratory investigation. J. Neurosurg. *107*, 1023–1026.

Shi, C., Shenkar, R., Du, H., Duckworth, E., Raja, H., Batjer, H.H., and Awad, I.A.

(2009). Immune response in human cerebral cavernous malformations. Stroke *40*, 1659–1665.

Sorg, G., and Stamminger, T. (1999). Mapping of nuclear localization signals by simultaneous fusion to green fluorescent protein and to beta-galactosidase. BioTechniques *26*, 858–862.

Stockton, R.A., Shenkar, R., Awad, I.A., and Ginsberg, M.H. (2010). Cerebral cavernous malformations proteins inhibit Rho kinase to stabilize vascular integrity. Journal of Experimental Medicine *207*, 881–896.

Thompson, M.E. (2005). An Amino-terminal Motif Functions as a Second Nuclear Export Sequence in BRCA1. J. Biol. Chem. *280*, 21854–21857.

Tim O'Brien, E., Cribb, J., Marshburn, D., Taylor, R.M., II, and Superfine, R. (2008). Methods in Cell Biology (Elsevier).

Trotman, L.C., Wang, X., Alimonti, A., Chen, Z., Teruya-Feldstein, J., Yang, H., Pavletich, N.P., Carver, B.S., Cordon-Cardo, C., Erdjument-Bromage, H., et al. (2007). Ubiquitination Regulates PTEN Nuclear Import and Tumor Suppression. Cell *128*, 141–156.

Uhlik, M.T., Abell, A.N., Johnson, N.L., Sun, W., Cuevas, B.D., Lobel-Rice, K.E., Horne, E.A., Dell'Acqua, M.L., and Johnson, G.L. (2003). Rac–MEKK3–MKK3 scaffolding for p38 MAPK activation during hyperosmotic shock. Nature Publishing Group *5*, 1104–1110.

Uhlik, M.T., Temple, B., Bencharit, S., Kimple, A.J., Siderovski, D.P., and Johnson, G.L. (2005). Structural and Evolutionary Division of Phosphotyrosine Binding (PTB) Domains. Journal of Molecular Biology *345*, 1–20.

Uyttendaele, H., Ho, J., Rossant, J., and Kitajewski, J. (2001). Vascular patterning defects associated with expression of activated Notch4 in embryonic endothelium. Proc. Natl. Acad. Sci. U.S.a. *98*, 5643–5648.

Verlaan, D.J., Laurent, S.B., Rochefort, D.L., Liquori, C.L., Marchuk, D.A., Siegel, A.M., and Rouleau, G.A. (2004). CCM2 mutations account for 13% of cases in a large collection of kindreds with hereditary cavernous malformations. Ann. Neurol. *55*, 757–758.

Verlaan, D.J., Siegel, A.M., and Rouleau, G.A. (2002). Krit1 missense mutations lead to splicing errors in cerebral cavernous malformation. Am. J. Hum. Genet. *70*, 1564–1567.

Vishteh, A.G., Zabramski, J.M., and Spetzler, R.F. (1999). Patients with spinal cord cavernous malformations are at an increased risk for multiple neuraxis cavernous malformations. Neurosurgery *45*, 30–2–discussion33.

Wang, Z., Dillon, T.J., Pokala, V., Mishra, S., Labudda, K., Hunter, B., and Stork, P.J.S. (2006). Rap1-mediated activation of extracellular signal-regulated kinases by cyclic AMP is dependent on the mode of Rap1 activation. Molecular and Cellular Biology *26*, 2130–2145.

Watanabe, N., Kato, T., Fujita, A., Ishizaki, T., and Narumiya, S. (1999). Cooperation between mDia1 and ROCK in Rho-induced actin reorganization. Nat. Cell Biol. *1*, 136–143.

Welch, C.M., Elliott, H., Danuser, G., and Hahn, K.M. (2011). Imaging the coordination of multiple signalling activities in living cells. Nat Rev Mol Cell Biol *12*, 749–756.

Whitehead, K.J. (2004). Ccm1 is required for arterial morphogenesis: implications for the etiology of human cavernous malformations. Development *131*, 1437–1448.

Whitehead, K.J., Chan, A.C., Navankasattusas, S., Koh, W., London, N.R., Ling, J., Mayo, A.H., Drakos, S.G., Marchuk, D.A., Davis, G.E., et al. (2009). The cerebral cavernous malformation signaling pathway promotes vascular integrity via Rho GTPases. Nature Medicine *15*, 177–184.

Wiggan, O., Shaw, A.E., DeLuca, J.G., and Bamburg, J.R. (2012). ADF/cofilin regulates actomyosin assembly through competitive inhibition of myosin II binding to F-actin. Developmental Cell *22*, 530–543.

Wittchen, E. (2008). Analysis of low molecular weight GTPase activity in endothelial cell cultures. Methods in Enzymology.

Wittchen, E.S. (2005). Rap1 GTPase Inhibits Leukocyte Transmigration by Promoting Endothelial Barrier Function. J. Biol. Chem. *280*, 11675–11682.

Wittchen, E.S., Aghajanian, A., and Burridge, K. (2011). Isoform-specific differences between Rap1A and Rap1B GTPases in the formation of endothelial cell junctions. Smallgtpases *2*, 65–76.

Wittchen, E.S., van Buul, J.D., Burridge, K., and Worthylake, R.A. (2005). Trading spaces: Rap, Rac, and Rho as architects of transendothelial migration. Curr. Opin. Hematol. *12*, 14–21.

Wolburg, H., and Lippoldt, A. (2002). Tight junctions of the blood-brain barrier: development, composition and regulation. Vascul. Pharmacol. *38*, 323–337.

Xu, K., Chong, D.C., Rankin, S.A., Zorn, A.M., and Cleaver, O. (2009). Rasip1 is required for endothelial cell motility, angiogenesis and vessel formation. Developmental Biology *329*, 269–279.

Xu, K., Sacharidou, A., Fu, S., Chong, D.C., Skaug, B., Chen, Z.J., Davis, G.E., and Cleaver, O. (2011). Blood Vessel Tubulogenesis Requires Rasip1 Regulation of

GTPase Signaling. Developmental Cell *20*, 526–539.

Yadla, S., Jabbour, P.M., Shenkar, R., Shi, C., Campbell, P.G., and Awad, I.A. (2010). Cerebral cavernous malformations as a disease of vascular permeability: from bench to bedside with caution. Neurosurg Focus *29*, E4.

Yajnik, V., Paulding, C., Sordella, R., McClatchey, A.I., Saito, M., Wahrer, D.C.R., Reynolds, P., Bell, D.W., Lake, R., van den Heuvel, S., et al. (2003). DOCK4, a GTPase activator, is disrupted during tumorigenesis. Cell *112*, 673–684.

Yamada, T., Sakisaka, T., Hisata, S., Baba, T., and Takai, Y. (2005). RA-RhoGAP, Rap-activated Rho GTPase-activating protein implicated in neurite outgrowth through Rho. J. Biol. Chem. *280*, 33026–33034.

Yamazaki, K., Gohda, J., Kanayama, A., Miyamoto, Y., Sakurai, H., Yamamoto, M., Akira, S., Hayashi, H., Su, B., and Inoue, J.I. (2009). Two Mechanistically and Temporally Distinct NF- B Activation Pathways in IL-1 Signaling. Science Signaling *2*, ra66–ra66.

Zabramski, J.M., Henn, J.S., and Coons, S. (1999). Pathology of cerebral vascular malformations. Neurosurg. Clin. N. Am. *10*, 395–410.

Zawistowski, J.S. (2005). CCM1 and CCM2 protein interactions in cell signaling: implications for cerebral cavernous malformations pathogenesis. Human Molecular Genetics *14*, 2521–2531.

Zawistowski, J.S., Serebriiskii, I.G., Lee, M.F., Golemis, E.A., and Marchuk, D.A. (2002). KRIT1 association with the integrin-binding protein ICAP-1: a new direction in the elucidation of cerebral cavernous malformations (CCM1) pathogenesis. Human Molecular Genetics *11*, 389–396.

Zhang, G., Xiang, B., Ye, S., Chrzanowska-Wodnicka, M., Morris, A.J., Gartner, T.K., Whiteheart, S.W., White, G.C., Smyth, S.S., and Li, Z. (2011). Distinct roles for Rap1b protein in platelet secretion and integrin αIIbβ3 outside-in signaling. J. Biol. Chem. *286*, 39466–39477.

Zhang, J., Clatterbuck, R.E., Rigamonti, D., and Dietz, H.C. (2000). Cloning of the Murine Krit1 cDNA Reveals Novel Mammalian 5′ Coding Exons. Genomics *70*, 392–395.

Zhang, J., Clatterbuck, R.E., Rigamonti, D., Chang, D.D., and Dietz, H.C. (2001). Interaction between krit1 and icap1alpha infers perturbation of integrin beta1-mediated angiogenesis in the pathogenesis of cerebral cavernous malformation. Human Molecular Genetics *10*, 2953–2960.

Zhang, J., Rigamonti, D., Dietz, H.C., and Clatterbuck, R.E. (2007a). Interaction between krit1 and malcavernin. Neurosurgery *60*, 353-359.

Zhang, J., Rigamonti, D., Dietz, H.C., and Clatterbuck, R.E. (2007b). INTERACTION BETWEEN KRIT1 AND MALCAVERNIN. Neurosurgery *60*, 353???359.

Zheng, X., Xu, C., Di Lorenzo, A., Kleaveland, B., Zou, Z., Seiler, C., Chen, M., Cheng, L., Xiao, J., He, J., et al. (2010a). CCM3 signaling through sterile 20–like kinases plays an essential role during zebrafish cardiovascular development and cerebral cavernous malformations. J. Clin. Invest. *120*, 2795–2804.

Zheng, X., Xu, C., Di Lorenzo, A., Kleaveland, B., Zou, Z., Seiler, C., Chen, M., Cheng, L., Xiao, J., He, J., et al. (2010b). CCM3 signaling through sterile 20–like kinases plays an essential role during zebrafish cardiovascular development and cerebral cavernous malformations. J. Clin. Invest. *120*, 2795–2804.

Zhu, Y., Wu, Q., Fass, M., Xu, J.-F., You, C., Müller, O., Sandalcioglu, I.E., Zhang, J.-M., and Sure, U. (2011). In vitro characterization of the angiogenic phenotype and genotype of the endothelia derived from sporadic cerebral cavernous malformations. Neurosurgery *69*, 722–31–discussion731–2.

Zhu, Y., Wu, Q., Xu, J.-F., Miller, D., Sandalcioglu, I.E., Zhang, J.-M., and Sure, U. (2010). Differential angiogenesis function of CCM2 and CCM3 in cerebral cavernous malformations. Neurosurg Focus *29*, E1.

Zieba, B.J., Artamonov, M.V., Jin, L., Momotani, K., Ho, R., Franke, A.S., Neppl, R.L., Stevenson, A.S., Khromov, A.S., Chrzanowska-Wodnicka, M., et al. (2011). The cAMP-responsive Rap1 Guanine Nucleotide Exchange Factor, Epac, Induces Smooth Muscle Relaxation by Down-regulation of RhoA Activity. Journal of Biological Chemistry *286*, 16681–16692.